MEASUREMENTS OF THERMAL CONDUCTIVITY OF PIPE INSULATION SYSTEMS AT BELOW-AMBIENT TEMPERATURE AND IN WET CONDENSING CONDITIONS WITH MOISTURE INGRESS

By

WEIWEI ZHU

Bachelor of Engineering in HVAC

Suzhou University

Suzhou, China

2012

Submitted to the Faculty of
Mechanical and Aerospace Engineering
Oklahoma State University
in partial fulfillment of the requirements for
the Degree of
MASTER OF SCIENCE
May, 2015

MEASUREMENTS OF THERMAL CONDUCTIVITY OF PIPE INSULATION SYSTEMS AT BELOW-AMBIENT TEMPERATURE AND IN WET CONDENSING CONDITIONS WITH MOISTURE INGRESS

Thesis Approved:

Dr. Lorenzo Cremaschi

Thesis Adviser

Dr. Afshin Ghajar

Dr. Khaled Sallam

ACKNOWLEDGEMENTS

I would like to express the deepest appreciation to my committee chair, Professor Lorenzo Cremaschi, who continuously conveyed to me the spirit of adventure in scientific research and his excitement in teaching. Without his guidance and persistent help, this thesis would not have been possible.

I would like to thank one of my committee members, Dr. Afshin Ghajar, for your continuous suggestions and support of the papers on my thesis subject. I would also like to thank my other committee member, Dr. Khaled Sallam, for your patience in teaching the energy conversion course, which enlarged my knowledge scope.

I would like to thank Dr. Shanshan Cai, who designed and constructed this experimental apparatus, which allowed me to conduct the following tests. My appreciation then goes to Jeremy Smith, who has been resolving the problems occurred with the LabView software and other electrical and mechanical systems inside the lab. I could not have successfully finished my experiments without him. I would also like to thank all my current and previous lab mates, Ardiyansyah Yatim, Andrea Bigi, Pratik Deokar, Pedro Perez, Biswas Auvi and Xiaoxiao Wu for all the efforts in maintaining our lab equipment and making the experimental work sustainable. I appreciate and treasure the time working with you all. You made all my sleepless nights and weekends in the lab less intolerable.

Acknowledgements reflect the views of the author and are not endorsed by committee members or Oklahoma State University.

Name: WEIWEI ZHU

Date of Degree: MAY, 2015

Title of Study: MEASUREMENTS OF THERMAL CONDUCTIVITY OF PIPE INSULATION SYSTEMS AT BELOW-AMBIENT TEMPERATURE AND IN WET CONDENSING CONDITIONS WITH MOISTURE INGRESS

Major Field: MECHANICAL & AEROSPACE ENGINEERING

Abstract:

When pipes are used for chilled water, glycol brines, refrigerants, and other chilled fluids, energy must be spent to compensate for heat gains through the wall of the pipes. Higher fluid temperature at the point of use decreases the efficiency of the end-use heat exchangers and increases the parasitic energy consumption. Mechanical pipe insulation systems are often used to limit the heat gains and save energy in commercial buildings. Pipe insulation systems play an important role for the health of the occupied space. When a chilled pipe is uninsulated or inadequately insulated, condensation might occur and water will drip onto other building surfaces possibly causing mold growth. The critical issue with cold pipes is that the temperature difference between the pipe and its surrounding ambient air drives water vapor in to the insulation system and condensation commonly occurs when the water vapor comes in contact with the chilled pipe surface. This thesis experimentally studies this issue for pipe insulation systems operating at below ambient temperature. The moisture content and the associated thermal conductivity of several pipe insulation systems were measured at various wet condensing conditions with moisture ingress. Accelerated type tests in laboratory showed the propensity of moisture accumulation in several insulation systems due to the cylindrical configuration, split joints, and micro-imperfections in the jacketing system. The data in the present work showed that the thermal conductivity increased systematically when water vapor entered the pipe insulation system.

TABLE OF CONTENT

LIST OF TABLES

Table Page

LIST OF FIGURES

Figure Page

Figure Page

Figure Page

Figure Page

NOMENCLATURE

B	: bias uncertainty for spatial distribution	-
D	: diameter	in. or (m)
G_f	: geometric factor	-
k	: thermal conductivity	Btu-in/hr-ft^2-°F or (W/m-°C)
L	: length of the test section	in. or (m)
m	: weight	lbm or (kg)
PIT	: Pipe Insulation Test apparatus	
$Q_{Al,pipe}$	: total heat transfer rate into the aluminum pipe	Btu/h or (W)
Q_{heater}	: electric power in the tape resistor heater	Btu/h or (W)
$Q_{leak,in}$	: heat transfer rate leaking in from the ambient through the external insulation	Btu/h or (W)
Q_{sand}	: heat transfer rate across the sand inside the aluminum pipe	Btu/h or (W)
T	: temperature	°F or (°C)
U	: uncertainty	-
V	: volume	ft$^{3/}$m^3
X	: uncertainty variables	-
Y	: uncertainty variables	-
P	: density	lbm/ft^3 or (kg/m^3)
δ	: thickness	in. or (m)
λ	: thermal conductivity	Btu-in/hr-ft^2-°F or (W/m-°C)

Subscripts

Al	: aluminum
amb	: ambient
avg	: average
Cu	: Copper
ins	: insulation
max	: maximum
min	: minimum
j	: actual time during test period
t	: total
v	: vapor
w	: water

CHAPTER I

1. INTRODUCTION

1.1 Background and motivations for this research project

Indoor heat exchangers are used to provide air conditioning, cooling, and dehumidification to buildings. A cold fluid, usually water or water-glycol solution, is used to transport and to distribute the refrigerating capacity from central chillers to the hydronic liquid-to-air heat exchangers and a network of chilled water pipelines commonly run inside the buildings. The exterior surface temperature of these pipelines is often at 38 to 40°F (3.3 to 4.4°C) and below the dew point temperature of the surrounding ambient air. Mechanical insulation systems are installed around such cold pipes to limit the heat gain and to prevent moisture condensation on the pipe wall surfaces. Insulation jackets, vapor retarders, and vapor sealing of the joints and fittings are normally adopted to create a barrier to the moisture ingress into permeable insulation. However, experience shows that mechanical pipe insulation systems are not completely vapor tight and in time moisture inevitably accumulates in permeable insulation systems. The fact that the pipe surface temperature is below the ambient room temperature has three main implications:

- There is a temperature gradient across the insulation system that drives a radial inward heat flow, that is, sensible heat is leaking in from the room at ambient conditions to the cold pipe through the cylindrically shaped insulation material and, when present, vapor retarder jacketing.
- There is a gradient of the water vapor partial pressure across the pipe insulation, which is often such that moisture in the ambient air is driven through the permeable insulation system

toward the cold pipe surface. When the surface temperature of the pipe is below the dew point temperature of the ambient air, moisture that migrates through the insulation system condenses upon contact with the cold pipe surface, resulting in the formation of water droplets. The water condensate may accumulate within the insulation system, thereby increasing the insulation thermal conductivity and sometimes drips onto the building's interior surfaces. Furthermore, in unconditioned spaces, surface mold sometimes results on the insulation jacket.

- The moist flow also represents an additional heat flux leaking into the insulation system and it increases the insulation apparent thermal conductivity of the system (Guldbrandsen et al., 2011).

According to Ogniewicz and Tien (1981), heat and moisture transport in insulation materials, especially porous insulation, is generally a complex multidimensional problem including air-vapor mixture flow due to free convection and infiltration through openings, heat transfer by conduction and convection, vapor transport by diffusion and convection, flow of liquid due to gravity and capillary action, and condensation with a possibility of re-evaporation accompanied by release or consumption of latent heat. He found out that, in porous media, especially fibrous insulation materials, the vapor transport mechanism usually happen in three stages. The first stage is a relatively short initial transient stage where temperature and vapor concentration fields are developing within the porous material. Second occurs the steady-state situation where temperature and vapor concentration fields are invariant with time. This stage is maintained as long as the liquid content is small enough to have an insignificant effect on properties. Finally, a transient stage follows when the liquid saturation reaches high enough values so as to affect the properties significantly. As the liquid content increases further, the liquid starts to flow out of the wet regions by gravity or capillary action. For closed cell type insulation materials, the cell walls are generally continuous and do not allow fluid or air to freely travel through. It could also be

predicted from the mechanism of moisture migration that, if the boundary conditions are reversed after the insulation is saturated with water, it would take less time for the water condensation to evaporate and condense again on the new cold surface. This could be explained by two facts. First one is that some of the water is already half way inside the insulation, and is therefore closer to the cold surface. The other one is that during the initial period of moisture migration, some preferential paths could have been created, which allows water vapor to pass through more easily. Therefore, it could be concluded that the process of water content migration is not reversible if the boundary conditions are reverses, that is, it will not take the same amount of time for the moisture to evaporate from the hot surface and condense on the cold surface.

To limit moisture accumulation inside pipe insulation systems, two methods are commonly used in the field, which are ventilation and the use of vapor barriers. Ventilation aims to exchange the high moisture content air with air having lower moisture content, while vapor barriers are used to limit the migration of moisture into the insulation and onto the pipe surface. In the literature, a few studies proposed to continuously remove the condensate from the pipe surface by utilizing a wicking action of hydrophilic fabrics (Crall, 2002; Korsgaard, 1993). While this approach has some value, it is generally recognized that the mechanical insulation systems for cold pipes suffer from moisture accumulation issues and the ASHRAE Handbook includes a discussion of such issues since the 1980s. Currently the standard ASTM C 335 (ASTM, 2010b) is used to determine the thermal conductivity of pipe insulation systems. However, this standard is based on a heated pipe, with the heat flow outward, and it is generally for use in above room temperature applications. When testing at below-ambient temperature, theoretical analysis shows that the experimental heat flow direction is unimportant for a perfect homogenous material but if the properties of the insulation vary in the radial direction, the experimental heat flow direction will affect the measured thermal conductivity (Wilkes et al., 2002). In addition, if the pipe is above room temperature moisture accumulation and water vapor condensation phenomena are virtually

absent since the moisture is driven outward, that is, from the pipe surface to the ambient. Another approach in the literature is to approximate the effective thermal conductivity of the materials used in pipe insulation systems with the thermal conductivities of materials used for insulation panels (ASTM, 2010a, 2010c). Often, the materials for such panels have been tested in flat slab configurations, which are originally intended for building walls, refrigeration and freezer boxes. Unfortunately the radial configuration and split joints typical of pipe insulation systems can produce significantly different thermal conductivity than flat slabs.

To address these challenges, a novel experimental methodology was developed to measure the apparent thermal conductivity of insulation systems for cold pipes and a new test apparatus was designed and realized under the ASHRAE Project RP-1356 (Cremaschi et al. (2012)). The thermal conductivity of pipe insulation systems was measured below-ambient temperatures in both dry non-condensing and wet-condensing conditions with moisture ingress. The tests of RP-1356 demonstrated the capabilities of the test apparatus and the feasibility of the experimental methodology. Several lessons were learnt from the ASHRAE RP-1356 research project and the main findings can be summarized as follows:

- The measured values of the apparent thermal conductivity of pipe insulation systems diverged from the values of thermal conductivity obtained from measurements on flat slabs. This result confirmed previous findings in the literature and it was explained due to possible variation of the density and anisotropy of the cells or fibers along the radial direction.
- The measured values of the apparent thermal conductivity of pipe insulation depended on the wall thickness of the pipe insulation. This was due to the variation of the heat path resistance, which took into account not only the anisotropy of the material but also the edge effects of split joints. Pipe insulation systems are typically split in two C-shaped sections or shells, for easy installation on previously installed chiller pipes.

- The measured thermal conductivity of pipe insulation was affected by the uniformity of both cold and hot side surface temperatures. For the aluminum surface, there was a critical need to accurately control the aluminum pipe surface temperature along the axial direction. For the outer surface of the pipe insulation, the surrounding air must be as uniform as possible for both temperature and humidity levels. Only if these boundary conditions were true, an average value of the pipe insulation thermal conductivity could be obtained. This observation implies that for achieving good accuracy and repeatability of the thermal conductivity measurements of pipe insulation, the ambient air should be extremely well controlled, and air direct impingement must be avoided at all times during the tests. This type of tests could be performed in a room whose environmental conditions are well controlled, such as a psychrometric chamber or a refrigerated room.
- The apparent thermal conductivity for the case of cold pipes increases as moisture entered in the insulation material. Preliminary results indicated that moisture content and thermal conductivity followed an asymptotic trend and the "time to drip" of water droplets from the wet pipe insulation onto the building floor ranged from 2 weeks up to several months of continuous exposure to humid environment. This time to drip was directly measured in accelerated-type laboratory tests, in which vapor barrier was intentionally removed from the pipe insulation. The time to drip of pipe insulation systems in true as-installed operating conditions can be estimated from the accelerated type laboratory experiments. The time to drip was depended on the ambient conditions, surface area of the insulation exposed to the ambient, density, permeability of the insulation or of the vapor retarder or exterior jacketing system, and the wall thickness of the pipe insulation.

From the above list, the ASHRAE project RP-1356 advanced the state-of-the-art knowledge in this area but there is still a large gap of information that must be provided in order to extend the findings to a wider range of pipe insulation systems. In particular there is a lack of quantitative

data about the impact of moisture ingress on the apparent thermal conductivity of pipe insulation systems for cold pipe applications. These data can be provided by experimental work in laboratory, which have equipment designed to control both cold pipe and ambient boundary conditions. The present work aims to provide such data and the project extends the experimental measurements of thermal conductivity for pipe insulation systems in the wet condensing conditions beyond the insulation materials and experimental conditions that were originally investigated in ASHRAE RP-1356.

CHAPTER II

2 LITERATURE REVIEW

2.1 Review of Methods to Measure Thermal Conductivity of Flat Slab Insulation Systems

Several criteria for the laboratory measurement of thermal conductivity of flat slab specimen were documented in the ASTM standards. One of the most popular methods is the Guarded Hot Plate (GHP) method for measurement of steady state heat flux and thermal transmission properties (ASTM C 177). This test method is applicable to the measurement of a wide range of specimens and environmental conditions. It should be noted that if the test specimen has inhomogeneities in the heat flux direction, the measured thermal properties by using GHP method may be location specific, and should be avoided. While most GHP method operates in double sided mode, ASTM C1044 specifies the Guarded Hot Plate method in the single side mode. Al-Hammad et al. (1994) utilized the GHP method for testing insulation samples, and made a comparison of experimental values with the manufacturer's data. The results indicated that the published thermal conductivity values do not necessarily represent the values for certain climatic conditions. Another widely used method for steady state thermal property measurement is the Heat Flow Meter method (HFM) documented in ASTM C 518. The HFM method generates one-dimensional heat flux thorough the test specimen by maintaining constant boundary temperature on the two parallel plates. The thermal conductivity can be obtained by applying the Fourier's Law of heat conduction. However, one disadvantage of the HFM method is that the thermal resistance of test specimen smaller than 0.1 m^2K/m could not be measured. Tseng and Kuo (2002) applied the HFM method, and obtained the correlation of effective thermal conductivity of

phenolic foam insulation with temperature. He tested both the dry samples and moisture saturated samples of phenolic foam insulation, and found out that the k_{eff} of saturated samples was about 20% higher than that of dry samples. ASTM C1363 also specifies the Hot Box method, which is applicable on building materials and envelope assemblies of homogeneous or non-homogeneous specimens. This method permits operation under natural or forced convective conditions at the specimen surface. Wilkes and Childs (1995) used the Guarded Hot Box facility to measure the thermal performance of fiberglass and cellulose attic insulations with an attic test module, and found that natural convection contributed to heat flow through the insulation and reduced the measured thermal resistance. This method was also utilized by Ye et al. (2006), and he obtained the thermal resistance of wool and wool-hemp insulations. Moore et al. (1985) used another technique for measuring the apparent thermal conductivity of flat insulations, which consisted of an electrically heated flat Nichrome-screen wire sandwiched between a pair of samples. He pointed out that the thermal conductivity of pipe insulation was easier to measure than flat slabs. This was mainly because that the radial configuration of the pipe tester ensured better accuracy than for flat insulations systems.

While steady state heat flow techniques are very precise for thermal conductivity measurements and have lower uncertainties and better repeatability, they require a relatively large sample size and a long time period to reach steady state. Transient methods can usually do measurements on a smaller sample and take a shorter time period. ASTM C1113 specifies the Transient Hot Wire method (THW), which applies the transient radial heat flow technique. Another commonly used method is Transient Line Source Technique (TLS) documented in ASTM D5930. The TLS has the advantages of simple and fast measurement, and it also has the highest accuracy because it eliminated the thermal contact resistance. Batty et al. (1981) validated and utilized the line source thermal probe technique to measure the apparent thermal conductivity of commercial fiberglass blankets, and measured the apparent thermal conductivity of 0.039W/K-m of dry insulation

samples at 20°C mean insulation temperature. The Transient Hot Strip (THS) method was developed by Gustafsson et al. (1978). According to him, the THS method was more preferable than the THW method, because the reduction of the thickness of the heat source and the thermal contact problems considerably decreased the absolute and statistical error of the measurements. Log (1993) pointed out that, this THS method might give large experimental errors when applied to insulation materials with low heat capacity. He further discussed the precautions that should be taken in order to eliminate the potential experimental errors when applying the THS method. On the other hand, Sabuga and Hammerschmidt (1995) found that, for the experimental data obtained by THS method, there was no relation between the uncertainty and the measured values due to the statistical nature of the estimation procedure. He improved it by developing a new algorithm to evaluate the THS measurement curves.

Ohmura (2007) compared the thermal conductivity values of insulation materials obtained by both steady state methods and transient methods. He found the variation in the results was about ±10%, and therefore he proposed that it would be practical to improve the accuracy of measurement in the absence of reference materials by comparing thermal conductivities obtained with different measurement methods. Salmon and Tye (2011) compared the thermal conductivity of thin specimens by using both the steady state and transient methods, and they found out that the transient values were generally higher than steady state values by as much as 3.2%. However, if taking into account the inhomogeneity of the material and the measurement uncertainties, the results could still be considered to be in good agreement. Bezjak and Zvizdić (2011) did the comparison of insulator thermal conductivity obtained by the THW method and the GHP method. He found out that for insulation materials of glass wool, stone wool, Expanded Polystyrene and Extruded polystyrene, the results obtained by both methods were within 6% variation. But for the case of polyurethane, the discrepancy was bigger due to the manufacturing stabilization process.

2.2 Review of Methods to Measure Thermal Conductivity of Pipe Insulation Systems

The ASTM C335 test method for steady state heat transfer properties of horizontal pipe insulation and ASTM C1033 test method for steady state heat transfer properties of vertically installed pipe insulation are the only two methods documented in the ASTM standards to measure thermal conductivity of pipe insulation systems. ASTM C335 specifies the guarded end or calibrated end pipe apparatus. This apparatus utilizes the guarded end sections to limit axial heat transfer and is based on a heated pipe. The thermal conductivity obtained by this method includes the effects of the insulation and its fits upon the pipe, circumferential and longitudinal joints and variations in construction. Therefore, thermal properties measured by this method are different from those obtained from the similar material in flat form using the GHP method. Whitaker and Yarbrough (2002) utilized the horizontal pipe apparatus test method, and presented the thermal conductivity of pipe insulation systems including calcium silicate, mineral fiber, cellular glass, expanded perlite and fiber glass. A wide variation was detected due to different physical properties of those pipe insulation systems. Zehendner (1983) used a similar heated pipe test apparatus placed in a test enclosure, and demonstrated the influence of material type, bulk density, cellular structure on the thermal conductivity of the insulation systems.

Wilkes et al. (2002) developed a pipe insulation test apparatus based on a cold pipe, where the main heat flow was radially inward through the test specimen to central fluid cooled tube. Fiberglass, polyisocyanurate foam and elastomeric rubber insulation were tested on this new apparatus, and their thermal conductivities were successfully correlated with insulation mean temperature in linear trends. Another cold pipe based testing method was the calibrated hot box method, first utilized by Musgrave (1979) on the thermal properties of urethane foam cryogenic

piping insulation. This method required that the humidity inside the box to be reduced before test and critically controlled during the test period by applying proper vapor barrier systems.

Ramsden (1985) and Rawlins (2005) used the concentric cylinder comparative method to measure the thermal conductivity of chilled water pipe insulation systems. This method was suitable for testing pipe insulation with heat flux both inward and outward with the heat flux pads attached on the insulation surface to measure heat flow through the insulation system. Nevertheless, it was possible that the heat flux pads could create air gaps between the test insulation and the cold pipe. It was also likely that the heat flux pads can change the path of heat transfer by compressing the test insulation material in certain locations, leading to inaccurate experimental results.

While some of the steady state methods suffer from the disadvantage that the time taken to reach equilibrium might be too long, transient methods have also been used to determine the thermal conductivity of pipe insulation systems. Kulkarni and Vipulanandan (2006) applied the transient hot wire (THW) method to investigate the thermal conductivity of pure polymer insulation and polymer composites. This method was suitable for measuring thermal conductivity in the range from 0.55 to 13.9 Btu-in/hr-ft^2-F (0.08 to 2.0W/m-K).

2.3 Review of Methods to Measure Thermal Conductivity of Pipe Insulation Systems with Moisture Ingress

To date, there is no standard method for testing thermal conductivity of pipe insulation systems in wet conditions. Both the steady state method Guarded Heated Plate, and the transient method thermal probe technique were used in previous studies for wet insulation samples. However, it is important to be noted that the results depend not only on the testing method used, but also how the wet insulation samples are prepared. McFadden (1986) investigated the moisture effects on Extruded Polystyrene Insulation using both the GHP and a thermal probe technique. The

advantage of the GHP method is the better accuracy. However, the initial thermal conductivity values measured by GHP were usually very high due to the fact that the moisture content inside the insulation sample was still reaching equilibrium status. The thermal probe technique utilizes a thermal conductivity probe inserted into the insulation and measures the thermal conductivity of a specific location. Compared with the GHP method, it requires a shorter time period to obtain results. Batty et al. (1981) also concluded that the steady state method GHP was not suitable for wet insulations because the steady state would not reach until all the moisture has redistributed. In other words, in the starting period of moisture conditions, results measured by GHP method were not appropriate. The heat flux meter (HFM) method was applied by Kumaran (1987) to monitor and measure the heat flux across a moist insulation specimen. He pointed out that the HFM method actually calculated two moisture transport characteristics, one of which was when the moisture content in the test insulation specimen was redistributing to reach equilibrium, and the other was when the moisture transfer was complete and the insulation specimen behaved as a dry material. Chyu (Chyu et al. (1997a), 1997b)) also applied this HFM method and measured the effective thermal conductivity of insulation specimen saturated with water and in steady state.

2.4 Review of Methods to Moisturize Pipe Insulation Systems

One of the methods to prepare wet insulation samples is immersion, which was first used by Batty et al. (1981). He prepared the moistened insulant by complete immersion in water, and controlled the dampness by conditioning it in an environmental chamber. Chyu investigated the effect of moisture content on the Polyurethane insulation thermal performance by submersion insulation specimen in water until saturated with moisture. The insulation was considered saturated with water when air or gas emission from the water ceased. The thermal conductivity was measured under isothermal conditions. However, Chalumeau and Felix-Henry (2006) pointed out that immersion under pressure might lead to different moisture distribution, because the heat and mass transfer inside the wet insulation could be affected by the water temperature in the

reservoir, which would cause different interfacial tension and the variation of vapor partial pressure. This method is only suitable for pipe insulations applied in a flooded condition, but not for HVAC mechanical pipe insulation applications which are normally installed in indoor or outdoor ambient conditions.

Another method is to prepare the wet samples in laboratory conditions. Laboratory moisturized samples usually have a more uniform moisture distribution than those from the field. However, McFadden (1988) pointed out that by using this method, the moisture content accumulated in the insulation specimen was usually lower than in the field. The other disadvantage was that the water distribution might be different from insulation in real fields, which would affect the measurement of thermal conductivity.

Spraying or injecting water into the insulation test samples is another method for measuring wet insulation thermal conductivity. Kumaran (1987) prepared wet insulation samples by injecting different amount of water inside the insulation specimen using a hypodermic syringe. The HFM method was used to measure the thermal conductivity of wet insulation samples in his work. It was found out that at the beginning the moisture distribution might be in transient conditions since water at the hot surface would be vaporized and transported to the cold surface. And therefore the thermal conductivity measure at the initial status might not be steady state. Langlais et al. (1983) proved this assumption later by developing a mechanism of moisture migration in fibrous insulations, and he defined this initial moisture transportation stage as quasi equilibrium. According to McFadden (1986), during the transient state, the insulation thermal conductivity was a function of the location of the high moist regions and the thermal conductivity of pipe insulation systems depended on whether the high moist regions were closer to the hot side or the cold side. Once the moisture on the hot side finished redistributing to the cold side, the insulation specimen reached the final steady state condition, and the thermal conductivity was the same as in dry conditions. It was also found by Langlais et al. (1983) that the large increase of thermal

conductivity observed at quasi steady state for low moisture content was caused by additional heat transfer by vapor diffusion. Because of the position of high moist content regions is quite sensitive for the overall thermal conductivity of pipe insulation systems, the injection method is not suitable for simulating the water distribution in HVAC pipe insulation systems.

The other method is to adopt a temperature, humidity and air speed controlled ambient and simultaneously impose a cold surface on one side of the insulation test specimen. Modi and Benner (1985) prepared wet insulation specimen by exposing them on a cold surface while a conditioned ambient on the exterior side of the insulation. Cremaschi et al. (2012) tested several pipe insulation systems in a psychrometric chamber. Their approach required a large amount of equipment and it had a very high capital cost. The psychrometric chamber is able to better simulate the actual operating conditions of HVAC mechanical pipe insulation systems. The pipe insulation systems were installed on a cold aluminum pipe and exposed to hot and humid ambient conditions. Moisture is driven into the insulation due to water vapor partial across the radial direction, and the water vapor finally condenses when it reaches the cold pipe. Accelerated type of ambient conditions was usually applied for the pipe insulation systems to achieve measurable moisture contents.

2.5 Conclusions

The experimental methodologies for measuring the apparent thermal conductivity of pipe insulation systems were discussed above. Both steady state and transient methods were used by previous researchers to investigate the thermal performance of pipe insulations and insulation slabs. Comparisons were made between results generated by the two different methods. It was observed that steady state methods for pipe insulation systems were commonly applied for measuring an average thermal conductivity. Steady state methods are simpler and easier to operate in dry conditions than transient methods, and they are also very precise for thermal

conductivity measurements, and have lower uncertainties and better repeatability. However, steady state methods often require a relatively larger sample size and a longer time period to reach equilibrium. In addition, heat flow direction will also impact the thermal conductivity results when applying steady state methods. Transient methods can usually do measurements on a smaller sample and take a shorter time period. They provide faster measurement and simpler installation. However, transient methods are more suitable for measuring thermal conductivity of a certain location on a test specimen, and the thermal probe sensors physical characteristics can also affect the measured apparent thermal conductivity.

For the measurement of thermal conductivity of pipe insulation systems with moisture ingress, several moisturizing strategies were utilized to prepare moistened insulation samples. The advantages and disadvantages of each method were discussed. The steady state method was not suitable for measuring the apparent thermal conductivity of wet insulation samples because the initial moisture redistribution would bring additional heat transfer by vapor diffusion and thus increase the measured thermal conductivity of the insulation specimen. Preparing the moistened insulation samples in a high humidity environment with one cold side surface of the test specimen could provide similar moisture ingress as in the field. However, this technique required a large equipment investment and more strict control of the ambient conditions. Compared with steady sate methods, transient methods were not appropriate for measuring thermal conductivity of wet insulations because of the sensitivity of test results to moisture content of the certain location where the thermal probe is placed.

To date, there are still challenges in measuring the apparent thermal conductivity of pipe insulations in dry conditions and in wet conditions with moisture ingress. The main aspects to be further considered include the thermal performance of joint sealants and the moisture redistribution in radial configurations of pipe insulation systems. The temperature and humidity controlled chamber can well simulate the boundary conditions during pipe insulation field service.

However, due to its high capital cost, long time period for construction and calibration, a compact, easy to install and inexpensive sensor is still needed for future research.

CHAPTER III

3 OBJECTIVE

The overall objective of this research project is to measure the apparent thermal conductivity of mechanical pipe insulation systems at below ambient temperatures in both dry non-condensing conditions and in wet condensing conditions with moisture ingress into the insulation systems. The specific objectives are summarized as follows:

(a) To measure the apparent thermal conductivity of twelve (12) materials/systems under dry conditions and nine (9) materials/systems under wet (condensing) conditions. All nine of the materials/systems tested under wet conditions were also among the twelve materials/systems tested under dry conditions.

(b) To experimentally determine the amount of moisture absorbed in the pipe insulation systems during the wet tests.

(c) To provide data of the impact of moisture ingress on the apparent thermal conductivity of pipe insulation systems.

Materials/systems that were tested under dry conditions but NOT in wet conditions

(1) 2” thick glass fiber with no vapor retarder. This test is to be run as the very first sample tested in this project.

(2) 2” thick glass fiber with no vapor retarder. This test is to be run near the end of the project.

(8) 2” thick elastomeric rubber with no vapor retarder.

Materials/systems that were tested under dry and wet condition

(3) 2” thick glass fiber with no vapor retarder. The wet test of this system was run at two different ambient conditions, which were 90°F ambient temperature, 83% R.H. ambient relative humidity and 78°F ambient temperature, 55% R.H. ambient relative humidity.

(4) 1.5” thick glass fiber with ASJ vapor retarder. The wet test of this system was run at 78°F ambient temperature, 55% R.H. ambient relative humidity.

(5) 1.5” thick glass fiber with ASJ vapor retarder

(6) 1.5” thick glass fiber with ASJ vapor retarder and then covered with 20 mil thick PVC jacketing sealed at the joints

(7) 1.5” thick glass fiber with Polyester Foil Polyester (PFP) vapor retarder. The PFP should be a zero permeance product consisting of ~1 mil thick aluminum foil sandwiched between two layers of 0.5 mil thick Polyester

(9) 1.5” thick elastomeric rubber with joint sealant and no additional vapor retarder

(10) 1.5” thick cellular glass with the joints sealed but with no additional vapor retarder

(11) 1” thick polyisocyanurate (PIR) with Polyvinylidene Chloride (PVDC) vapor retarder

(12) 1.5” thick polyisocyanurate (PIR) with no vapor retarder, the wet test of this system was run at 107°F ambient temperature, 81% R.H. ambient relative humidity, and with a pipe temperature of 40°F.

Same conditions were set for all of the wet testing. These were 38°F pipe temperature, 90°F ambient temperature and 83% ambient relative humidity, except for system (3), system (4) and system (12).

CHAPTER IV

4 SUMMARY OF THE PIPE INSULATION TEST APPARATUS AND ASSOCIATED INSTRUMENTATION

This chapter provides an overview of the test apparatus and test facility. The experimental methodology and design criteria will be further discussed in the following sections. The experimental apparatus consisted of three parts: the pipe insulation tester (PIT), a chiller system, and a psychrometric chamber. The PIT was installed inside the psychrometric chamber at Oklahoma State University Research laboratory, which provided accurate control of the ambient temperature and humidity.

4.1 Pipe Insulation Tester (PIT)

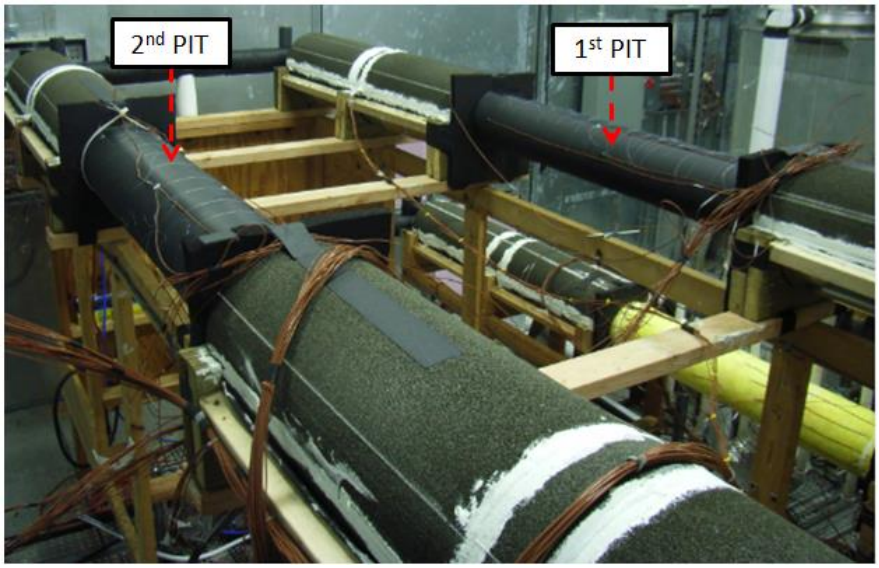

Figure 4.1 Photo of the four Pipe Insulation Test apparatus (PIT): the 1st PIT is used to measure the thermal conductivity of the test insulation specimen; the 2nd PIT is used to measure its moisture content.

Four pipe insulation testers (PITs), shown in ERROR! REFERENCE SOURCE NOT FOUND. were constructed and were installed in parallel with respect to the heat transfer fluid flow. The four PITs were divided into two groups of PITs, and each group consisted of a first PIT and a second PIT. Each PIT was 11.6 ft. (3.5 m) long and had two end sections acting as thermal guards. Each PIT consisted of a 0.5 in. (12.7 mm) inner copper tube, sand filling, and an aluminum pipe of 3 in. (76.2 mm) NPS pipe (referred to as aluminum pipe). Figure 4.2 shows a schematic of one PIT with relevant dimensions. The test specimen was 4 ft. (1.2 m) long, but the actual measuring section was only the center part of it, that is, 3ft. (0.9m) across the center line of pipe insulation system. The copper pipe was centered and aligned inside the aluminum pipe.

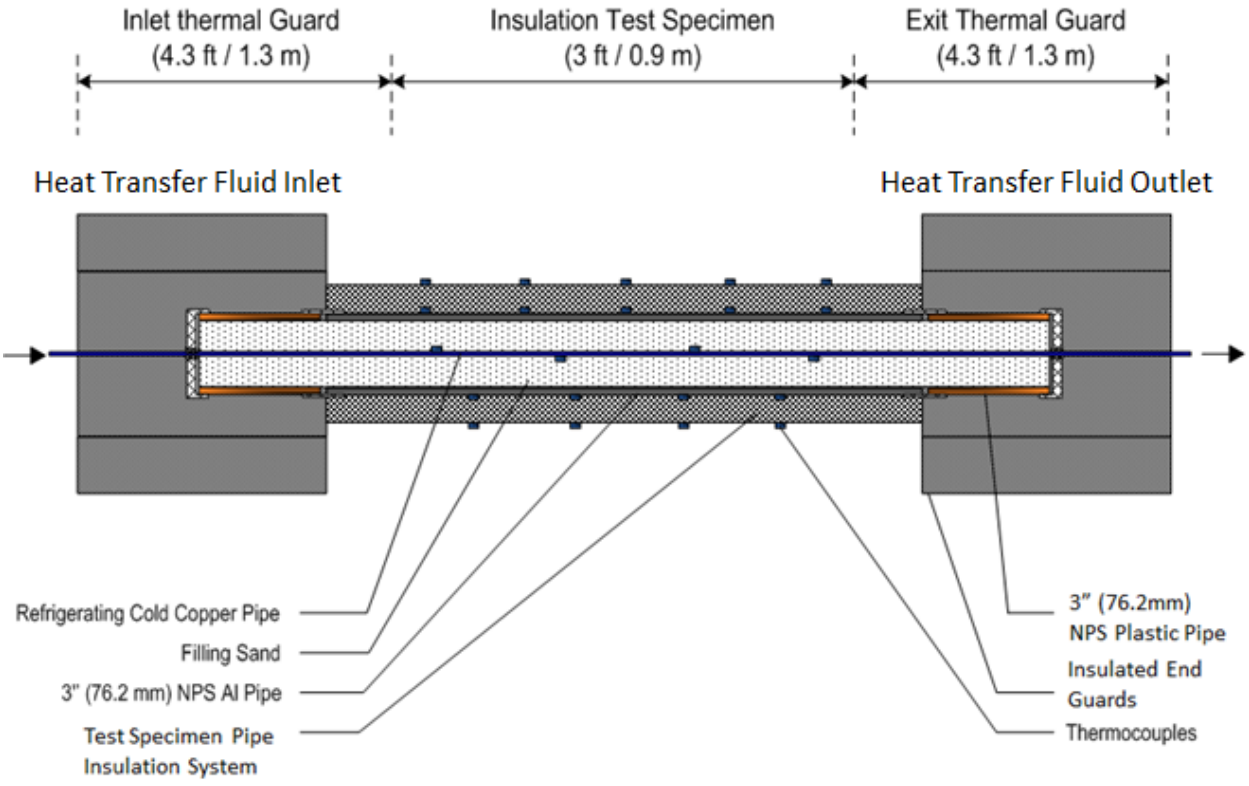

Figure 4.2: Schematic of the Pipe Insulation Test apparatus (PIT).

The aluminum surface temperature was adjusted to about 38°F ± 0.5°F (3.3°C ± 0.3°C) or 40°F ± 0.5°F (4.4°C ± 0.3°C) to be close to the typical surface temperatures in chilled water applications. With reference to Figure 4.2, a heat transfer fluid was circulated in the inner copper tube. The chilled copper tube at the central core of the aluminum pipe created a thermal gradient across the sand, which was the filling material for the annulus region between the copper pipe and the aluminum pipe. The temperature gradient controlled the inward heat flux and, at the same time, the heat transfer fluid was maintained at a high flow rate in the cold pipe to limit the temperature increase along the axial direction within 1°F (0.5°C). Since the bulk temperature of the heat transfer fluid was fairly constant along the axial length of the test apparatus, the surface temperature of the copper pipe tended also to be uniform along the axial and angular directions. Thus axial heat losses were minimized. Pre-dried play sand was selected because of easiness of filling, compact structure, and appropriate thermal conductivity for the radial heat flux measurements. The suitable thermal conductivity of sand provided large temperature gradients between the inner copper tube and the aluminum pipe surface during the experiments. Sand was inexpensive and available in several local warehouses. It filled the annulus region in between the copper tube and the aluminum pipe without requiring special tools or any pre-fabrication processes. Sand formed a fairly homogenous and compact filling in the entire space inside the aluminum pipe and it can be replaced without damaging the thermocouples attached on the inner copper tube. When water vapor diffused into the aluminum pipe, sand provided some resistance to the local water accumulation because it limited water traps due to its compactness. In addition, sealing of the end sections of the aluminum pipe was performed with vapor resistance mastic and, to prevent possible moisture ingress into the sand, the sand was sealed in vapor barrier plastic bags and plastic plugs were used to seal each side of the aluminum pipe. Figure 4.3 (a) illustrates the end sides of the aluminum pipe, the plastic bags and plastic plug used as vapor barrier for the sand, and various phases of the assembly process of the aluminum pipe core section. Four cross-

shaped plastic supports, shown in Figure 4.3 (b), were inserted inside the aluminum pipe to align the copper pipe at the center line of the aluminum pipe. These supports were necessary to prevent copper pipe from bending when full of refrigerant and compressing the sand at the bottom section. Any misalignment of the copper pipe with the aluminum pipe and any non-uniformity of the sand in the annulus region could cause a systematic error in the radial heat flux measurements. Preliminary tests were conducted to check that the entire device was assembled satisfactorily. In these tests the temperature distribution along the aluminum pipe surface was measured and it was reasonably uniform along both axial and angular directions.

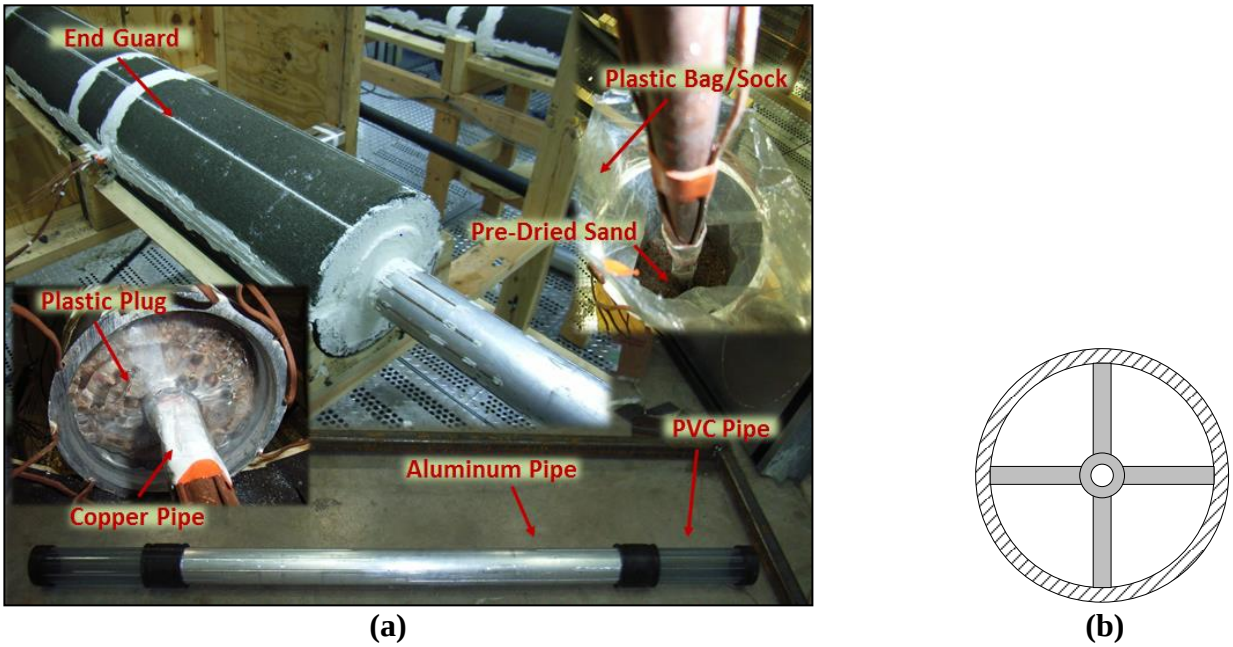

Figure 4.3: (a) Photos of the construction stages of Pipe Insulation Test apparatus (PIT) (b) Pipe support for the copper pipe inside the PIT.

During the later period of this research project, the surfaces of the aluminum pipes of all PITs were covered with aluminum adhesive tape with zero or closed to zero permeability. The tape covered the thermocouple wire housed in the grooves on the aluminum pipe surface as shown in Figure 4.4. These grooves were identified as potential paths for the water vapor intrusion into the insulation systems. Water vapor might be able to enter at the end side of the aluminum pipe,

travel along the paths created by the thermocouple grooves, and enter the pipe insulation from its inner surface. To avoid this potential mechanism of water vapor ingress in the pipe insulation system, the gaps between the test pipe and the end thermal guards were sealed with silicone gel. Then the thermocouple wires running on the aluminum pipe were completely covered with aluminum tape, which was wrapped around the aluminum pipe surface as shown at the top of Figure 4.4. This tape created a vapor barrier between the grooves of the aluminum pipe and the insulation test specimen, thus eliminating the possibility of water vapor ingress into the test specimen from the grooves of aluminum pipe surface. In addition, in order to eliminate the radiation heat transfer effect caused by the low emissivity of the aluminum surface, the aluminum pipes were painted black by using a latex based paint (Eco-Guard latex enamel). The photos for the black pipes are shown in Figure 4.5.

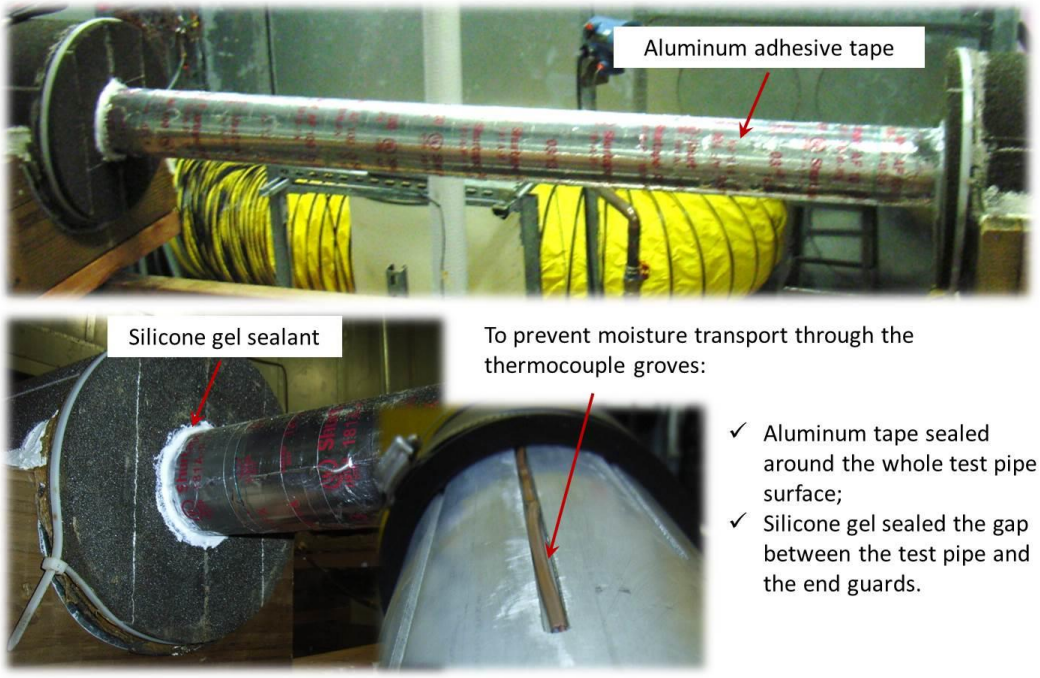

Figure 4.4: Photos of the grooves sealed with aluminum adhesive tape and edge seal with silicone gel.

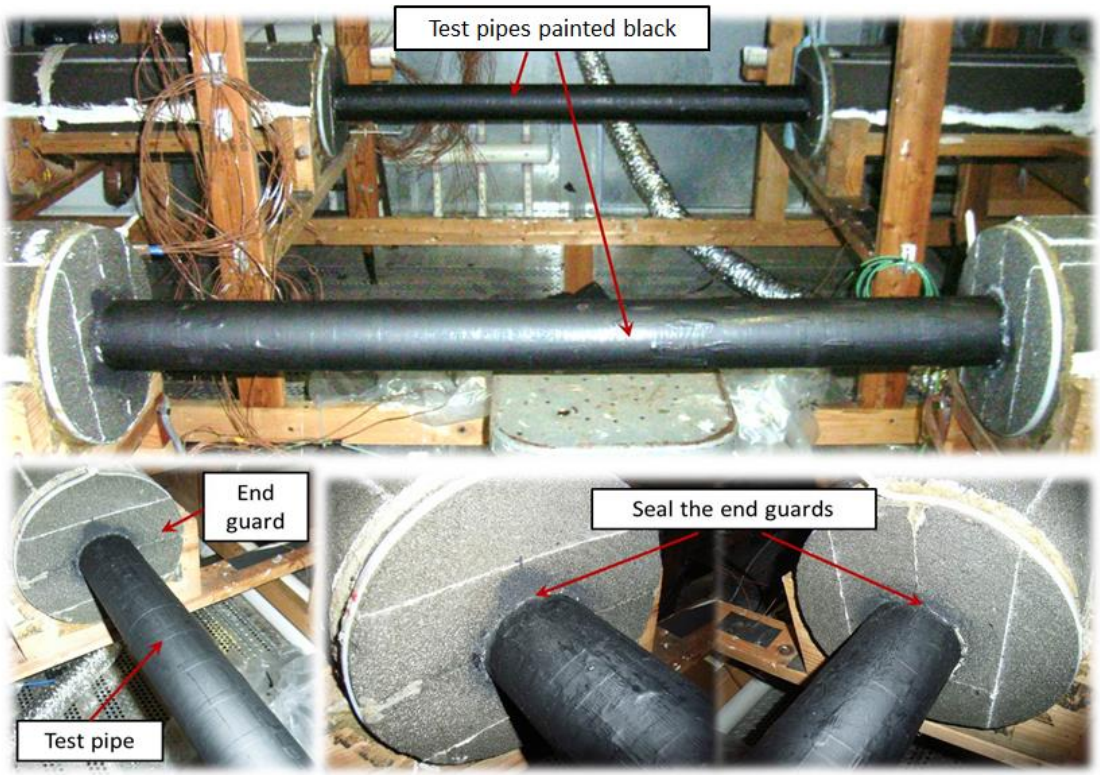

Figure 4.5: Photos of the aluminum pipes painted black and details of the edge seals.

4.2 Chiller System

A chiller system was used to cool the copper pipe temperature in the range from -5 to +25°F (-21 to -4°C). The chiller had a capacity of 2 tons at -5°F (-21°C) and used Dynalene HC50 as the heat transfer fluid for the PITs. The chiller system was installed adjacent to the chamber but outside the indoor room where the PITs were located. This location of the chiller system minimized the disturbance of the ambient air that surrounded the PITs. The flow rate was controlled by a variable speed gear pump in the range from 34 to 48 lb/min (0.26 to 0.36 kg/s). The gear pump circulated the heat transfer fluid through the PITs with a high velocity so that the resulting temperature increase across the PITs was within 1°F (0.5°C). Four PITs were connected in parallel with respect to the heat transfer fluid flow as shown in Figure 4.6. The four PITs were identical. They were divided into two groups, and each group consisted of a 1st PIT and a 2nd PIT.

The 1st PIT and the 2nd PIT were built at the same time. The temperature sensors on the first PIT aimed to measure the apparent thermal conductivity of the pipe insulation specimen, while the second PIT was used to measure the moisture content in the pipe insulation system at intermediate time intervals during the wet tests. The measurements of moisture content from the second PIT provided an indication of the moisture accumulation rate (McFadden (1988)) in the mechanical pipe insulation system during the wet test period.

The parallel configuration of the PITs guaranteed that all the insulation test specimens were exposed to exactly the same temperature boundary conditions and radial heat flux at all time. The chiller system provided sufficient cooling capacity at low temperatures required for conducting the dry and wet tests. A 25 gallon tank was used to stabilize the heat transfer fluid temperature for long periods of testing scheduled for the experiment campaign of this project. The temperature control of the heat transfer fluid entering the PITs was also perfected by using a custom made PID controller that modulated the electric power of an immersion heater installed in the supply line of the chiller system. The immersion heater was installed after the gear pump as shown in the schematic of Figure 4.6. The control algorithm was tuned ad-hoc to control the inlet temperature of the heat transfer fluid to the PITs with a precision of $\pm 0.2°F$ ($\pm 0.1°C$) of the set point temperature during the period of the experiments. This was found to be a key factor in order to guarantee the repeatability of the test results.

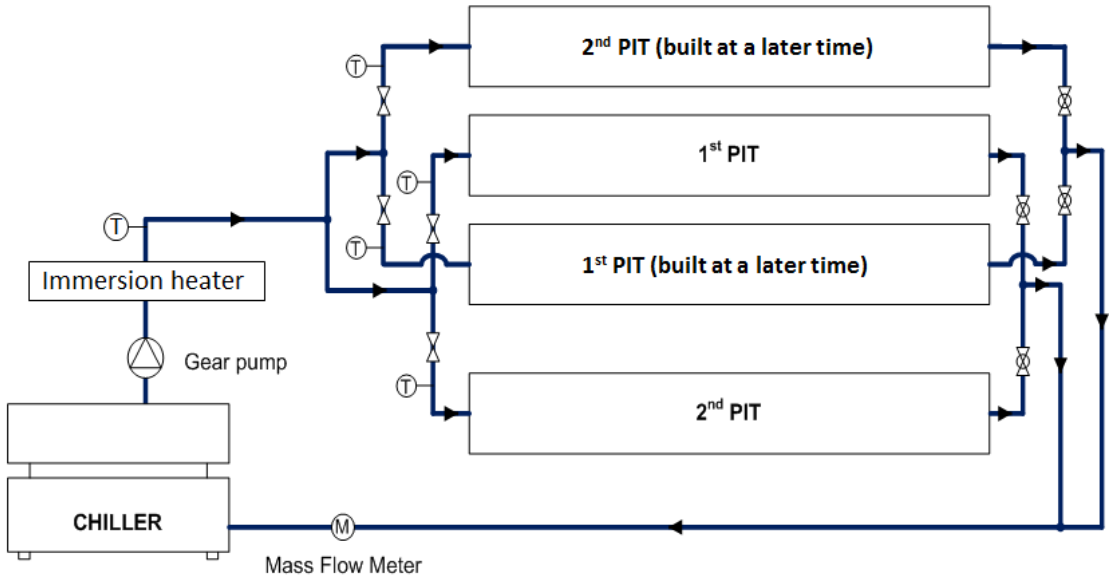

Figure 4.6: Schematic of the test facility consisting of four PITs installed in parallel with respect to the heat transfer fluid flow.

4.3 Psychrometric Chamber

Measurement of the apparent thermal conductivity of pipe insulation systems under controlled ambient temperature and humidity could be performed in psychrometric chambers. In this project, a psychrometric chamber was designed so that a slow motion of the air was controlled during the tests, with air ascending vertically in the room and coming from perforated grids on the floor. An under floor air plenum was used to distribute the air flow uniformly across the entire floor area of the psychrometric chamber. The displacement ventilation system, shown in Figure 4.7, consisted of an air conditioning loop, an under floor air plenum supply, and a set of adjustable ceiling filters. Air was circulated through the conditioning loop first, shown on the right side in Figure 4.7, by using variable speed fans. The air flow rate was adjusted with the fan and a set of electro-mechanical dampers. With reference to Figure 4.7, during the first process, the air that goes inside the conditioning loop is cooled and dehumidified through water-to-air cooling coils. The coil surface temperature and capacity were controlled by a variable speed pump, electronic mixing

valves and bypass valves. These parameters were adjusted so that the air is cooled and dehumidified at about 43°F (6°C) of air dew point temperature. This was the minimum air dew point temperature that the cooling coils of the chamber were able to provide. To guarantee dry non-condensing conditions, the ambient air dew point temperature must be below the aluminum pipe surface temperature of 38°F (3.3°C). In order to reach this condition, an additional mechanical dehumidifier was utilized to dehumidify further the ambient air in the room and the air was dehumidified to a dew point temperature lower than the aluminum pipe surface temperature. Once the ambient dew point temperature was below the aluminum pipe surface temperature, the electric heaters of the chamber were activated to reach the desired dry bulb temperature of the test. The electric heaters of the psychrometric chamber allowed for precise temperature control and rapid response time during the test period. The controls adjusted the heaters power until the average room dry bulb temperature was within ±0.1°F (±0.05°C) of the desired set point temperature.

For the wet tests, when the ambient conditions required maintaining high humidity levels, the air stream was humidified using an electric stream humidifier. Moisture was added in the bottom section of the conditioning loop by steam wands, shown as "Humidification Wand" in Figure 4.7. It is important to emphasize that the introduction of moisture in the ambient air was far away from the PITs, giving enough time for good mixing of the air stream and the water vapor in the under-floor air plenum before the resulting moist air stream reached the PITs. This strategy was critical because uniform ambient conditions must be generated around the PITs, in order to measure one value of thermal conductivity that was well representative of the entire insulation test specimen thermal conductivity.

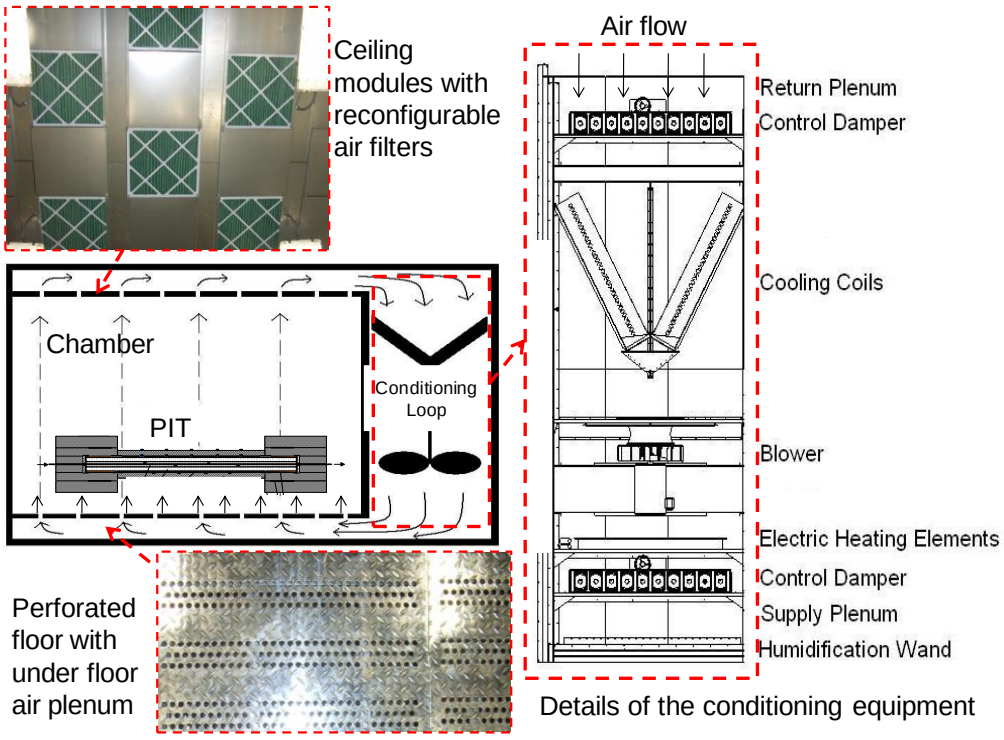

Figure 4.7: View of psychrometric chamber with details of the ceiling with reconfigurable air filters, of the perforated floor with under floor air plenum, and of the chamber conditioning equipment to create dry and wet conditions of the ambient air surrounding the PIT.

Two dry bulb and two wet bulb probes were used to measure the dry-bulb and wet-bulb temperatures of ambient air surrounding the PITs. The probes measured an average value of the ambient air via mechanical samples at various locations along the two sides of the PITs. The sampling tree of the dry/wet-bulb probe was made of plastic white PVC and is shown in Figure 4.8 on the left side next to the PIT. Four additional humidity sensors and six thermocouples were installed around the PIT to measure the local air humidity and local dry-bulb temperature, respectively. A panel of elastomeric rubber insulation was positioned directly underneath the pipe insulation test specimen as shown on the bottom of Figure 4.8. This configuration avoided direct impingement of the air on the bottom exterior surface of the insulation test specimen, which was positioned at about 33 in. (0.8 m) of elevation from the floor. Each PIT was supported from the two end side thermal guard sections by a wood frame, as shown in Figure 4.9. The measurements of the

air temperature and humidity at the various locations surrounding the PITs indicated uniform ambient conditions. The local ambient dry-bulb temperatures were typically within ±0.3°F (0.15°C) of the average room dry-bulb temperature and the local relative humidity measurements were typically within ±4% RH of the average relative humidity of the room.

Figure 4.8: View of Pipe Insulation Test apparatus (PIT) with indication of the local ambient dry-bulb temperature sensors and local relative humidity sensors

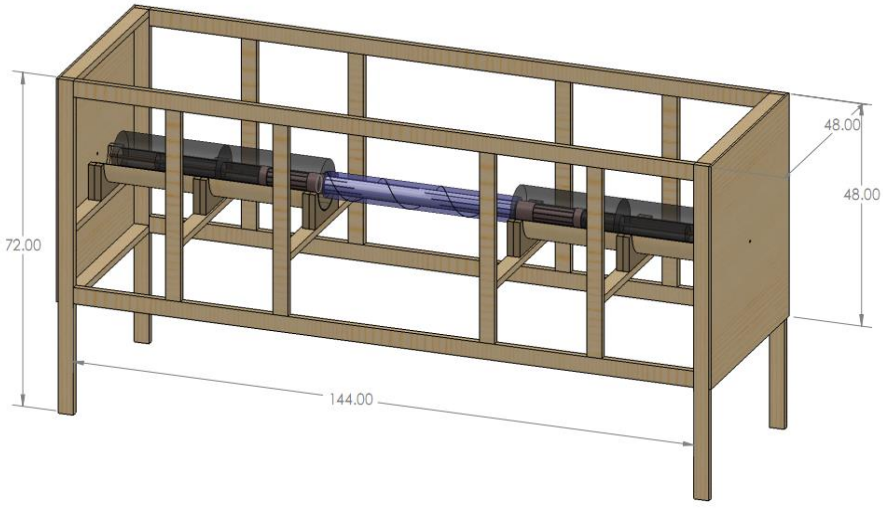

Figure 4.9: 3-D drawing of the PIT showing structural supports and wood frame (dimensions are in inches).

CHAPTER V

5 EXPERIMENTAL PROCEDURES AND DATA REDUCTION

In this chapter, the test procedures for the thermal conductivity measurements are summarized, and the data reduction is presented.

5.1 Experimental Test Conditions

Different types of pipe insulation systems with nominal wall thickness from 1 to 2 in. (25.4 to 50.8 mm) were investigated in dry tests. Dry conditions were achieved when the air dew point temperature was lower than the aluminum pipe surface temperature; thus avoiding the risk of condensation on the aluminum pipe surface. The thermal conductivity of the pipe insulation test specimen was measured for insulation mean temperature ranging from 57 to 73°F (14 to 23°C), that is, a cold surface side of 38 to 40°F (3.3 to 4.4°C) and a hot surface side from 75 to 107°F (24 to 42°C). The hot surface temperature was controlled by varying the ambient temperature of the surrounding air from 75 to 107°F (24 to 42°C). As described in previous chapter, over 50 temperature sensors were used to monitor the interior and exterior local surface temperatures of the pipe insulation test specimens. An example of the axial and angular temperature measurements is shown in Figure 5.1. It should be noted that the position of the thermocouples varies along a spiral path along the surface of the pipes. Pipe insulation surface temperatures were measured by 20 thermocouples positioned around the exterior surface of insulation specimen and following a similar spiral configuration. By blocking the air stream right below the test specimen with a panel of elastomeric rubber insulation, the temperature distribution of the pipe insulation exterior surface was within ±0.8°F (0.4°C) of the average temperature. The 20 thermocouples that were

installed along the longitudinal grooves on the aluminum pipe exterior surface measured local aluminum pipe surface temperatures that were within ±0.6°F (0.3°C) with respect to the average aluminum pipe surface temperature. The deviation was both for axial and angular directions, as shown in the central plot of Figure 5.1. With 6 thermocouples attached to the copper tube, the temperature variation in both axial and angular directions was within ±1.8°F (1°C) from the average copper pipe temperature, as shown in the bottom plot of the figure.

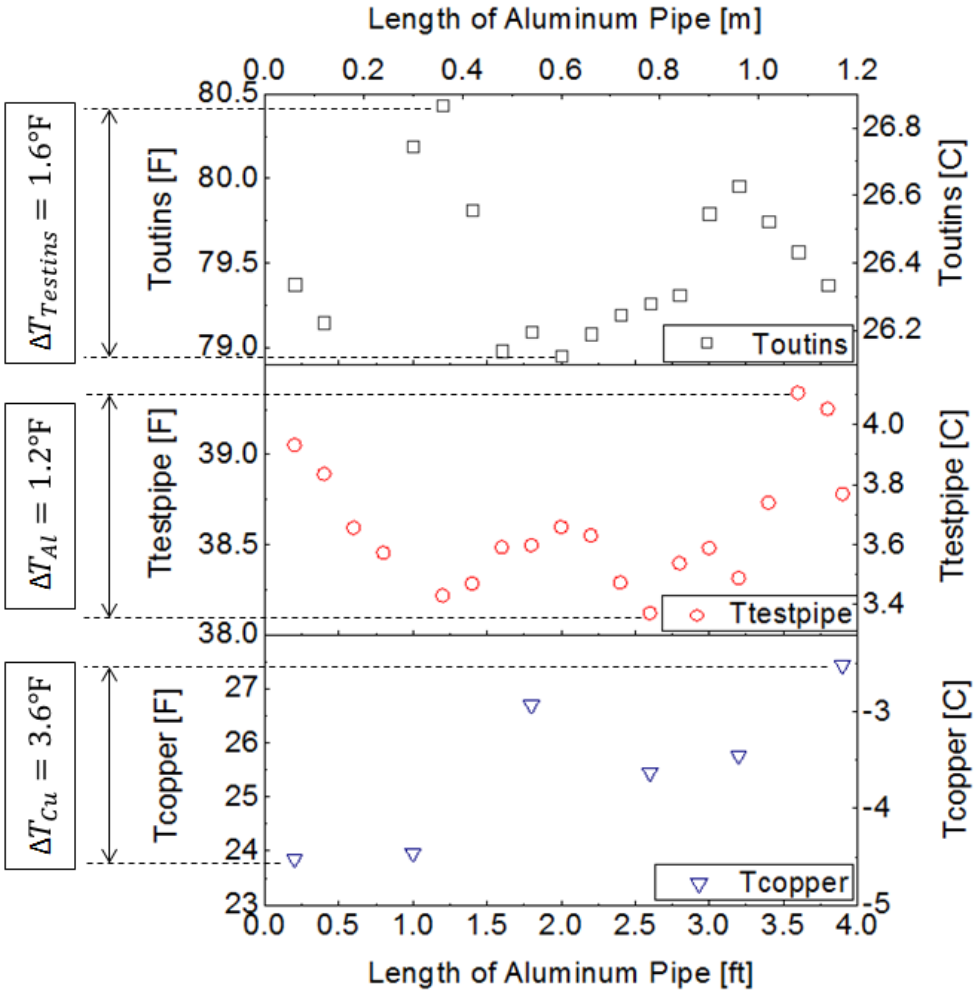

Figure 5.1: Example of surface temperature measurements during a dry test on cellular glass (note that thermocouples are positioned along the axial and angular directions that follow a spiral path along the pipe surface).

During the wet tests, the ambient was controlled at a high temperature and high humidity to accelerate the moisture ingress in the pipe insulation test specimens. The ambient temperature was controlled at 90°F (32.2°C), with average relative humidity adjusted at 83%. Under such conditions, the air dew point temperature was about 84°F (29°C), which was significantly higher than the aluminum pipe surface temperature. Figure 5.2 shows the surface temperature measurements on the first day of cellular glass pipe insulation during the wet test. The temperature distributions along the surfaces were quite similar to the dry test case and the discrepancy of all temperature sensors reading the pipe insulation exterior surface decreased by 0.1°F (0.17°C), that is, from $\Delta T_{test,ins}$ was 1.6°F in dry non-condensing conditions (see Figure 5.1) to $\Delta T_{test,ins}$ of 1.5°F for the first day of the wet test (see Figure 5.2). The temperature distribution on the surfaces after 60 days of exposure to humid ambient conditions for cellular glass pipe insulation is shown in Figure 5.3. The temperature profiles on the insulation specimen exterior surfaces were not as uniform as the ones measured for dry tests. This was due to local wet regions created by water condensate that accumulated around the joint sealant regions on the exterior surface of the pipe insulation test specimen. These wet regions were visually observed and documented during the wet tests using digital photos. As can be observed in Figure 5.3, $\Delta T_{test,ins}$ gradually increased from 1.5°F (0.8°C) at day 1 up to 2 °F (1.1°C) at day 60. It should be noted that a temperature difference might be due to local values of the temperature readings in which the water condensate droplets were adjacent to the thermocouple beads. Thermal bridges might have occurred due to local regions of wet insulation. The temperature readings were not uniform because the insulation material was not homogeneously wet along the axial and angular directions. Since 20 thermocouples were installed on the surface, the average surface temperature calculated from all temperature readings was still a good representation of the exterior temperature of the pipe insulation surface. With all 3D effects introduced for wet insulation conditions, the assumption of a 1-D heat transfer model is an approximate approach that was simple but accurate

enough to be useful in practice. The thermal conductivity value calculated in wet conditions was representative of the average conductance of heat across the pipe insulation test specimen in wet conditions with moisture accumulated (non-uniformly) on the insulation system.

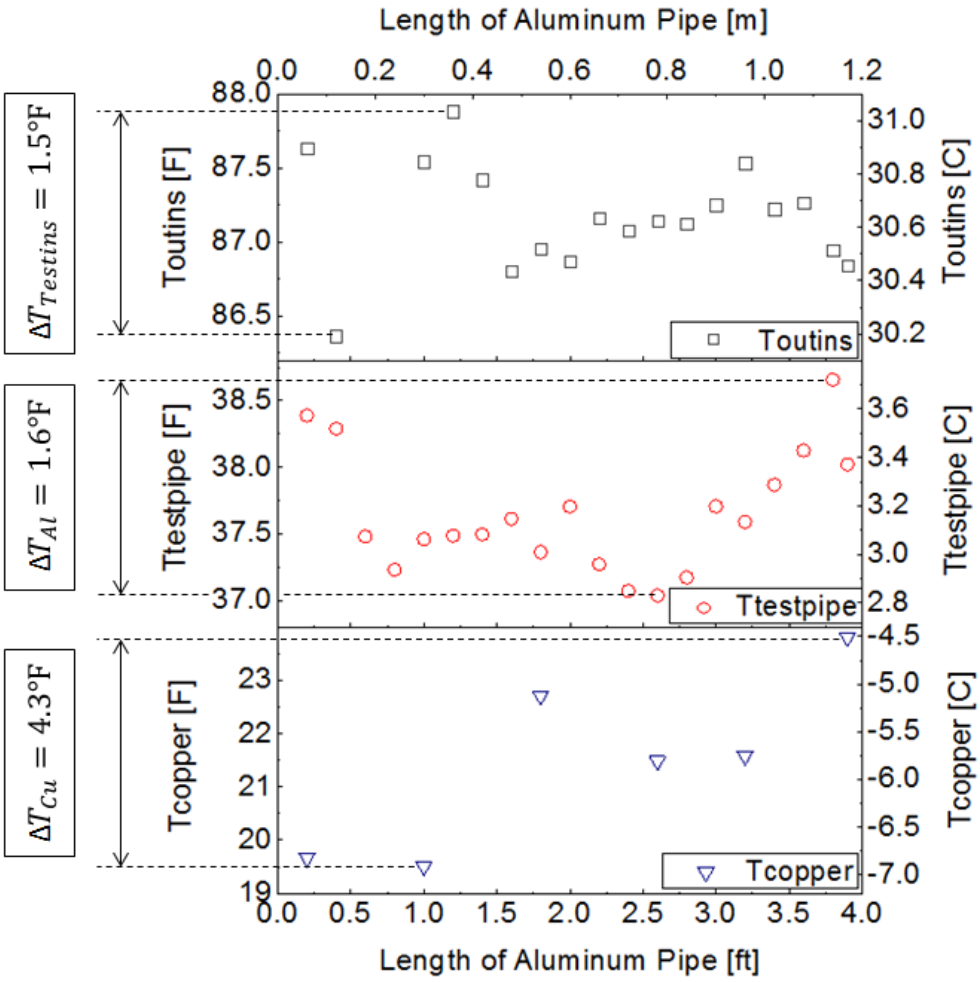

Figure 5.2: Example of surface temperature measurements on the 1st day of cellular glass wet test (note that thermocouples are positioned along the axial and angular directions that follow a spiral path along the pipe surface).

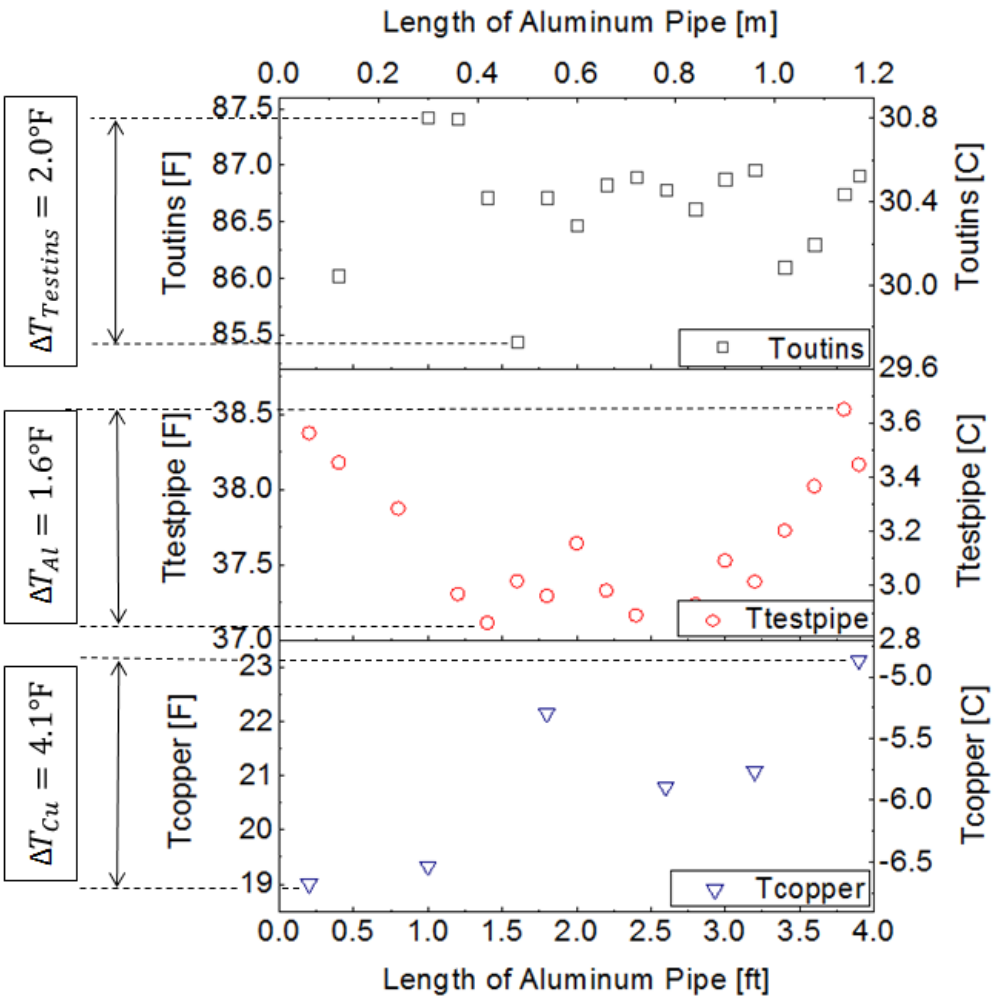

Figure 5.3: Example of surface temperature measurements on the 60th day of cellular glass wet test (note that thermocouples are positioned along the axial and angular directions that follow a spiral path along the pipe surface).

5.2 Experimental Procedures

5.2.1 Experimental Procedures for Calibration Test

For both tests under dry non-condensing and wet conditions, calibration was required for determining the effective thermal conductivity of the sand. Although the sand was completely sealed in the plastic bag, with two plugs tightly blocked at the ends of the test pipe, a calibration test was necessary to detect any potential moisture intrusion into the aluminum pipe from the small cracks of the seals between plugs and metal pipe surfaces, if present. The calibration served for correcting any potential variation of the sand thermal conductivity due to moisture accumulation.

During the calibration, two tape electric heaters were installed on the surface of the aluminum pipes and they were controlled by a variable transformer. A watt transducer was used to measure the power to the electric heaters. A large volume of rubber foam insulation was applied around the heaters to limit the heat gains from the ambient. From preliminary tests, it was found that thermocouple readings were quite sensitive to the power of the tape heaters due to the electric interferences from the direct contact of the electric tape heater with the aluminum pipe surface. Therefore, a layer of wax paper was tightly wrapped around the aluminum pipe and underneath the tape heaters to provide an extra layer of electrical insulation. Another layer of thin film aluminum foil was tightly installed on the top of the tape heaters, in order to distribute the heat from the electric heater to the aluminum pipe and avoid local hot spots that could potentially damage the thermocouple wires. The entire aluminum pipe and corresponding thermocouples were electrically grounded to reduce electric noise.

5.2.2 Experimental Procedures for Dry Non-Condensing Tests

The steps for the experimental procedure are shown in the flow chart provided in Figure 5.4. By following this procedure, each PIT can be used for thermal conductivity measurement if needed.

This means two pipe insulation systems can be tested at the same time in dry conditions. Before each dry test, a calibration test was conducted to determine the initial relation between the sand thermal conductivity and the sand average temperature and the exterior temperature difference between the ambient and the cold pipe surface, $k'_{sand} = f(T,\Delta T)$. For example, f was a polynomial curve fit function of the 2nd order. After the calibration test, the dry test started and then it was followed by the wet test. At the end of the wet test, a second calibration test was conducted for checking the sand thermal conductivity. A new correlation from the second calibration was obtained, for example $k''_{sand} = g(T,\Delta T)$, where g was another polynomial curve fit function of the 2nd order. It should be noticed that f and g were not necessarily the same. Assuming the sand thermal conductivity varied linearly with time between beginning and end of the test, the revised values of $k_{sand,j}$ on each day of the test was found by interpolation from the two sets of data of the beginning and of the end of the test. For example, according to the temperature profile recorded on the j^{th} day, the sand thermal conductivity was computed as $k'_{sand,j}$ by applying the correlation $f(T,\Delta T)$, which was developed from the initial calibration. With the same temperature profile, but applying the other correlation, $g(T,\Delta T)$, from the second calibration test, the sand thermal conductivity was $k''_{sand,j}$. Therefore, on day j^{th}, the corrected sand thermal conductivity $k_{sand,j}$ that was used for the radial heat flux meter was calculated as follows:

$$k_{sand,j} = k'_{sand,j} + \frac{j}{m}(k''_{sand,j} - k'_{sand,j}) \tag{5.1}$$

where m is the total time (in day) of the test period, j is the actual time (in day) during the test period, Table 5-1 below gives an example of how j was calculated for one test period.

Table 5-1: Example of how the j was calculated during the test period

Actual time during the test period j [day]	Actual time during the test period j [hour]	Status of test period
0.0	0	First test of dry tests series
0.3	7.2	Second test of dry tests series
0.5	12	Third test of dry tests series
⋮	⋮	⋮
n	⋮	Last test of the dry tests series
n+k	⋮	First test of the wet tests series
n+k+0.2	⋮	Second test of wet tests series
n+k+0.5	⋮	Third test of wet tests series
⋮	⋮	⋮
m	⋮	Last test of wet tests series

j varied gradually from 0 to n, where n was the number of days it took to complete the dry test. Then j increased gradually from n+k to m, where m was the total number of days of the test and it included both the days for dry tests and the days for completing the wet tests. For example, m=60 days for the cellular glass pipe insulation system while m = 68.85 for the fiberglass system FG7. The parameter k accounted for the fact that it took few hours to start the wet test and achieve thermal equilibrium and steady state conditions after a dry test was completed. This period was also required for setting and verification of the equipment and for taking few additional dry tests of the test insulation specimen. The aluminum pipe temperature was set to in the neighborhood of 38°F, that is, at 38°F-1°F (37°F) and to 38°F+1°F (39°F), while the ambient temperature was set to 90°F (32.2°C). Dry thermal conductivity values were measured to develop baseline data of thermal conductivity in dry conditions. These data were used as benchmark for the thermal conductivity in wet conditions when the aluminum pipe temperature varied from 37 to 39°F.

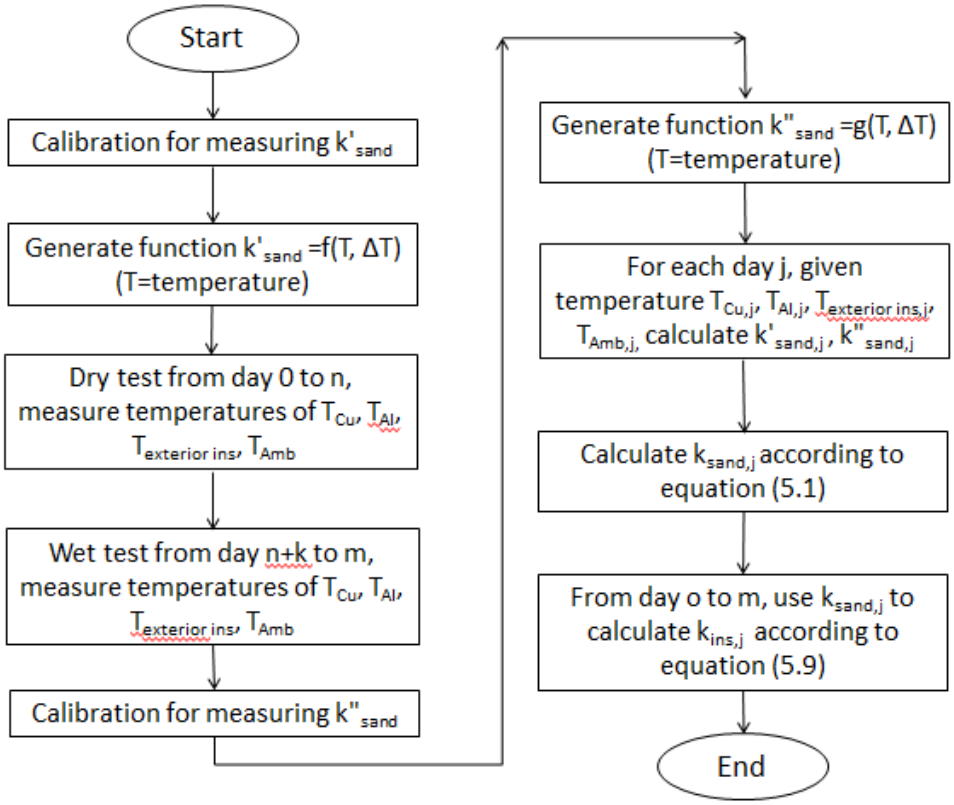

Figure 5.4: Algorithm for calculating the thermal conductivity of pipe insulation systems.

The apparent thermal conductivity of the pipe insulation system measured in both dry and wet conditions was updated by using the corrected sand thermal conductivity, $k_{sand,j}$, shown in equation (5.1). By following this procedure, the variation on the sand thermal conductivity due to any potential moisture ingress into the sand was considered in the data reduction for the insulation test specimen thermal conductivity. Table 5-2 provides an example of the calculation procedure for the system FG7, and it reports the corrected thermal conductivity of the sand filling the annulus region between the copper pipe and the aluminum pipe and apparent thermal conductivity of the insulation test specimen for entire period of the dry and wet tests. The other systems are reported in similar tables in the Appendix C.

Table 5-2: Example of the corrected sand thermal conductivity, $k_{san,j}$ (see eq. (5.1)), and apparent insulation system thermal conductivity, $k_{ins,j}$, calculated during the dry and wet test period for the pipe insulation system FG7

Actual time during the test period j [day]	Actual time during the test period j [hour]	Status of test period	$k_{sand,j}$ [Btu-in/hr-ft^2-°F]	$k_{ins,j}$ [Btu-in/hr-ft^2-°F]
0.0	0	First test of dry tests	3.2230	0.2597
0.13	3.12	Second test of dry tests	3.2115	0.2593
0.17	4.08	Third test of dry tests	3.2024	0.2590
⋮	⋮	⋮	⋮	⋮
3.60	86.40	Last test of dry tests	3.1681	0.2687
4.73	113.52	First test of wet tests	3.1897	0.2665
4.44	106.56	Second test of wet tests	3.1870	0.2611
4.51	108.24	Third test of wet tests	3.1893	0.2716
⋮	⋮	⋮	⋮	⋮
68.85	1652.4	Last test of wet tests	3.0634	0.3002

5.2.3 Experimental Procedures for Wet-condensing Test with Moisture Ingress

In the wet tests, when recommended by the manufacturer, joint sealant was applied on the longitudinal joints to glue the bottom and top C-shells together. The joint sealant was applied at the cross sectional ends of the pipe insulation system to prevent water vapor diffusion from the end sections. It should be noted that throughout the report the terminology "apparent thermal conductivity or simply thermal conductivity of the pipe insulation system" refers to the coefficient k_{ins} that is or can be used in the following Equation (5.2).

$$Q_{ins} = \frac{2\pi \cdot k_{ins} \cdot L \cdot (T_{\text{exterior surface pipe insulation}} - T_{\text{exterior surface Al pipe}})}{\ln \frac{D_{\text{exterior,pipe insulation}}}{D_{\text{Al pipe}}}} \qquad (\mathbf{5.2})$$

where L is the length of the center section of the pipe insulation test specimen installed on the PIT, that is, 36 in. (3ft. or 0.9m) across the center line of pipe insulation system. $D_{exterior,\ pipe\ insulation}$ is the actual measured diameter of the exterior surface of the pipe insulation system in inches (or

mm). $D_{Al\ pipe}$ is 3.5 in. (88.9mm). $T_{exterior\ surface\ pipe\ insulation}$ is the spatial average measured temperature of the exterior surface of the mechanical pipe insulation system in °F (or °C). $T_{exterior\ surface\ Al\ pipe}$ is the average spatial measured temperature of the aluminum pipe in °F (or °C). Q_{ins} is the heat transfer rate in Btu/hr or Watts across the 3ft. long center section of the pipe insulation test specimen. This coefficient k_{ins} accounts for insulation material thermal conductivity, vapor retarder thermal conductivity (when present), joint sealant thermal conductivity, joint sealant thickness, and air thermal conductivity (if present), since small gaps of air might have been present in some cases in between the inner surface of the pipe insulation and the outer surface of the aluminum pipe. The pipe insulation system is a 3D geometry consisting of multiple C-shells of finite length and joints together. Its thermal conductivity is an average lumped value that differs from the thermal conductivity of the insulation material. In other words, the pipe insulation thermal conductivity reported throughout the next sections combines all geometric effects, edge effects, and material effects into one representative value for the conductance of the heat across the radial direction of the pipe insulation system.

Before each wet test, it was critical to determine an initial reference point for the thermal conductivity of the pipe insulation system. Similar cylindrical insulation systems might not have the same thermal conductivity, even if taken from the same material bun. Location in the bun, transportation, storage, and actual installation might have an effect on the actual thermal conductivity of the pipe insulation system. To eliminate these effects, the pipe insulation system was installed on the PIT and its thermal conductivity was measured in dry conditions first. The time for the experiments to determine the reference points of the pipe insulation system thermal conductivity was part of the time n, as mentioned in Table 5-1.

A vapor repellent sealant was applied at two end sides of the pipe insulation test specimen, which were in contact with the end thermal guards. At the same time, a second test specimen of the same insulation material batch was cut into six cylindrical sections. Each section was about 6 in.

(152.4mm) long. Then, the sections were mounted to the second PIT and they served to measure the moisture content accumulating on the pipe insulation test specimen during the wet test period. Figure 5.5 shows an example of the schematic of the PITs with vapor retarder jacket systems and joint sealant. Each of the 6 in. samples was removed at regular time intervals from the second PIT and replaced with a dry 6 in. section of the same insulation material. Each sample was weighed, conditioned in an oven, and weighed again to obtain the amount of water mass accumulated in the insulation sample. The amount of water mass accumulated in the sample was obtained as the mass difference between the wet sample and the dry sample. At the end of the wet test period, the last 6 in. long sample on the second PIT was removed at the same time in which the entire test specimen on the first PIT was removed. We postulated that similar moisture ingress occurred in the two test specimens during the wet test. Since the insulation test specimens were identical and were exposed to similar thermal and humidity boundary conditions, the above assumption seemed reasonable. The only difference was that each 6-in. long section was a small replica of the test specimen installed on the 1st PIT. This means that the longitudinal and end joints and sealant of the test specimen installed on the 1st PIT were also replicated for each small section installed on the 2nd PIT.

The moisture content of the insulation test specimen installed on the 1st PIT was directly measured only at the beginning and at the end of the wet test period. The rate of moisture absorption in the pipe insulation test specimen was obtained by data regression of the moisture content measurements obtained from the samples removed at regular time intervals from the second PIT. The order that the small sections of insulation were taken out from the insulation test sample mounted on the 2nd PIT, was the same for all the systems tested in wet conditions. This order is shown in Figure 5.6. The water mass accumulated on the insulation was measured by using the difference in weight of the test specimen in wet conditions with respect to dry insulation.

This weight difference represented the moisture mass accumulated in the insulation during the period of exposure to the wet ambient conditions.

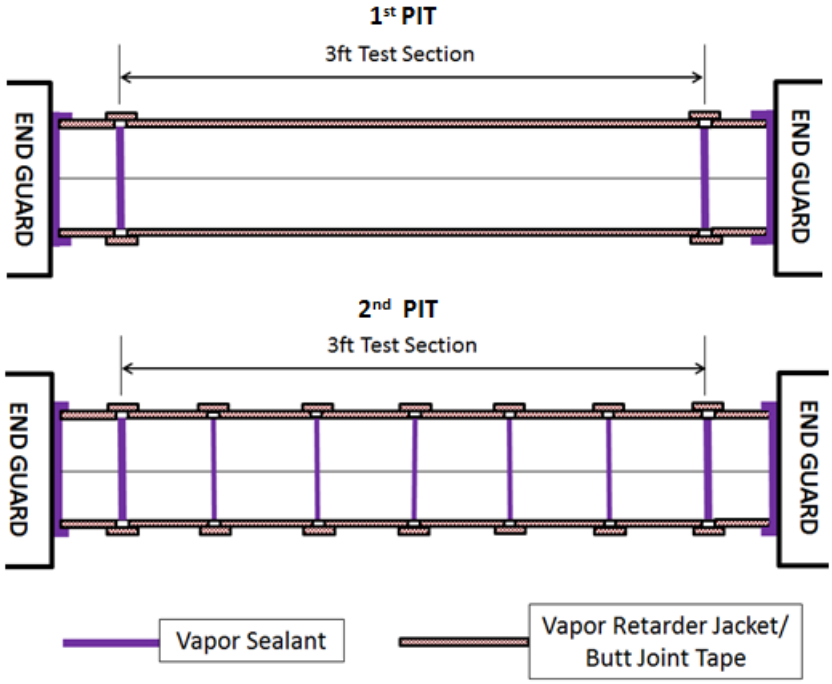

Figure 5.5: Schematic showing the preparation of the insulation test specimens for the wet test.

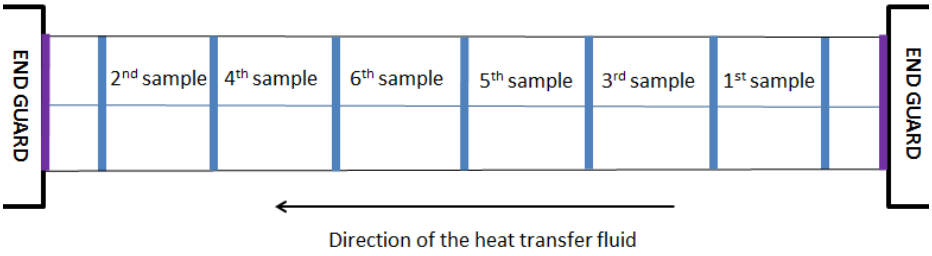

Figure 5.6: schematic showing the order that the 6-in test insulation samples were taken on the 2nd PIT

For some types of pipe insulation, like cellular glass and PIR, joint sealant was recommended to glue two C-shells together along the longitudinal joints. A procedure to remove the vapor sealant by cutting a piece of insulation out of the test specimen taken from the second PIT is shown in Figure 5.7. The insulation sample, without any vapor sealant, was placed in an electric oven at a

temperature ranging from 170 to 250 °F (77 to 121 °C) for at least 8 hours. The time and temperature of the drying process varied with moisture content and types of insulation. Usually for highly permeable materials, such as fiberglass, the drying process for the entire pipe insulation test specimen was up to three days. Each insulation sample was conditioned in the oven for a period long enough such that its weight did not change in between two consecutive weight measurements. Each weight measurement took place in ambient room temperature every 12 to 24 hours. If two consecutive weight measurements of the same sample were within 0.0022 lb_m (1 gram), then the insulation sample was considered to have achieved dry conditions. The final weight measurement after the drying process was assumed to be the weight of the dry insulation test specimen. The total amount of water mass accumulated in the insulation sample during wet operating conditions was determined from the difference between the wet weight of the sample and the dry weight of the insulation sample.

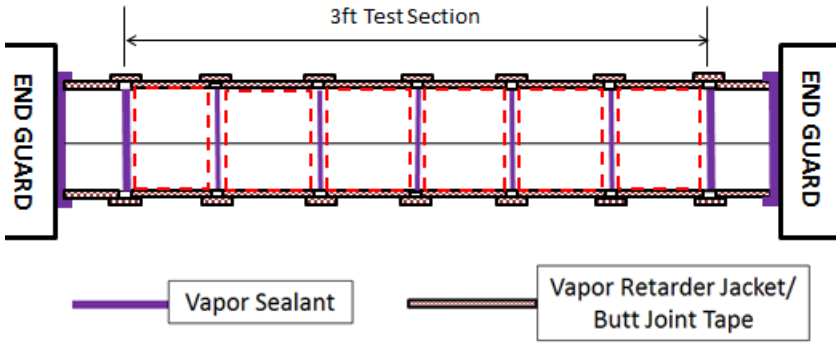

Figure 5.7: Schematic showing the insulation cuts for collecting insulation material without any vapor sealant and adhesive before drying process.

The thermal conductivity of the pipe insulation system in dry condition was measured in about 1 week, for at least four pipe insulation mean temperatures. This provided a baseline for the thermal conductivity of the specific pipe insulation test specimen. Then, the dry-bulb temperature was set to 90°F (or in some cases 78°F, 107°F) and the humidity in the chamber was raised gradually until 83% R.H. (or in some cases 55%R.H., 81%R.H.) in about 12 to 24 hours.

5.3 Data Reduction

5.3.1 Calibration of the PIT

Calibration was conducted before each dry test to determine the actual thermal conductivity of the sand that filled in the 3-in. (76.2 mm) NPS aluminum pipe. The cross section of the radial flux meter that used in the calibration test is shown in Figure 5.8.

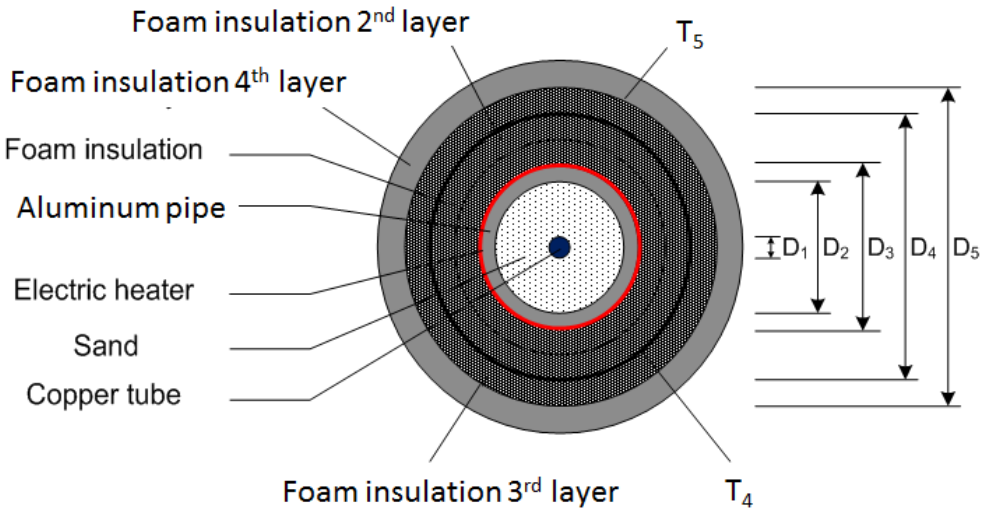

D_1: $D_{copper\ pipe}$ D_2: $D_{interior,Al\ pipe}$ D_3: $D_{exterior,Al,pipe}$ D_4: $D_{exterior,\ layer\ 2}$ D_5: $D_{exterior,\ layer\ 3}$

T_4: $T_{exterior,\ layer2}$ T_5: $T_{exterior,\ layer3}$

Figure 5.8: schematic of the radial cross section with electric heaters installed during the calibration phase of the PIT.

When the electric heater was energized, the total heat transfer into the aluminum pipe, $Q_{Al,pipe}$, was estimated by considering both the electric power in the tape resistor heater, Q_{heater}, and a small amount of heat transfer leaking in from the surrounding ambient through the foam rubber insulation layer and from the end sections of the test apparatus due to axial heat conduction, $Q_{Al,pipe}$, as given in equation (5.3):

$$\mathbf{Q_{Al,pipe} = Q_{heater} + Q_{leak,in}} \quad (5.3)$$

where $Q_{Al,pipe}$ is the total heat transfer rate into the aluminum pipe; Q_{heater} is the heating capacity measured by the watt transducer; $Q_{leak,in}$ is the heat transfer rate leaking in from the environment.

The control volume was selected as shown in Figure 5.8. $Q_{leak,in}$ is estimated by using the following expression for conduction heat transfer in a cylindrical insulation material, as shown in Equation (5.4).

$$\mathbf{Q_{leak,in} = \frac{2\pi k_{foam} L(T_5 - T_4)}{\ln \frac{D_5}{D_4}}} \quad (5.4)$$

where k_{foam} is the estimated thermal conductivity of outside rubber foam insulation; $D_{exterior,\ layer3}$ is the exterior diameter of the 3rd foam insulation layer (see Figure 5.8); $D_{exterior,\ layer2}$ is the exterior diameter of the 2nd foam insulation layer (see Figure 5.8); L is the length of test section; T_5 is the exterior surface temperature of the 3rd foam insulation layer; T_4 is the exterior surface temperature of the 2nd foam insulation layer (see Figure 5.8).

During the calibration of the PIT the ambient temperature was adjusted such that the temperature difference across the insulation on the outside of the electric heater was within 5.4°F (3°C). This caused $Q_{leak,in}$ to vary from 3.5 to 4.2 Btu/hr (1.0 to 1.2 W), which represent 7 to 10 percent of the total heat measured from the heater. $Q_{leak,in}$ was accounted for during the calibration procedures to eliminate a systematic error on the actual thermal conductivity of the sand filling the aluminum pipe. It should be noted that according to equation (5.4), $Q_{leak,in}$ is highly dependent on the ambient conditions. When the test condition is controlled at a higher temperature, the temperature difference between the exterior surface of the pipe insulation and the aluminum pipe increases, and $Q_{leak,in}$ weights more in Q_{sand}, when compared to the low temperature condition. In order to include the impact from the variation on the boundary conditions, the calibration phase was required at two different ambient temperatures of 56˚F (13.3˚C) and 90˚F (32.2˚C). For each of

the ambient conditions, k_{foam} was estimated from Wilkes' correlation (Wilkes et al. (2002)) of elastomeric rubber flat slab insulation, as in equation (5.5), for calculating the apparent thermal conductivity of the elastomeric rubber insulation we used for calibration procedures. This allows us to estimate the amount of heat flux leaking into the pipe insulation from the ambient conditions during the calibration phase. Since the electric tape heaters were energized, the local temperature of the insulation foam was close to ambient temperature. When applying equation (5.5) to calculate the foam insulation thermal conductivity, it was assumed that for each of the ambient condition, the outer surface elastomeric rubber insulation mean temperature was the same as the ambient temperature.

$$\boldsymbol{\lambda = 0.000133T + 0.03684} \qquad (5.5)$$

where $\boldsymbol{\lambda}$ is the apparent thermal conductivity in W/m-K, T is the insulation mean temperature in °C, which equals to the ambient temperature.

It should be emphasized that the actual thermal conductivity of the sand inside the aluminum pipe was slightly different than the thermal conductivity of pure dry sand because the measured values during the calibration procedure accounted for the end effects of the thermal guards, the contribution due to small axial heat flow, and the effects due to the non-uniformity and non-homogenous properties of the sand inside the aluminum pipe. The thermal conductivity of the sand also depended on the percent of quartz and residual moisture in the sand batch used for filling the pipe. Calibration of the PIT at the same thermal conditions, as that of the actual experiments, allowed estimating a value of the sand thermal conductivity that can be used during the dry and wet tests to calculate the radial heat flux. The sand thermal resistance and the axial heat conduction effects of the PIT were approximated as an equivalent sand thermal conductivity that could be used in a 1-D valid heat conduction equation following Fourier's law. By applying the energy balance on the aluminum pipe surface, there is:

$$\mathbf{Q_{Al,pipe} = Q_{sand}} \tag{5.6}$$

where Q_{sand} represents the heat transfer rate into the sand filling the aluminum pipe

The axial temperature gradient along the aluminum pipe was less than 0.43% of the radial temperature gradient across the sand. Based on this finding it was reasonable to assume that the axial heat losses on the aluminum pipe were small and a heat balance across the sand yields

$$\mathbf{Q_{sand} = \frac{2\pi k_{sand} L(T_{Al\ pipe} - T_{copper\ pipe})}{\ln \frac{D_{interior,Al\ pipe}}{D_{copper\ pipe}}}} \tag{5.7}$$

where k_{sand} is the effective thermal conductivity of sand; $D_{interior,Al,pipe}$ is the inside diameter of test pipe (Figure 5.8); $D_{copper\ pipe}$ is the diameter of copper tube (Figure 5.8); $T_{copper\ pipe}$ is the surface temperature of copper tube; $T_{,Al,pipe}$ is the surface temperature of the aluminum pipe.

The average sand temperature is

$$\mathbf{T_{sand} = \frac{T_{copper\ pipe} + T_{Al\ pipe}}{2}} \tag{5.8}$$

By measuring the power of the electric heater and the temperatures, the thermal conductivity of the sand inside the aluminum pipe was obtained using equations (5.1) to (5.7).

Two correlations between sand thermal conductivity and average sand temperatures were derived from the measurements under these two ambient conditions in the calibration phase. With interpolation between these curves, the sand thermal conductivity was developed as a second power curve fit to both the average sand temperature and the exterior temperature difference between the ambient and the aluminum pipe, shown in Equation (5.9). This correlation included the impact of the variation on the boundary conditions on the average sand thermal resistance inside the PIT.

$$\mathbf{k_{sand} = b_1 T_{sand}^2 + b_2 T_{sand} + b_3 \Delta T_{exterior}^2 + b_4 \Delta T_{exterior} + b_5} \quad (5.9)$$

where b_1 to b_5 are empirical coefficients, $\Delta T_{exterior}$ represents the temperature difference between the ambient and the aluminum pipe in °C, while sand thermal conductivity k_{sand} is in W/m-K.

5.3.2 Pipe Insulation Thermal Conductivity Measurements

Once the thermal conductivity of the sand filling the aluminum pipe, $k_{sand,j}$, was obtained from the calibration procedure, a 1-D heat balance equation along the radial direction was applied to the PIT, as shown in the schematic of Figure 5.9. As a result, the pipe insulation thermal conductivity, $k_{ins,j}$, was determined directly by the following expression (5.10):

$$\mathbf{k_{ins,j} = k_{sand,j} \times \frac{(T_{exterior\ Al\ pipe,j} - T_{copper\ pipe,j})}{(T_{exterior\ ins,j} - T_{exterior\ Al\ pipe,j})} \times G_f} \quad (5.10)$$

where G_f is a geometry factor that depends on the ratios of pipe insulation exterior diameter, the aluminum pipe outer diameter, and refrigerating copper tube outer diameters, as shown in Figure 5.9, The diameters of the pipe insulation were measured according to the standard ASTM C585 (ASTM, 2009).

The average temperature of the test insulation specimen was calculated from the measurements of the surface temperature sensors as follows:

$$\mathbf{T_{ave\ ins,j} = \frac{T_{extrior\ Al\ pipe,j} + T_{exterior\ ins,j}}{2}} \quad (5.11)$$

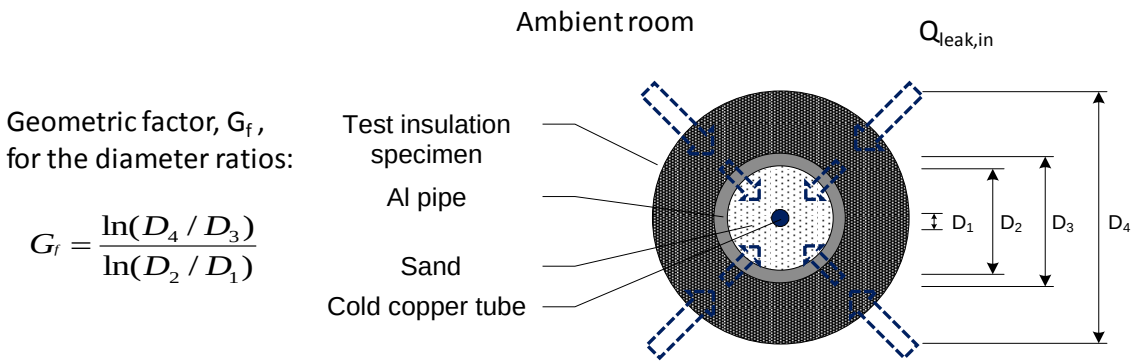

Figure 5.9: Schematic of the 1-D model of the Pipe Insulation Tester (PIT) and corresponding diameters.

5.3.3 Moisture Content Measurements in the Pipe Insulation System

The moisture content in the pipe insulation systems during the wet tests was calculated as percentage of the water volume per unit volume of pipe insulation. Moisture mass was measured from the weight difference of the samples in wet and dry conditions. Then the water mass was divided by a reference density of water, which was assumed constant at 62.4 lbm/ft^3 (1000 kg/m^3) (at 39.2°F/ 4°C). The volume of pipe insulation system was measured from its actual geometry. The overall expression for moisture content is as follows:

$$\mathbf{V_{moisture}}(\%) = \frac{(\mathbf{m_{wet,specimen}} - \mathbf{m_{dry,specimen}})}{\boldsymbol{\rho}_{\mathbf{water}}} \cdot \frac{\mathbf{1}}{\mathbf{V_{specimen}}} \times \mathbf{100} \cdot \qquad (5.12)$$

where $V_{moisture}$ is the volume of water present in the insulation system; $V_{specimen}$ is the volume of the insulation system; $m_{wet,specimen}$ is the weight of the wet insulation system; $m_{dry,specimen}$ is the weight of the dry insulation system after being dried in the oven; ρ_{water} is the water density at 39.2 °F (4 °C).

5.4 Experimental Uncertainty

5.4.1 Uncertainty on the Thermal Conductivity

A complete uncertainty analysis was conducted by using EES, Engineering Equation Solver, (Klein, 2006), and the experimental data for the axial and radial temperature measurements were used as input to the uncertainty propagation table of EES. The uncertainty on the apparent thermal conductivity was estimated according to the Taylor series expansion method as follows (Taylor, 1997):

$$\mathbf{U_Y} = \sqrt{\sum_{\mathbf{i}} \left(\frac{\partial \mathbf{Y}}{\partial \mathbf{X_i}}\right)^2 \mathbf{U_{Xi}^2}} \tag{5.13}$$

where U_Y represents the uncertainty of the variable Y and U_X represents the precision accuracy of the measured variable X. The uncertainty on the pipe insulation thermal conductivity was calculated following a similar approach and it resulted as in equation (5.14):

$$\begin{aligned} \mathbf{U_{k_{ins}}^2} = &\left(\frac{\partial \mathbf{k_{ins}}}{\partial \mathbf{k_{sand}}}\right)^2 \mathbf{U_{k_{sand}}^2} + \left(\frac{\partial \mathbf{k_{ins}}}{\partial \mathbf{k_{Al,pipe}}}\right)^2 \mathbf{U_{T_{Al\ pipe}}^2} \\ &+ \left(\frac{\partial \mathbf{k_{ins}}}{\partial \mathbf{k_{cold,copper,pipe}}}\right)^2 \mathbf{U_{T_{cold,copper,pipe}}^2} \\ &+ \left(\frac{\partial \mathbf{k_{ins}}}{\partial \mathbf{k_{exterior,ins,specimen}}}\right)^2 \mathbf{U_{T_{exterior,ins,specimen}}^2} + \left(\frac{\partial \mathbf{k_{ins}}}{\partial \mathbf{G_f}}\right)^2 \mathbf{U_{G_f}^2} \end{aligned} \tag{5.14}$$

where each term in parenthesis represents the coefficient of sensitivity for the variable of interest (X_i) and the U_{Xi} on the right hand side of equation (5.13) are the uncertainty associated with the variable X_i. The uncertainty on the thermal conductivity depended on the thermocouple accuracy and on the time averaged spatial uniformity of the temperatures along the axial and angular directions of the PIT device. All temperature sensors were calibrated in-situ and the bias

uncertainty was computed according to the approach provided by Johnson et al. (1998) and summarized below:

$$\mathbf{B_{Tdistribution}} = (\mathbf{T_{max}} - \mathbf{T_{min}}) / \mathbf{N} \quad (5.15)$$

$$\mathbf{B_T} = \sqrt{\mathbf{B^2_{Tdistribution}} - \mathbf{B^2_{Tuniform}}} \quad (5.16)$$

where $B_{Tdistribution}$ is the bias uncertainty resulting from the actual non-uniform temperature distribution, $B_{Tuniform}$ is the bias uncertainty present even with a uniform temperature distribution and it was estimated from equation (5.15) with T_{max} and T_{min} set as the acceptable limits for ideal condition of uniform surface temperature, B_T is the total bias uncertainty, and N is the total number of measuring points on the surface.

Accuracy and precision of the sensors used during the measurements are given in Table 5-3. The uncertainties on the effective thermal conductivity of sand and the apparent thermal conductivity of the test specimen were plotted with radial heat flux, shown in Figure 5.10.

It was observed that in both cases the uncertainty on the effective thermal conductivity of the sand filling the aluminum pipe was the main factor affecting the uncertainty of the pipe insulation thermal conductivity. The two uncertainties followed similar trends with the latter being amplified by the accuracy of the temperature measurements. Because of an improved calibration of the temperature sensors at low heat flux, as shown in Table 5-3, the uncertainty in the present work was reduced, especially in the low heat flux range. In the current test apparatus, when the radial heat flux was larger than 10.4 Btu/hr-ft (10 W/m) it was estimated that the experimental uncertainty on the pipe insulation thermal conductivity was about ±5 % and the uncertainty of the sand thermal conductivity was within ±4%, as shown in Figure 5.10. With the temperature boundary conditions of the aluminum pipe surface temperature at 38°F (3.3°C) and room temperature between 56 to 90˚F (13.3 to 32.2˚C), the PITs measured the pipe insulation thermal

conductivity with heat flux as low as 8.2 Btu/hr-ft (7.9 W/m). In wet conditions, the radial heat flux through pipe insulation systems was often in the range of 10.4 Btu/hr (10 W/m), or higher. It should be noted that the uncertainty increased when the heat flow was below 8.2 Btu/hr-ft (7.9 W/m). This limitation was due to the fact that the measured heat transfer from the tape heaters during the PIT calibration phase became too small and in particular was below 1% of range of the watt transducer used to measure the power in input to the electric heaters. In these conditions the uncertainty of the heat flux measurements increased drastically. In the low range of the electric heater, the heat gain from the ambient into the sand became a higher fraction of the total heat gain, and the uncertainty on the heat gain from the ambient became a significant contributor to the overall experimental uncertainty of the sand thermal conductivity.

Table 5-3: Accuracy and maximum spatial variation of the temperature measurements of the PIT

Parameter	**Manufacturer**	**Model**	**Accuracy**	**Max Spatial Variation**	**Uncertainty**
Foam insulation thermal conductivity	Armacell	Armaflex	± 10%		± 10%
Watt transducer	Flex-Core	AGW-001E	± 0.04% F.S. (± 0.2W)		± 0.04% F.S. (± 0.2W)
Thermocouples (copper tube)	Omega	T-type	± 0.14 °F (± 0.08 °C)	± 1.8 °F (± 1.0 °C)	± 0.33 °F (± 0.18 °C)
Thermocouples (aluminum pipe)	Omega	T-type	± 0.11 °F (± 0.06 °C)	± 1.1°F (± 0.6 °C)	± 0.14 °F (± 0.08 °C)
Thermocouples (insulation and ambient)	Omega	T-type	± 0.14 °F (± 0.08 °C)	± 1.3 °F (± 0.7 °C)	± 0.18 °F (± 0.10 °C)
Diameter (copper pipe)	N/A	N/A	± 0.010 in (± 0.254 mm)	N/A	± 0.010 in (± 0.254 mm)
Diameter (aluminum pipe)	N/A	N/A	± 0.015 in (± 0.381 mm)	N/A	± 0.015 in (± 0.381 mm)
Diameter (pipe insulation)	N/A	N/A	± 0.0625 in (± 1.6 mm)	N/A	± 0.0625 in (± 1.6 mm)

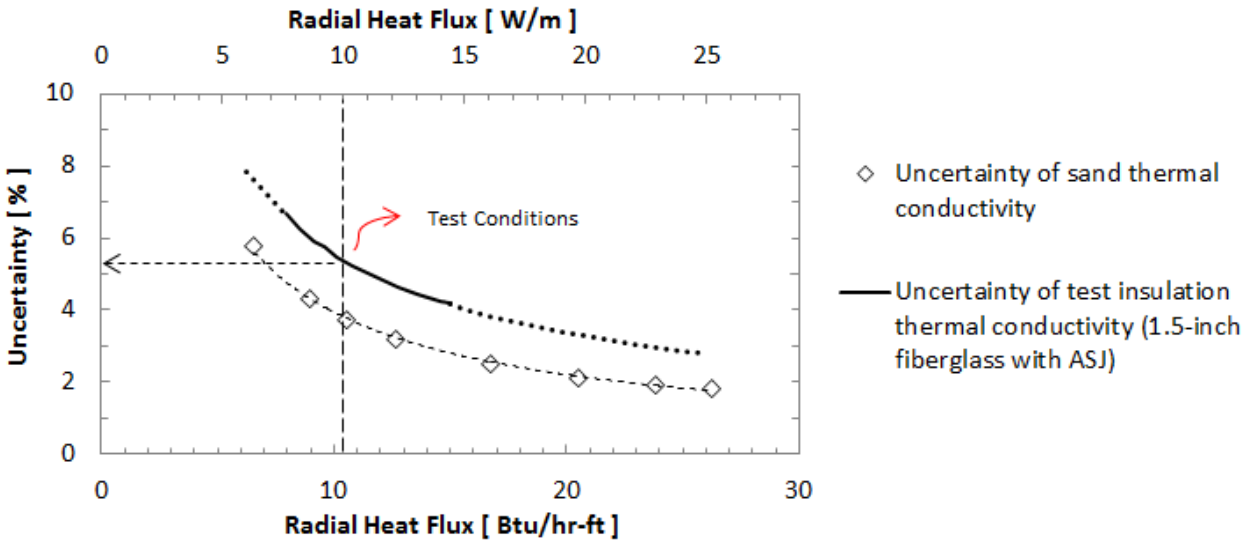

Figure 5.10: Uncertainties of the sand thermal conductivity and of the pipe insulation thermal conductivity versus radial heat flux per unit length (data from the calibration phase of the PIT with electric heater around the aluminum pipe).

5.4.2 Uncertainty on the Moisture Content in the Pipe Insulation Test Specimen

The moisture content was computed from dividing the moisture mass by the volume of the insulation sample, which was estimated from the insulation actual geometry. The uncertainty on the moisture content was determined by the accuracy of the scale and human error in measuring the insulation dimensions as listed in Table 5-4 and Table 5-5. It should be noted that during the research period, two digital scales with different accuracy were used to measure the moisture content of the insulation specimen. The first scale (Model AMW-13) had an accuracy of $\pm$0.1oz (3g), and it was used to measure the moisture content of pipe insulation systems FG3A, FG3B, FG4, FG5, ER1.5, CG, PIR1 and PIR1.5. However, because of its low accuracy, moisture content lower than 0.035oz (1g) could not be measured. To solve this issue, a second scale (Model AND EJ-200) was used in order to more accurately measure the moisture content of pipe insulation systems FG6 and FG7, which were tested with vapor retarder jackets and thus had very low

moisture content. This scale had an accuracy of ±0.004oz (0.1g) and provided a more precise measurement of the weight of dry and wet insulation samples.

Table 5-4: Accuracy of the moisture gains measurement during the tests in wet conditions (Scale model AMW-13)

Moisture Gain Uncertainty Table				
Parameter	Manufacturer	Model	Nominal Value	Accuracy
Scale	AMW	AMW-13	0~13lb (0~6kg)	±0.1oz (3g)
Length/Thickness/Diameter	N/A	N/A		±1/8in. (3.18mm)

Table 5-5: Accuracy of the moisture gains measurement during the tests in wet conditions (Scale model AND EN-200)

Moisture Gain Uncertainty Table				
Parameter	Manufacturer	Model	Nominal Value	Accuracy
Scale	A&D	AND EJ-200	0~210g (0~7oz)	±0.1g (0.004oz)
Length/Thickness/Diameter	N/A	N/A		±1/8in. (3.18mm)

The relative uncertainty of the moisture content decreased with moisture content increasing in the insulation, as shown in Figure 5.11 and Figure 5.12. (Figure 5.11 represents uncertainty derived with scale model AMW-13 and Figure 5.12 represents uncertainty derived with scale model AND EJ-200.) The relative uncertainty on moisture content of the test insulation specimen on the 1st PIT and 2nd PIT were different when the moisture content was below 4% if using the first scale (see Figure 5.11) and when it was below 0.2% if using the second scale (see Figure 5.12). For those ranges the experimental uncertainty values on 2nd PIT were higher than that on the 1st PIT. In Figure 5.11, if the moisture content was less than 1% by volume, the uncertainty on PIT2 was above ±15% while the uncertainty on PIT 1 was about 5%. In Figure 5.12, if the moisture content was less than 0.2% by volume, the uncertainty on the 2nd PIT was from 7 to 20% while on 1st PIT the uncertainty resulted below 9%. The scales accuracies were the limiting factors for the uncertainty of the moisture content when the moisture content was below 4% for the first scale and 0.2% with the second scale. For higher moisture contents, the error in the measurements of

the volume of the test samples dominated the overall uncertainty error and the two uncertainty curves of PIT1 and PIT 2 tended to converge to each other.

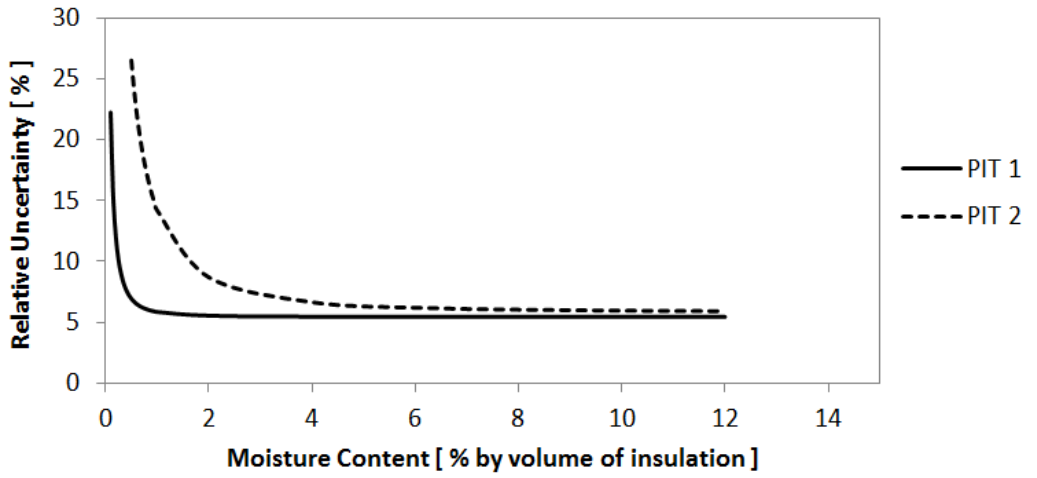

Figure 5.11: Relative uncertainty on the moisture content measured in the pipe insulation specimens using the first scale (model AMW-13).

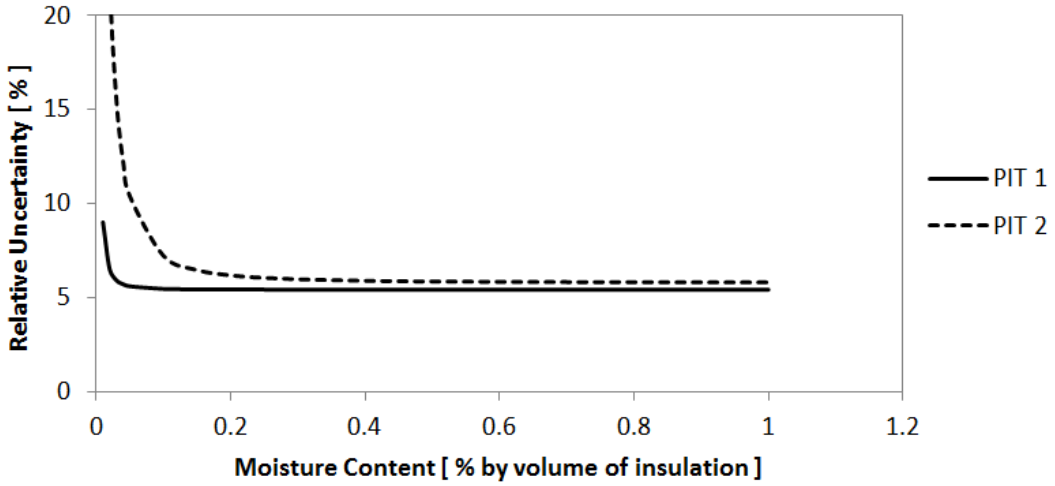

Figure 5.12: Relative uncertainty on the moisture content measured in the pipe insulation specimens using the second scale (model AND EJ-200).

CHAPTER VI

6 DISCUSSION OF THE EXPERIMENTAL RESULTS

This chapter discusses the experimental results for calibration tests of the sand thermal conductivity, k_{sand}, the measurements of thermal conductivity in dry conditions for twelve mechanical pipe insulation systems and the data from the wet tests. Empirical correlations were developed based on a curve-fit approach and they are discussed in detail in this chapter.

6.1 Calibration Tests Results of Sand Thermal Conductivity

Based on the outcome from the uncertainty analysis, the experimental uncertainty of sand thermal conductivity was found to be within 4% and it decreased if the heat flux and the temperature gradients in the PITs increased. During the calibration phase of the PIT, the tape heaters were controlled from 34.1 to 136.5 Btu/hr (about 10 to 40W) in order to control a high radial heat flux and impose a large temperature differences between the aluminum pipe surface and the copper pipe surface. The thermal conductivity of the sand, k_{sand}, was correlated with the average temperature of the sand, T_{sand}, and a quadratic polynomial function fitted well the experimental data. Equations (6.1) and (6.2), shown below, were used to calculate the thermal conductivity of the sand inside the 1st PIT.

$$\mathbf{k'_{sand}} = \mathbf{b_1 T_{sand}^2} + \mathbf{b_2 T_{sand}} + \mathbf{b_3 \Delta T_{exterior}^2} + \mathbf{b_4 \Delta T_{exterior}} + \mathbf{b_5} \qquad (6.1)$$

$$\mathbf{k''_{sand}} = \mathbf{c_1 T_{sand}^2} + \mathbf{c_2 T_{sand}} + \mathbf{c_3 \Delta T_{exterior}^2} + \mathbf{c_4 \Delta T_{exterior}} + \mathbf{c_5} \qquad (6.2)$$

where b_1 to b_5 are empirical coefficients developed from initial calibration, and c_1 to c_5 are empirical coefficients developed from the second calibration. The sand thermal conductivity was a linear interpolation between k'_{sand} and k''_{sand}, as shown in equation (5.1).

6.2 Thermal Conductivity Tests Results for Pipe Insulation Systems

The thermal conductivity of fiberglass (FG), elastomeric rubber (ER), cellular glass (CG) and polyisocyanurate (PIR) pipe insulation systems was measured during this project in dry non-condensing ambient conditions. Each system is given in Table 6-1. The test insulation mean temperature was varied between 57 to 73°F (14 to 23°C). The ambient dry bulb temperature was varied from 77 to 107°F (25 to 42°C). The ambient humidity was set as low as possible to reduce any moisture ingress into the pipe insulation systems and the dew point temperature of the ambient air was below the aluminum pipe surface temperature, which was around 38°F (3.3°C). It should be noted that the cellular glass pipe insulation systems CG was tested twice during the research period. CGA had the manufacture fabrication joints and was tested on the bare aluminum pipe, while CGB did not have any fabrication joints and it was tested on aluminum pipe painted black to limit any potential radiation effect.

Table 6-1: Pipe insulation systems tested under dry conditions

Test Samples (Ref. No.)	Nominal Wall Thickness In. (mm)	Joint Sealant (When Used)	Edge Seal	Vapor Retarder / Insulation Jacketing	Measured Average Density Range lb/ft^3 (kg/m^3)
(1)Fiberglass (FG1)	2 (50.8)	N/A	Foster 90-66	N/A	4.2-4.3 (~66 - 69)
(2)Fiberglass (FG2)	2 (50.8)	N/A	Foster 90-66	N/A	4.2-4.3 (~66 - 69)
(3A)Fiberglass (FG3A)	2 (50.8)	N/A	Childers CP-30	N/A	4.2-4.3 (~66 - 69)
(3B)Fiberglass (FG3B)	2 (50.8)	N/A	Childers CP-30	N/A	4.2-4.3 (~66 - 69)
(4)Fiberglass (FG4)	1.5 (38.1)	N/A	Childers CP-30	All Service Jacket (ASJ)(factory applied)	3.4-3.6 (~55 - 57)
(5)Fiberglass (FG5)	1.5 (38.1)	N/A	Foster 90-66	All Service Jacket(factory applied) (ASJ)	3.1-3.2 (~50 - 52)
(6)Fiberglass (FG6)	1.5 (38.1)	N/A	Foster 90-66	All service Jacket (ASJ) + PVC	3.1-3.2 (~50 - 52)
(7)Fiberglass (FG7)	1.5 (38.1)	N/A	Foster 90-66	Polyester Foil Polyester (PFP)	3.8-3.9 (~62 - 63)
(8)Elastomeric Rubber (ER2)	2 (50.8)	Stay-Seal with Protape	Aeroseal	N/A	2.4-2.6 (~38 - 41)
(9)Elastomeric Rubber (ER1.5)	1.5 (38.1)	Stay-Seal with Protape	Aeroseal	N/A	2.4-2.6 (~38 - 41)
(10A)Cellular Glass (CGA)	1.5 (38.1)	Boss 368	Boss 368	N/A	7.1-7.9 (~114 - 126)
(10B)Cellular Glass (CGB)	1.5 (38.1)	Boss 368	Boss 368	N/A	6.8-7.6 (~109 - 121)
(11)Polyisocyanurate (PIR1)	1 (25.4)	Childers CP-70	Foster 90-66	Polyvinylidene chloride (PVDC) vapor retarder	1.7-1.8 (~28 - 29)
(12)Polyisocyanurate (PIR1.5)	1.5 (38.1)	Childers CP-70	Foster 90-66	N/A	1.9-2.1 (~30 - 33)

6.2.1 Fiberglass Pipe Insulation Systems without Vapor Retarder Jackets

Four fiberglass pipe insulation systems FG1, FG2, FG3A and FG3B with the same thickness and density were tested under dry non-condensing conditions. All the four pipe insulation systems had a nominal wall thickness of 2 in. (50.8mm) and were tested without any vapor retarder jacket.

FG1 was tested at the very beginning of this research project, while FG2 was tested toward the end of the project in order to verify the repeatability of the measurement with the newly developed experimental test apparatus. The results are shown in Figure 6.1. During the measurements, the radial heat flux of system FG1 varied from 8.0 to 10.2 Btu/hr-ft (7.7 to 9.8 W/m), and that of system FG2 varied from 6.4 to 11.3 Btu/hr-ft (6.2 to 10.9 W/m). The radial heat flux of system FG3B varied from 6.7 to 10.4 Btu/hr-ft (6.4 to 10.0 W/m), and that of system FG3A was from 6.8 to 11.4 Btu/hr-ft (6.5 to 11.0 W/m). The uncertainty error of the thermal conductivity of system FG2 varied from 5.3% to 8.3%, and that of system FG3B ranged from 4.8% to 8.3%. As can be seen from the plot, the thermal conductivity values of all the four fiberglass pipe insulation systems are within the experimental uncertainty range.

The experimental results of FG1 and FG2 were also compared with one fiberglass pipe insulation system tested in research project ASHREA RP-1356. The experimental data from the research project RP-1356 was compared and validated with data from manufacturer catalog and previous researches (Cai (2013)). The results are shown in Figure 6.2. The experimental results from RP-1356 fiberglass pipe insulation system, shown in the green filled triangles in Figure 6.2, were about 8% lower than that from the current project. This shift was due to the difference in measured pipe insulation outside diameter. In RP-1356, the nominal diameter was used instead of the actual diameter of the fiberglass insulation exterior surface. The nominal exterior diameter of the fiberglass pipe insulation system was 7.5 in. (190.5mm), and possibly about 0.1 to 0.2 in. (2.5 to 5.1mm) smaller than the actual diameter. After the nominal diameter was modified with the actual diameter, the results are the green void triangles in Figure 6.2. The modified test results of RP-1356 fiberglass pipe insulation system showed about a 10% increase from the original experimental values, and they were within the uncertainty range of systems FG1 and FG2 tested in the second phase. This further demonstrated that the experimental thermal conductivity data produced in this present work was convincing and had good repeatability.

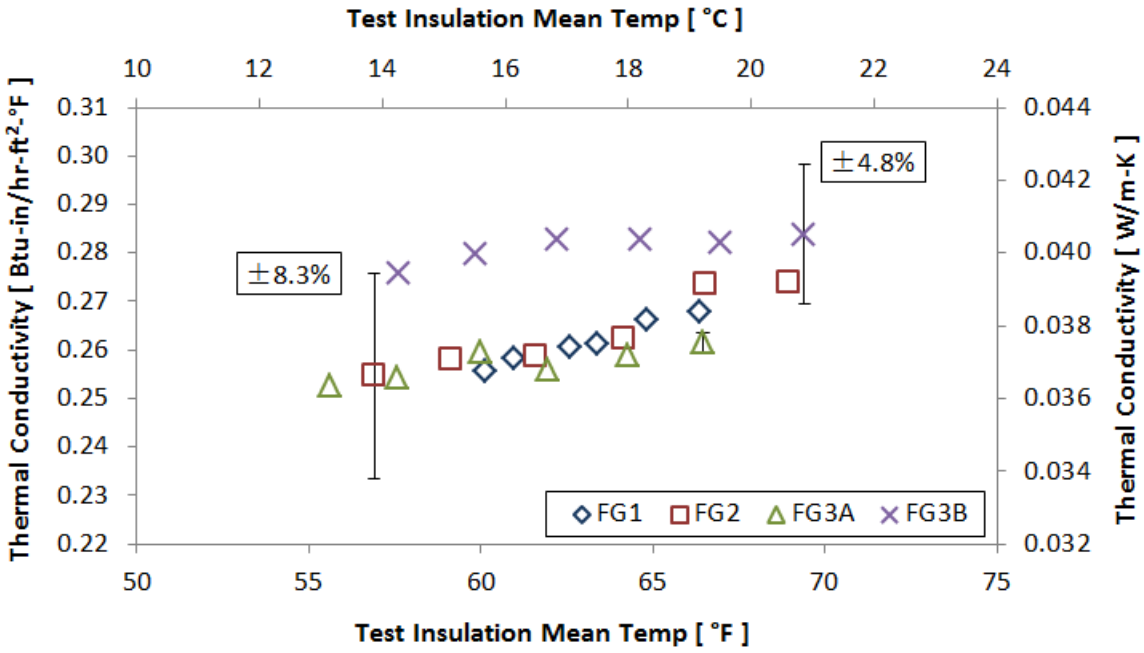

Figure 6.1: Thermal conductivity of three fiberglass pipe insulation systems FG1, FG2, FG3A and FG3B.

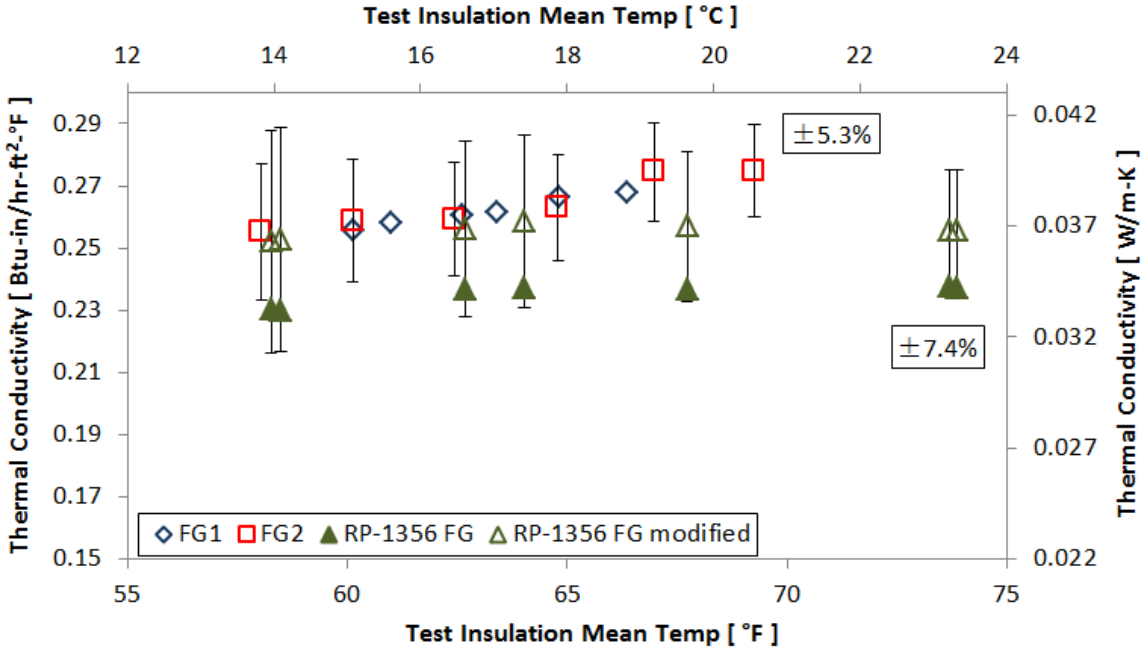

Figure 6.2: Thermal conductivity of three fiberglass pipe insulation systems FG1, FG2,and one FG system from RP-1356.

6.2.2 Fiberglass Pipe Insulation Systems with Vapor Retarder Jackets

Three fiberglass pipe insulation systems with the same nominal wall thickness 1.5 in. (38.1mm), but different vapor retarder systems and different densities were tested under the dry non-condensing conditions. System FG4 had a slightly different density of (3.5 lb/ft^3) 55.8kg/m^3 and was tested with ASJ vapor retarder jacket. FG5 had a density of (3.2 lb/ft^3) 50.8kg/m^3 and was tested with ASJ vapor retarder jacket. FG6 with the same density as FG5 was tested with ASJ vapor retarder jacket covered with a 20 mil thick PVC jacket. System FG7 had a higher density of (3.9 lb/ft^3) 62.3kg/m^3 and was tested with a Polyester Foil Polyester (PFP) laminate vapor retarder jacket. The experimental results are shown in Figure 6.3. The difference on the measured values of exterior diameters of FG3 and FG5 was the reason to cause the small difference between the two systems thermal conductivity. The thermal conductivity of all the four fiberglass pipe insulation systems is within the experimental uncertainty range. From the experimental results, it appeared that different vapor retarder systems and different densities did not affect the apparent thermal conductivity in dry conditions.

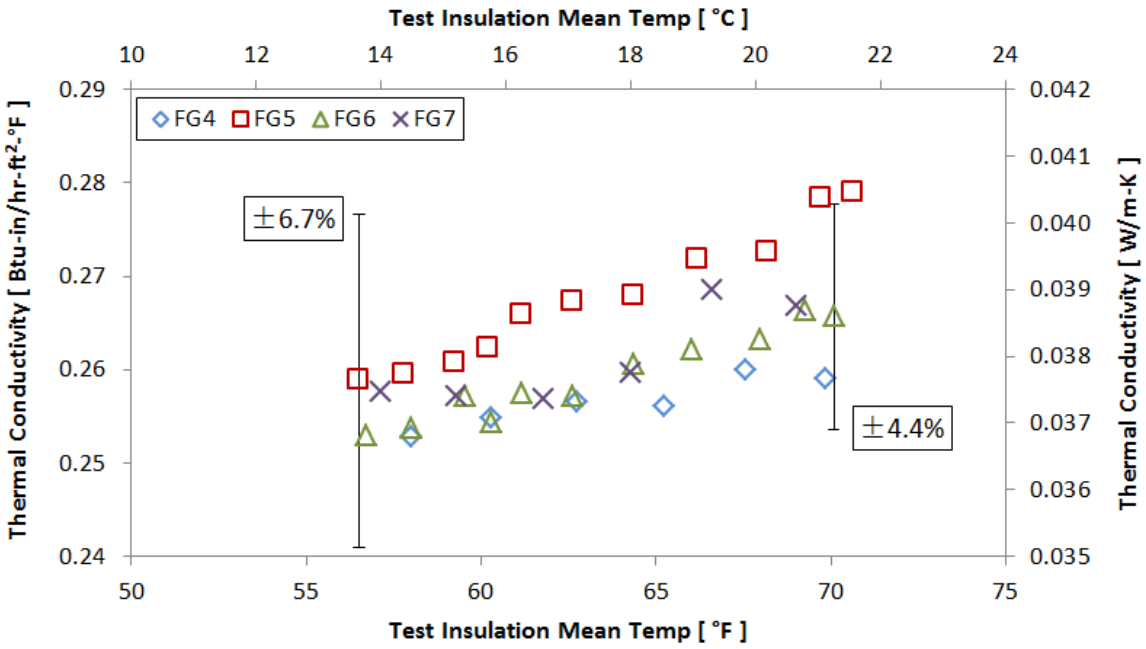

Figure 6.3: Thermal conductivities of fiberglass pipe insulation systems FG4, FG5, FG6 and FG7.

6.2.3 Elastomeric Rubber Pipe Insulation Systems

In this research project, two elastomeric rubber pipe insulation systems were tested under dry non-condensing conditions: ER1.5 with 1.5 in. (38.1mm) nominal wall thickness and ER2 with 2 in (50.8mm) nominal wall thickness and. During the measurements, the radial heat flux through the test sample varied from 7.9 to 13.3 Btu/hr-ft (7.6 to 12.8W/m) for ER1.5 and 6.3 to 10.7 Btu/hr-ft (6.1 to 10.3W/m) for ER2. The uncertainty for system ER1.5 was from ±4.5% to ±6.7%, and that for system ER2 was from ±5.0% to ±7.7%. The experimental results are shown in Figure 6.4. Both systems showed a similar trend of thermal conductivity with insulation mean temperature, and the test results were within the experimental uncertainty. In particular, the two systems had approximately the same slope of thermal conductivity versus test insulation mean temperatures.

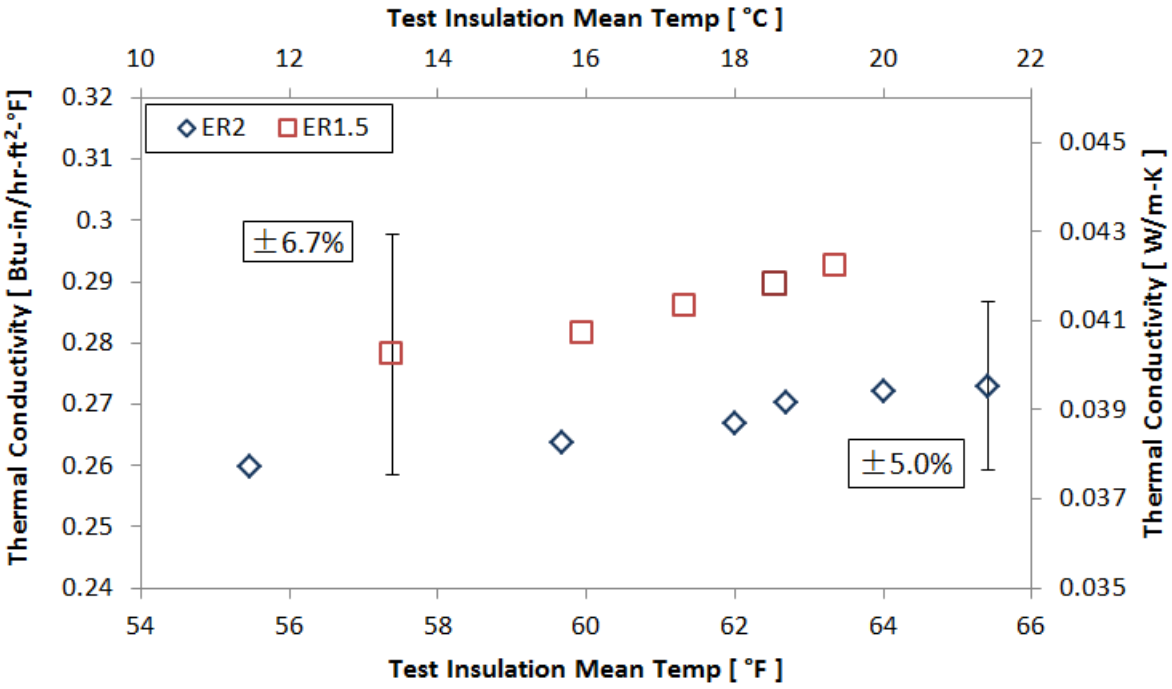

Figure 6.4: Thermal conductivities of elastomeric rubber pipe insulation systems ER2 and ER1.5.

6.2.4 Cellular Glass Pipe Insulation Systems

Cellular glass pipe insulation system with the nominal thickness of 1.5 in (38.1mm) was tested under dry non-condensing conditions. This pipe insulation system was tested twice on the bare aluminum pipe and on the black painted pipe, referred to as pipe insulation systems CGA and CGB, respectively. During the measurements, the radial heat flux for system CGA varied from 12.3 to 16.0 Btu/hr-ft (11.8 to 15.4 W/m), and that for system CGB varied from 10.6 to 17.4 Btu/hr-ft (10.2 to 16.7 W/m). The uncertainty for both systems was between ±4.3% and ±6.1%. The experimental results are shown in Figure 6.5. The values derived from the black pipe were about 5% lower than the thermal conductivity measured on the bare aluminum pipe. This could be explained by two reasons. The first reason is the existence of manufacturing fabrications joints in the testing insulation specimens for the system CGA. The manufacturing fabrications might increase the apparent insulation thermal conductivity. Fabrication joints were visibly observed for the insulation samples of CGA but not for the insulation samples of CGB. Another possibility for

the difference might be that the material came from different manufacturing batches, and thus their density was different as indicated in last column of Table 6-1. It was also observed from Figure 6.5 that the thermal conductivity of CGB was slightly decreasing with test insulation mean temperature. However, if taken into account of the experimental uncertainty, the thermal conductivity of systems CGB was practically constant.

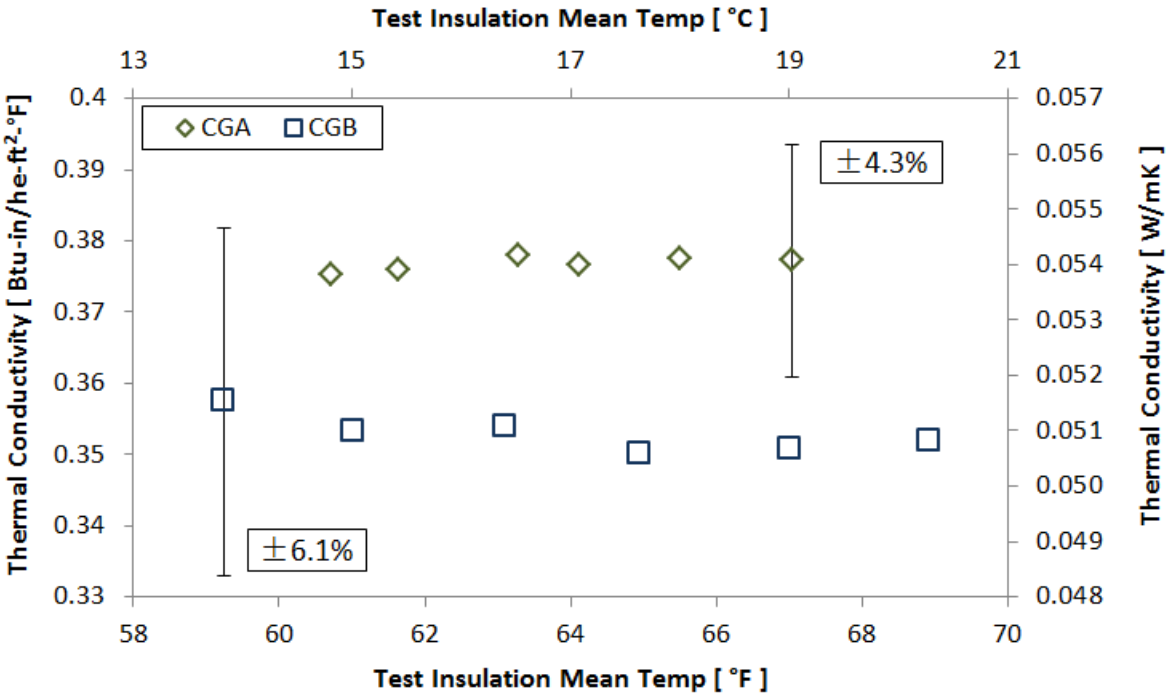

Figure 6.5: Thermal conductivities of cellular glass pipe insulation systems CGA and CGB

.

6.2.5 Polyisocyanurate (PIR) Pipe Insulation systems

System PIR1 pipe insulation system was tested with a nominal wall thickness of 1 in. (25.4mm) and with polymer polyvinylidene chloride (PVDC) film vapor retarder jacket. During the measurement, the radial heat flux through the insulation was from 9.8 to 17.2 Btu/hr-ft (9.4 to 16.5 W/m), and the uncertainty was between ±4.6% to ±6.9%. System PIR1.5 was tested with no vapor retarder jacket, and the redial heat flux range was 7.9 to 14.0 Btu/hr-ft (7.6 to 13.5 W/m), uncertainty varying from ±3.5% to ±6.3%. The experimental results are shown in Figure 6.6. For

system PIR1.5, the apparent thermal conductivity increased gradually with insulation mean temperature. The results for two systems are all within the experimental uncertainty. The data for PIR1 seems to indicate a slight decrease in thermal conductivity with average insulation temperature. This might be due to an aging phenomenon in the PIR test insulation sample or the uncertainty in the experimental results. Because of the limited temperature range and given that the uncertainty reported in Figure 6.6 for one representative point is applicable to all the other data points, the thermal conductivity of the system PIR1 remained fairly constant for insulation mean temperature ranging between 55 to 70°F (12.8 to 21°C).

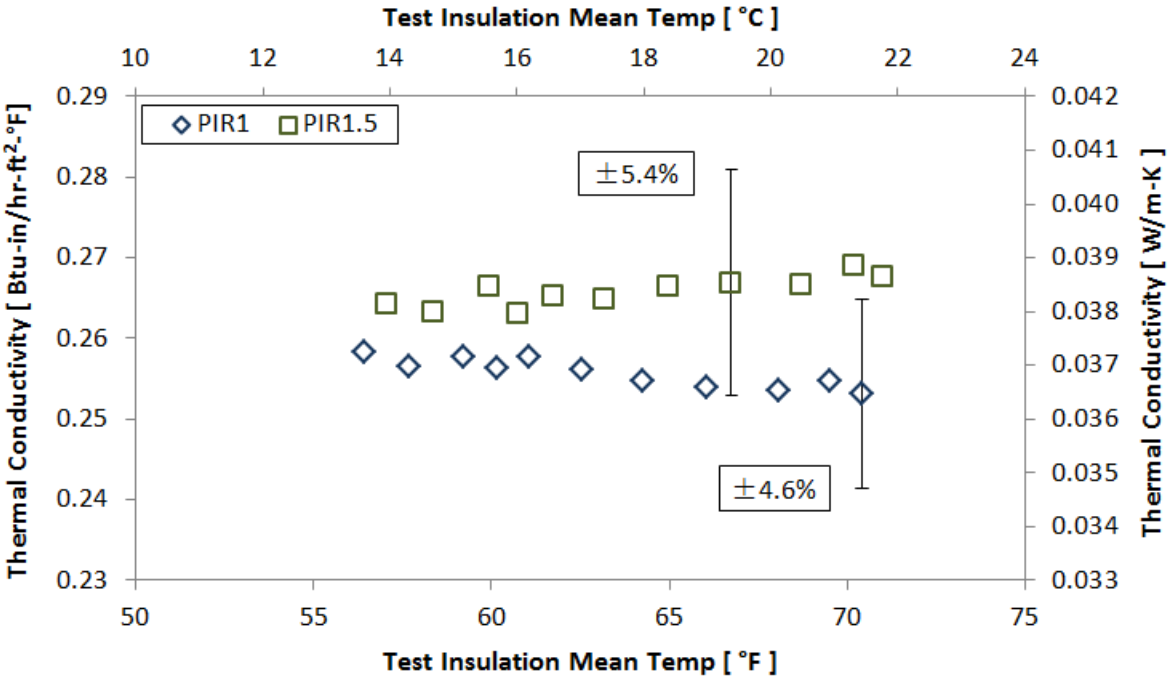

Figure 6.6: Thermal conductivities of PIR pipe insulation systems PIR1 and PIR1.5.

6.2.6 Summary of Dry Results

Linear correlations were developed based on the measured thermal conductivity and test insulation mean temperature of the 12 pipe insulation systems, listed in Table 6-2. For fiberglass, elastomeric rubber, one of the cellular glass pipe insulation systems and one of the PIR pipe

insulation systems, the overall thermal conductivity increased with the insulation mean temperature. For the same temperature range, the thermal conductivity of pipe insulation systems PIR1 and CGB was practically constant. It should be noticed here that in the second column of Table 6-2, the actual wall thickness of the pipe insulation systems was derived from the actual measured outside diameter of the insulation specimen once they were installed on the aluminum pipe, as illustrated in Figure 6.7.

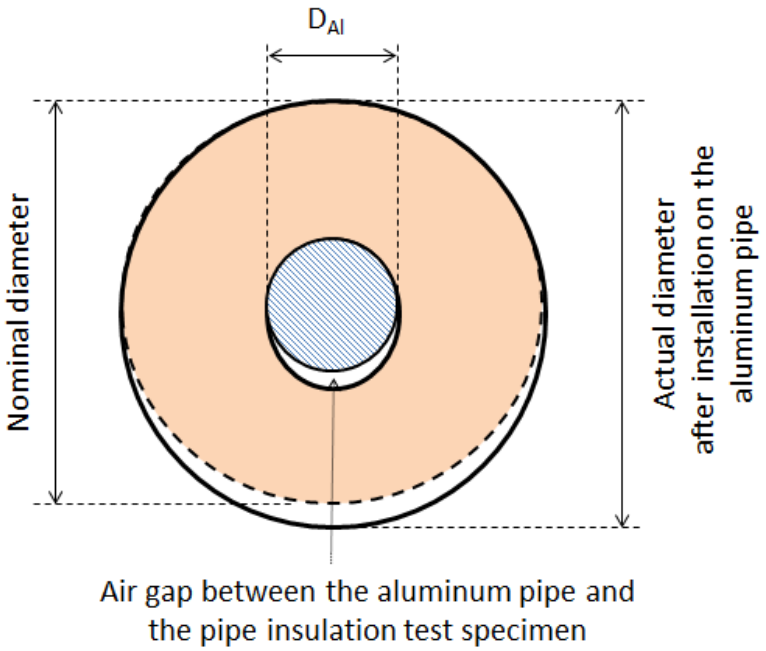

Figure 6.7: illustration of the actual wall thickness of pipe insulation specimen after installed on the aluminum pipe.

Table 6-2: Thermal conductivity of pipe insulation systems tested under dry conditions

Test Samples (Ref. No.)	Actual Wall Thickness in (mm)	$^{*}k_{pipe,insulation} = a \cdot T + b$ Btu-in/hr- ft^2-F (W/m-K) a	b	Heat flux per unit length Btu/hr-ft (W/m)
(1)Fiberglass (FG1)	2.1 (53.3)	0.0020 (0.0005)	0.1367 (0.0289)	9.3 (8.97)
(2)Fiberglass (FG2)	2.1 (53.3)	0.0017 (0.0004)	0.1568 (0.0304)	8.8 (8.46)
(3A)Fiberglass (FG3A)	2.1 (53.3)	0.0007 (0.0002)	0.2132 (0.0341)	9.1 (8.71)
(3B)Fiberglass (FG3B)	2.1 (53.3)	0.0005 (0.0001)	0.2451 (0.0378)	9.1 (8.72)
(4)Fiberglass (FG4)	1.6 (40.6)	0.0006(0.0001)	0.2212(0.0345)	9.9 (9.50)
(5)Fiberglass (FG5)	1.6 (40.6)	0.0014 (0.0004)	0.1809 (0.0325)	11.3 (10.82)
(6)Fiberglass (FG6)	1.7 (43.2)	0.0010 (0.0003)	0.1999 (0.0333)	10.6 (10.18)
(7)Fiberglass (FG7)	1.6 (40.6)	0.0010 (0.0002)	0.2028 (0.0337)	10.7 (10.27)
(8)Elastomeric Rubber (ER2)	2.1 (53.3)	0.0014 (0.0004)	0.1807 (0.0326)	8.9 (8.56)
(9)Elastomeric Rubber (ER1.5)	1.7 (43.2)	0.0013 (0.0003)	0.2059 (0.0356)	10.9 (10.52)
(10A)Cellular Glass (CGA)	1.7 (43.2)	0.0003 (0.0001)	0.3581 (0.0530)	14.0 (13.50)
(10B)Cellular Glass (CGB)	1.6 (40.6)	-0.0002 (-0.0001)	0.3664 (0.0518)	13.9 (13.37)
(11)Polyisocyanurate (PIR1)	1.1 (27.9)	-0.0003 (-0.0001)	0.2766 (0.0384)	13.3 (12.83)
(12)Polyisocyanurate (PIR1.5)	1.7 (43.2)	0.0003(0.0001)	0.2448(0.0368)	10.9 (10.50)

6.3 Thermal Conductivity of Pipe Insulation Systems in Wet Condensing Conditions with Moisture Ingress

6.3.1 Fiberglass Pipe Insulation System FG3A

According to literature, fiberglass is a fibrous insulation material that allows water vapor to pass through the gaps among the strands of the fibers if a vapor repellent jacketing is not present **(**McFadden (1988)). The condensation can be easily accumulated and filled in the void spaces inside the material due to the loose and fibrous interior structure. This fiber glass pipe insulation system FG3A was tested under severe conditions with a high temperature of 90.1°F (32.3°C) and

a high relative humidity of 84% for 54 days. In these conditions, the dew point temperature was 84.6°F (29.2°C), and the insulation surface temperature of the FG3A system ranged from 88.2°F (31.2°C) to 88.9°F (31.6°C). The nominal wall thickness was 2 in. (50.8mm). Figure 6.8 below shows the installation details of system FG3A.

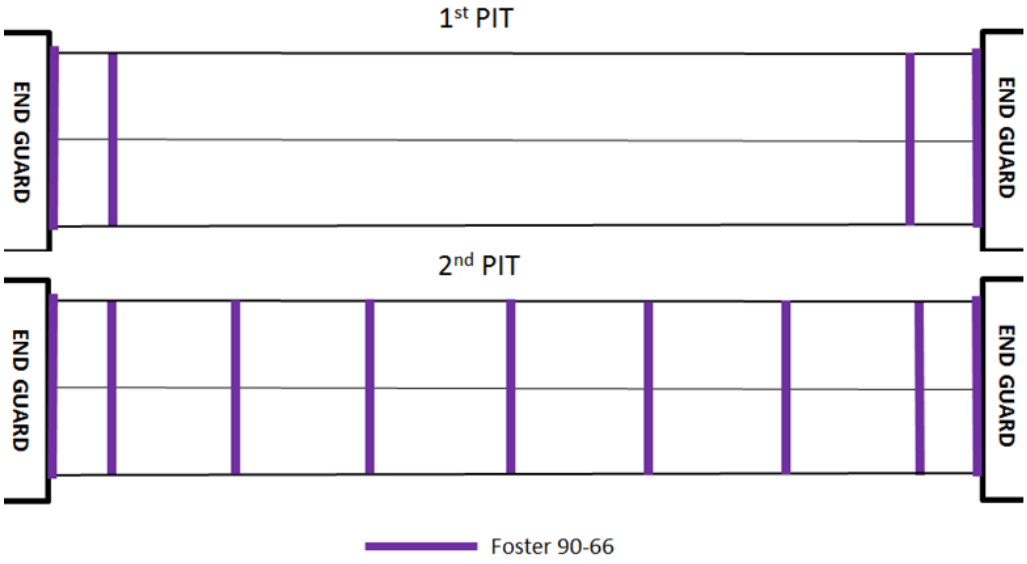

Figure 6.8: Schematics of installation of system FG3A for the wet test.

During the wet test period, only one small wet region was observed on the exterior surface of the bottom shell, and the wet region remained almost of the same size for the remaining period of the test as indicated inside the dashed red line circles in Figure 6.9. A large region of water marks was observed at the location. This location might be a less dense region for the insulation material and water vapor ingress was locally promoted. Figure 6.9 also shows the interior surface of both top and bottom shells of the fiberglass test sample in this system FG3A. There were not any visible water marks on the top shell, and the water droplets only coating along the surface of the fibers. The experimental results on the system thermal conductivity and moisture content are plotted in Figure 6.10. After 54 days of wet test, the system thermal conductivity ratio, defined as

wet over dry thermal conductivity at the same temperature, increased up to 3.5 with the total moisture content of about 15% by volume.

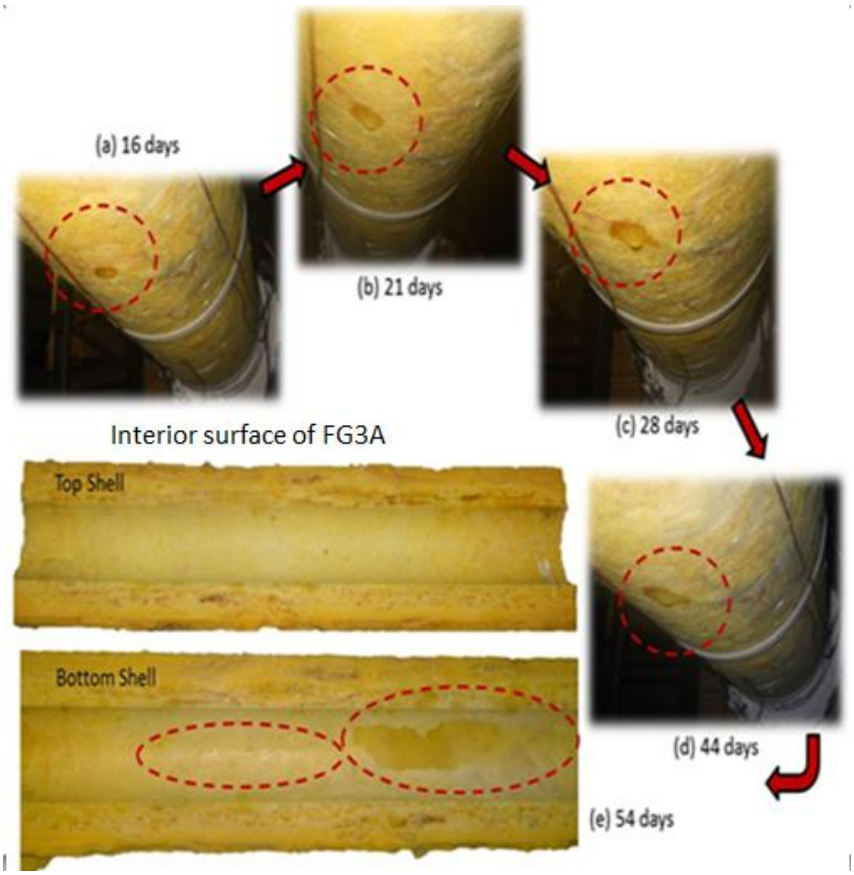

Figure 6.9: Development of wet regions on the exterior surface of pipe insulation system FG3A.

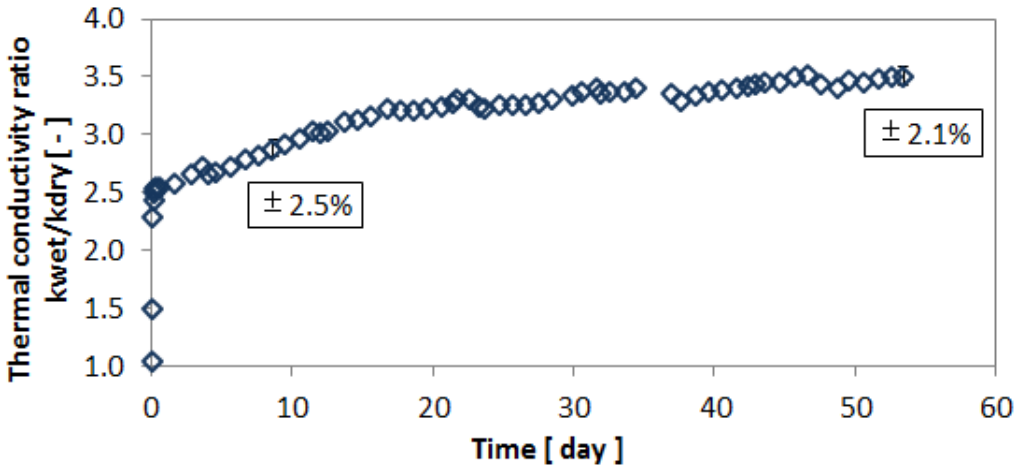

(a)

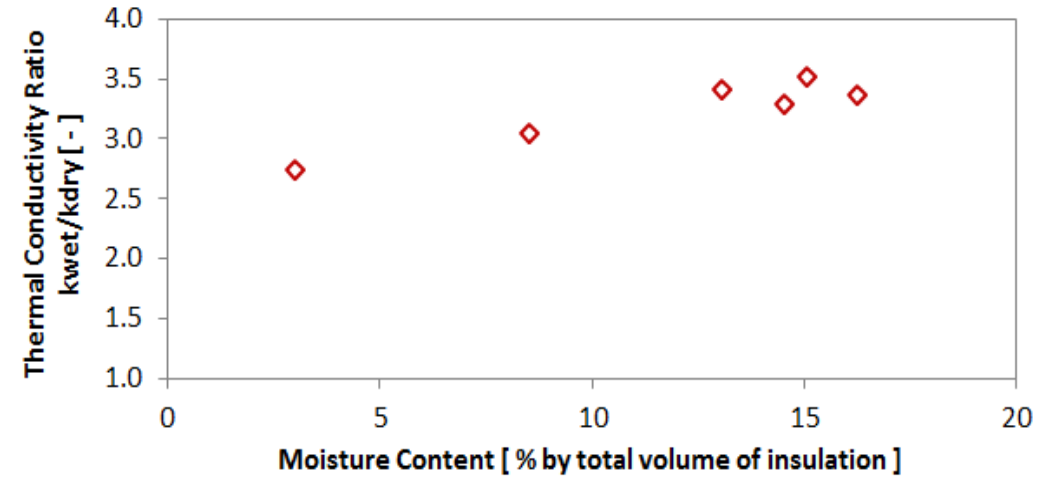

(b)

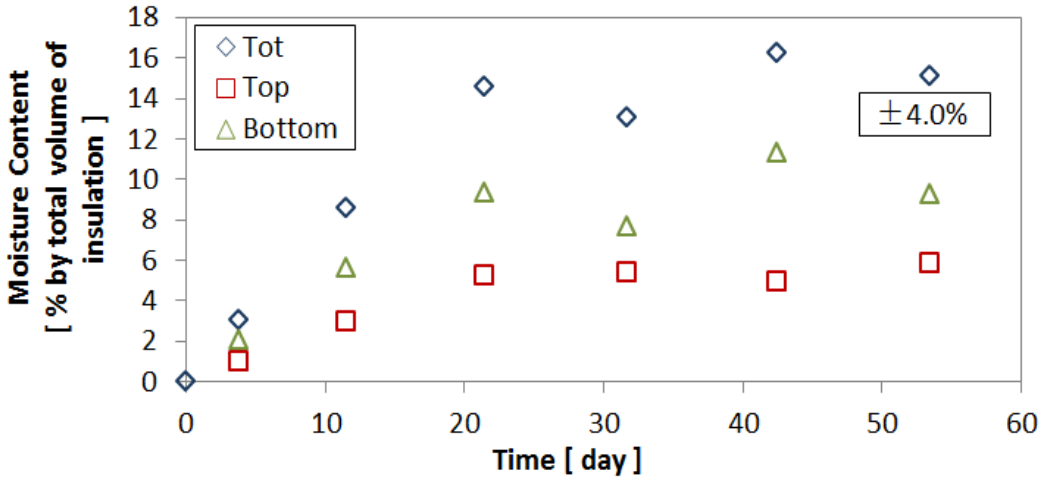

(c)

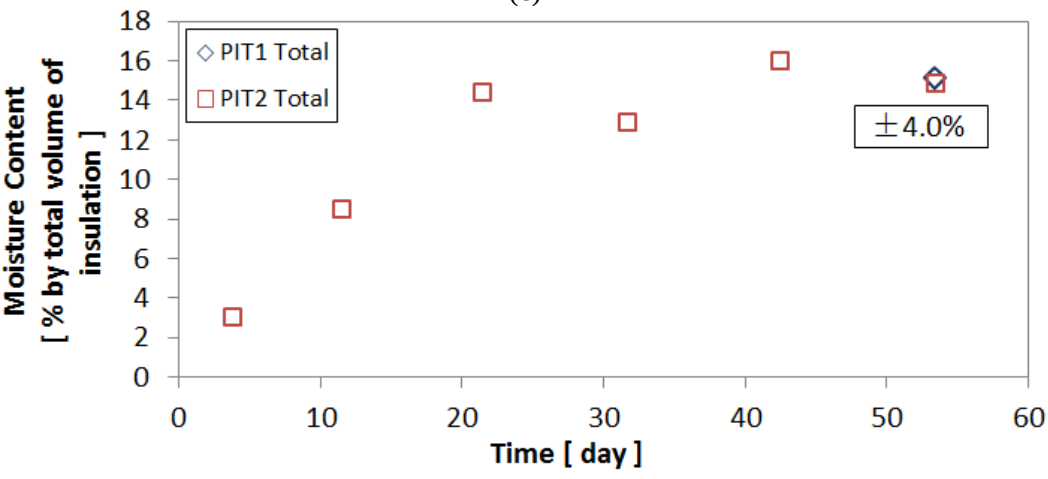

(d)

Figure 6.10: Experimental results on pipe insulation system FG3A: (a) system thermal conductivity versus time during the wet test period (b) moisture accumulation during wet test (c) effect of moisture content on the pipe insulation system thermal conductivity ratio (d) periodical measurement of moisture content on the 2nd PIT and moisture content on 1st PIT at the completion of wet test.

As shown in Figure 6.10 (a), during the beginning of the wet test, the performance on the system thermal conductivity showed a two-step variation process. The system thermal conductivity changed almost simultaneously with the ambient condition at the beginning of the wet test. The thermal conductivity ratio increased to 2.5 during the first several hours and then gradually increased to 3.5 during the remaining of the wet test period. The reason for this phenomenon could be explained by the additional heat transfer of vapor diffusion (Langlais et al. (1983)). It should be noted that the thermal conductivity measured during the wet tests was the equivalent thermal conductivity which included both sensible heat transfer and latent heat transfer as shown in Equation (6.3). The latent heat component of the equivalent thermal conductivity was calculated as in Equation (6.4).

$$\boldsymbol{\lambda = \lambda^{*} + \lambda_{v}} \tag{6.3}$$

$$\boldsymbol{\lambda_{v} = \frac{J_{v}}{\Delta T} \cdot L} \tag{6.4}$$

Where $\boldsymbol{\lambda^{*}}$ is the apparent thermal conductivity; $\boldsymbol{\lambda_{v}}$ is the latent heat component of the thermal conductivity; $\mathbf{J_v}$ is the density of vapor flow, $\mathbf{kg/m \cdot s}$; $\Delta\mathbf{T}$ is the temperature difference between the insulation surface and the aluminum pipe surface; $\mathbf{L}$ is the latent heat of vaporization of water, and was assumed as constant at 2260 $\mathbf{kJ/kg}$.

According to the moisture content variation of the fiberglass pipe insulation system FG3A, during the first 3.8 days, the moisture content increased by 3% by total volume of the insulation test specimen, which was a total of around 744g in mass. Then the density of vapor flow, $\mathbf{J_v}$, was calculated as $\boldsymbol{2.5 \times 10^{-6}}$ kg/m-s. By applying equation (6.4), the latent heat component of equivalent thermal conductivity of the fiberglass pipe insulation system FG3A was calculated at 0.226 W/m-K. This value was much higher when compared with the insulation dry thermal conductivity. As moisture kept accumulating inside the fiberglass pipe insulation specimen, the

temperature difference varies. In the meantime, it was assumed that the density of vapor flow during the transient period of the wet test remained unchanged and was independent of moisture content. Then according to equation (6.4), $\boldsymbol{\lambda_v}$ was calculated and plotted with time, as shown in Figure 6.11. By comparing Figure 6.11 with Figure 6.10 (a), it was observed that the significant increase of thermal conductivity in the transient stage at low moisture content was caused by the additional heat transfer of vapor diffusion. This also explained why the first few percentages of moisture content affect immediately the measured thermal conductivity of the fiberglass pipe insulation system, while a further supply of moisture has a relatively moderate effect.

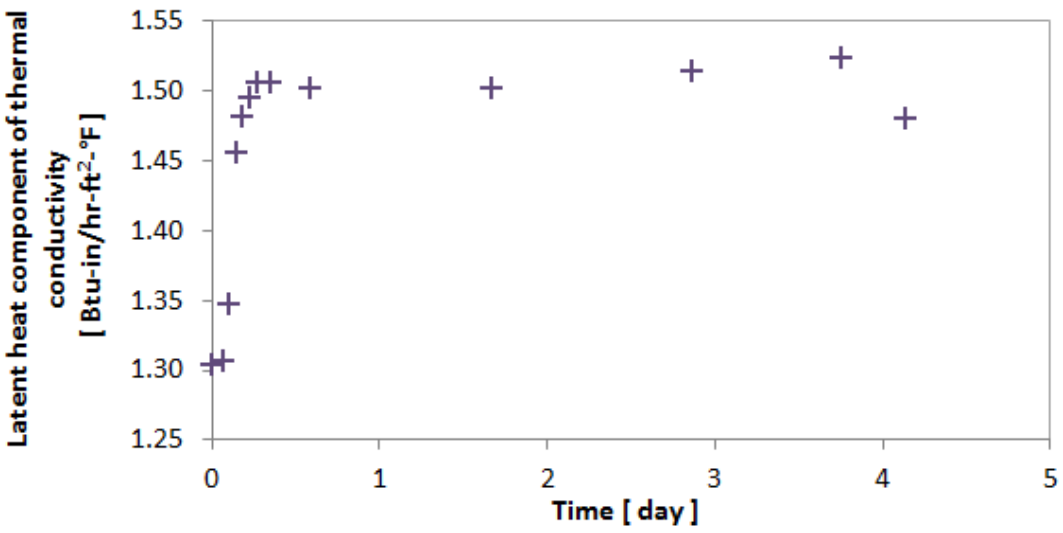

Figure 6.11: Calculation results on the latent heat component of thermal conductivity versus time during the transient stage of wet test of system FG3A.

6.3.2 Fiberglass Pipe Insulation System FG3B

In this wet condensing test, the 2 in. (50.8mm) nominal wall thickness fiber glass pipe insulation system FG3B was tested at the 78.1°F (25.6°C), 54.8% R.H. condition for 55 days. Photos of wet regions during the tests are shown in Figure 6.12. By the end of the wet test period, only two small wet regions were observed on the exterior surface of the bottom shell and next to the insulation ends of the test sample. The wet regions, showed inside the red dashed circles in the

photo, were observed on the 5th day of the wet test, and the wet regions remained almost the same size for the remaining period of the test. The figure also shows that a large amount of water was trapped on the exterior layer of the fiberglass pipe insulation system due to possible preferential paths for water vapor ingress near to the insulation end cross sections. Figure 6.12 shows the interior surface of the fiberglass insulation that was wrapped around the aluminum pipe. The interior surface of the top shell was basically dry, with only few water droplets on the surface layer of the fibers. On the bottom shell, larger wet regions were present next to the insulation end cross sections. This observation supported the hypothesis that preferential paths for moisture ingress were established at the end cross sections of the pipe insulation test specimen. The experimental results on the system thermal conductivity and moisture content are shown in Figure 6.13. By the end of the wet test, the system thermal conductivity in wet condition was 1.5 times higher than the thermal conductivity in dry condition at the same temperature. The maximum moisture content was about 1.7% by volume. From Figure 6.13 (a), it is observed that the system thermal conductivity also followed a two-step variation with time. The system thermal conductivity ratio increased to 1.5 with the moisture content less than 0.3% by volume at the beginning of the test. Then the thermal conductivity ratio was 1.5 for a long period during which the moisture content increased from 0.3 to 1.7% by volume. This could also be explained by the additional heat transfer of vapor diffusion. Both the top and bottom shells of this insulation system had similar moisture content. It should be noted that the uncertainty was above 20% when the moisture content was below 2% by volume. It was speculated that gravity had minor impact on the water redistribution between the top and bottom shells when the total amount of moisture content in the fiberglass insulation system was below 2%. It was also observed from Figure 6.13 (d) that on the last day of the wet test, the total moisture content of the last sample on the 2nd PIT was lower than that of the sample on the 1st PIT. This was caused by the preferential path on the 1st PIT that could be observed in Figure 6.12. Since this preferential path was only observed on

the 1st PIT, more water vapor actually entered the insulation sample on the 1st PIT and caused the moisture content to increase.

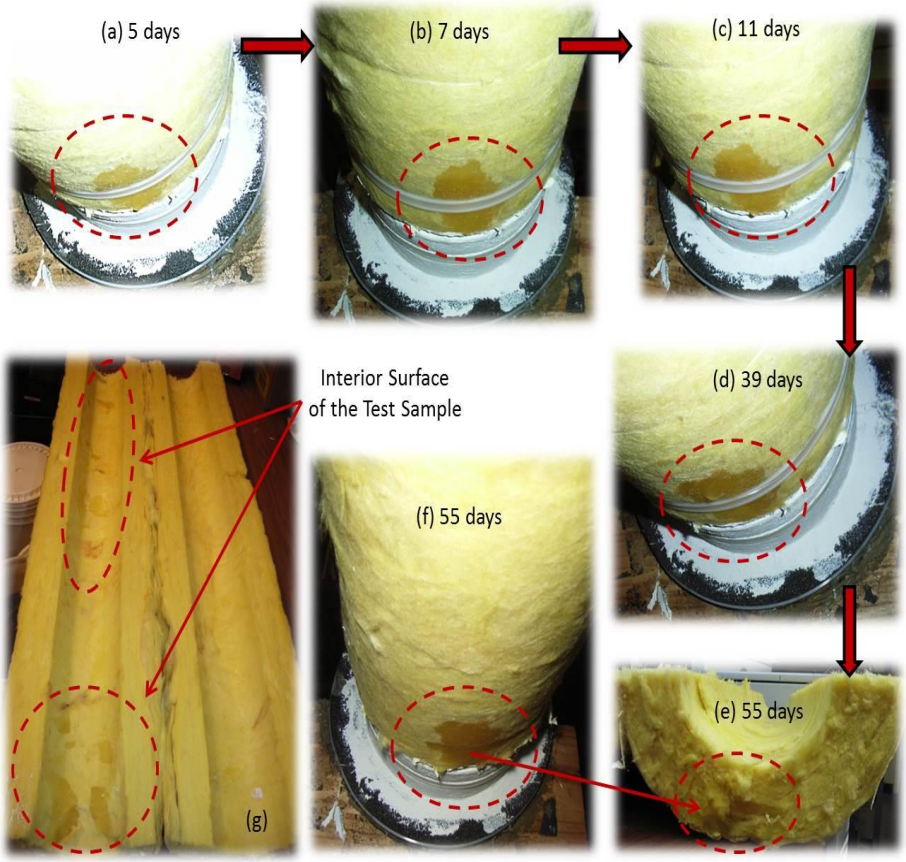

Figure 6.12: Development of wet regions on the exterior surface of pipe insulation system FG3B.

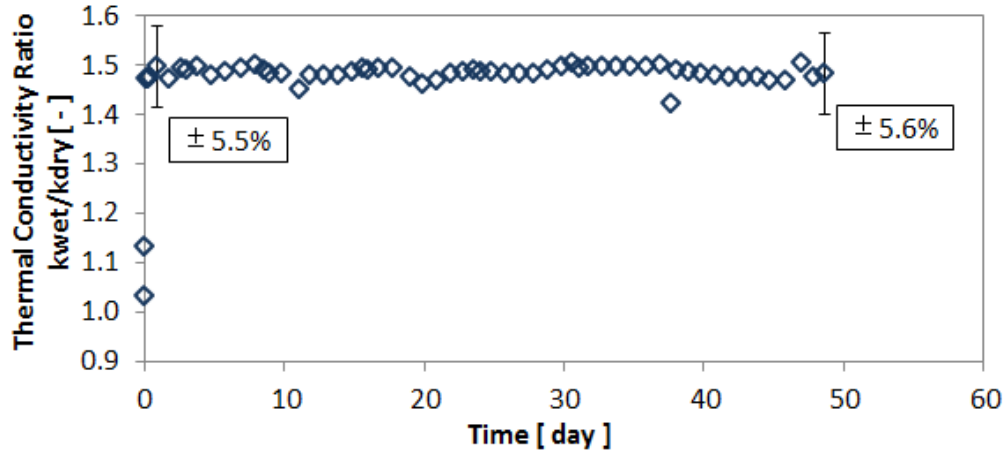
Thermal Conductivity Ratio
kwet/kdry [-]
1.6
1.5
1.4
1.3
1.2
1.1
1.0
0.9
± 5.5%
± 5.6%
0
10
20
30
40
50
60
Time [day]

(a)

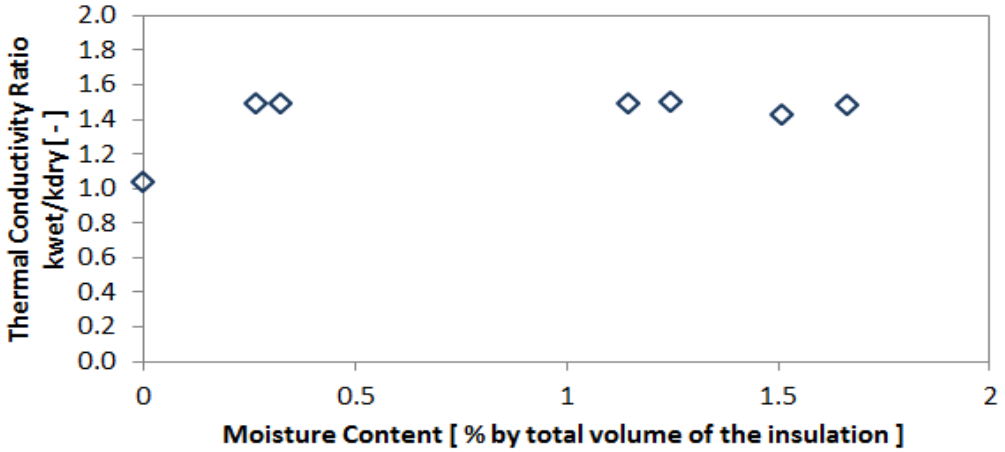
Thermal Conductivity Ratio
kwet/kdry [-]
2.0
1.8
1.6
1.4
1.2
1.0
0.8
0.6
0.4
0.2
0.0
0
0.5
1
1.5
2
Moisture Content [% by total volume of the insulation]

(b)

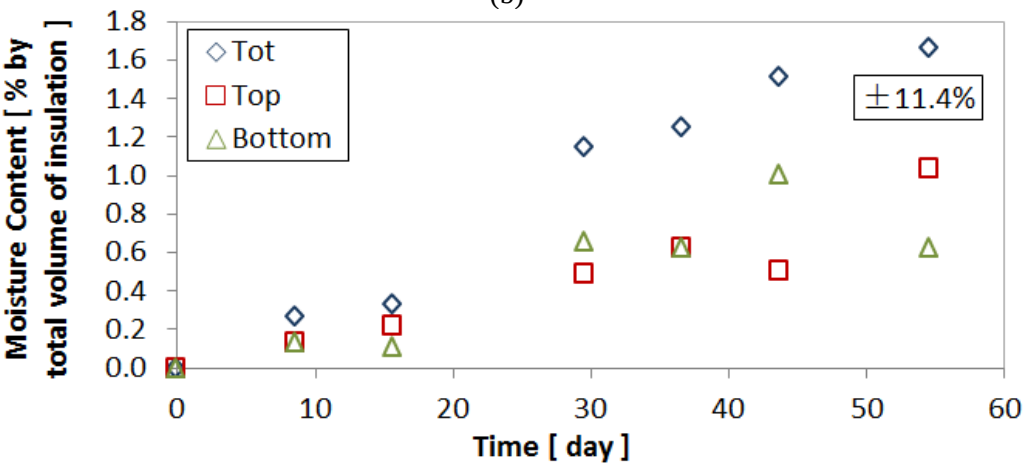
Moisture Content [% by total volume of insulation]
1.8
1.6
1.4
1.2
1.0
0.8
0.6
0.4
0.2
0.0
Tot
Top
Bottom
± 11.4%
0
10
20
30
40
50
60
Time [day]

(c)

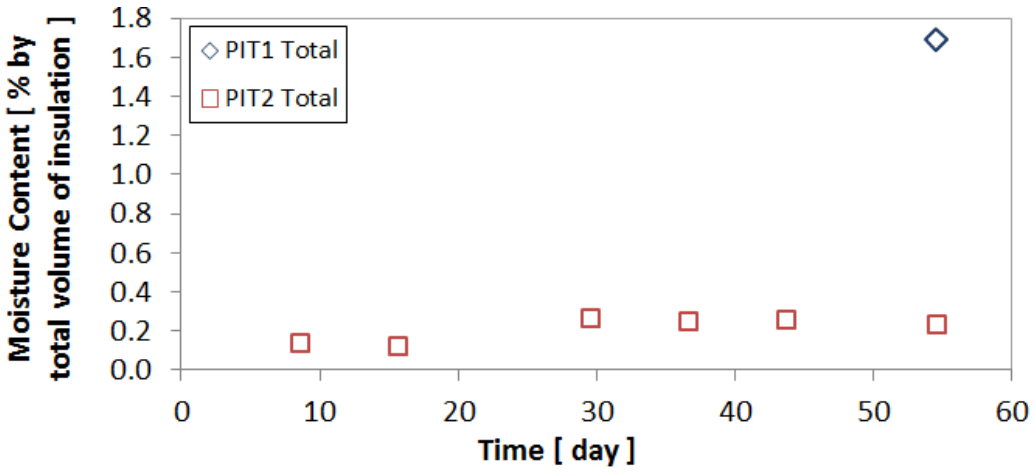

(d)

Figure 6.13: Experimental results on pipe insulation system FG3B: (a) system thermal conductivity versus time during the wet test period (b) moisture accumulation during wet test (c) effect of moisture content on the pipe insulation system thermal conductivity ratio (d) periodical measurement of moisture content on the 2nd PIT and moisture content on 1st PIT at the completion of wet test.

6.3.3 Fiberglass Pipe Insulation System FG4

The fiberglass pipe insulation system FG4 with ASJ vapor retarder jacket was operated in a wet condensing environment and it had a nominal wall thickness of 1.5 in. (38.1mm). It was tested at 78.1°F (25.6°C), 55% R.H. for 55 days. The conditions purposely simulated more closely the actual temperature and humidity of indoor spaces for mechanical insulation systems in commercial buildings. For this fiberglass system, both the 1st PIT and the 2nd PIT were used to measure the thermal conductivity of the fiber glass pipe insulation systems in order to confirm the repeatability of the data and to estimate the error due to operator installation. Figure 6.14 below shows the installation details of system FG4.

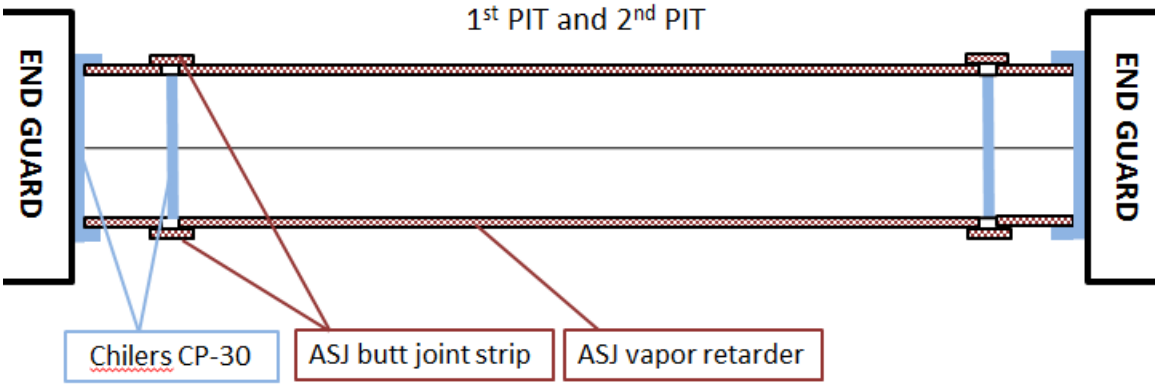

Figure 6.14: Schematics of installation of system FG4 for the wet test.

During the wet test, only the initial and final moisture content were measured for both PITs. There were not any wet regions observed during the 55 days of wet test period and the insulation interior surfaces appeared to be completely dry after taking out the samples from the PITs. It can be observed from Figure 6.15 (a) that, different from systems FG3A and FG3B, it didn't show a large increase during the first several hour of the wet test, and the thermal conductivity ratio increased slightly during the beginning of the moisture test. One reason to explain this phenomenon could be the very small amount of vapor diffusion in the system FG4 due to the existence of vapor retarder jacket and the low humidity environment. The water vapor trapped inside the fiberglass pipe insulation specimen started to condense on the cold surface during the transient stage of the wet test, causing the system thermal conductivity to slightly increase. Then after this period, because there was basically no vapor diffusion into the insulation specimen, the system thermal conductivity gradually decreased back to the dry thermal conductivity value. The previous researcher (Langlais et al. (1983)) also supported this phenomenon by pointing out that liquid water sprayed on the cold side of the insulation hardly affected its thermal conductivity. As shown in Figure 6.15(b), both systems FG4 on PIT1 and PIT2 had moisture content lower than 0.3% by total volume and they showed identical behavior, confirming the repeatability of the measurements with the newly developed test apparatus.

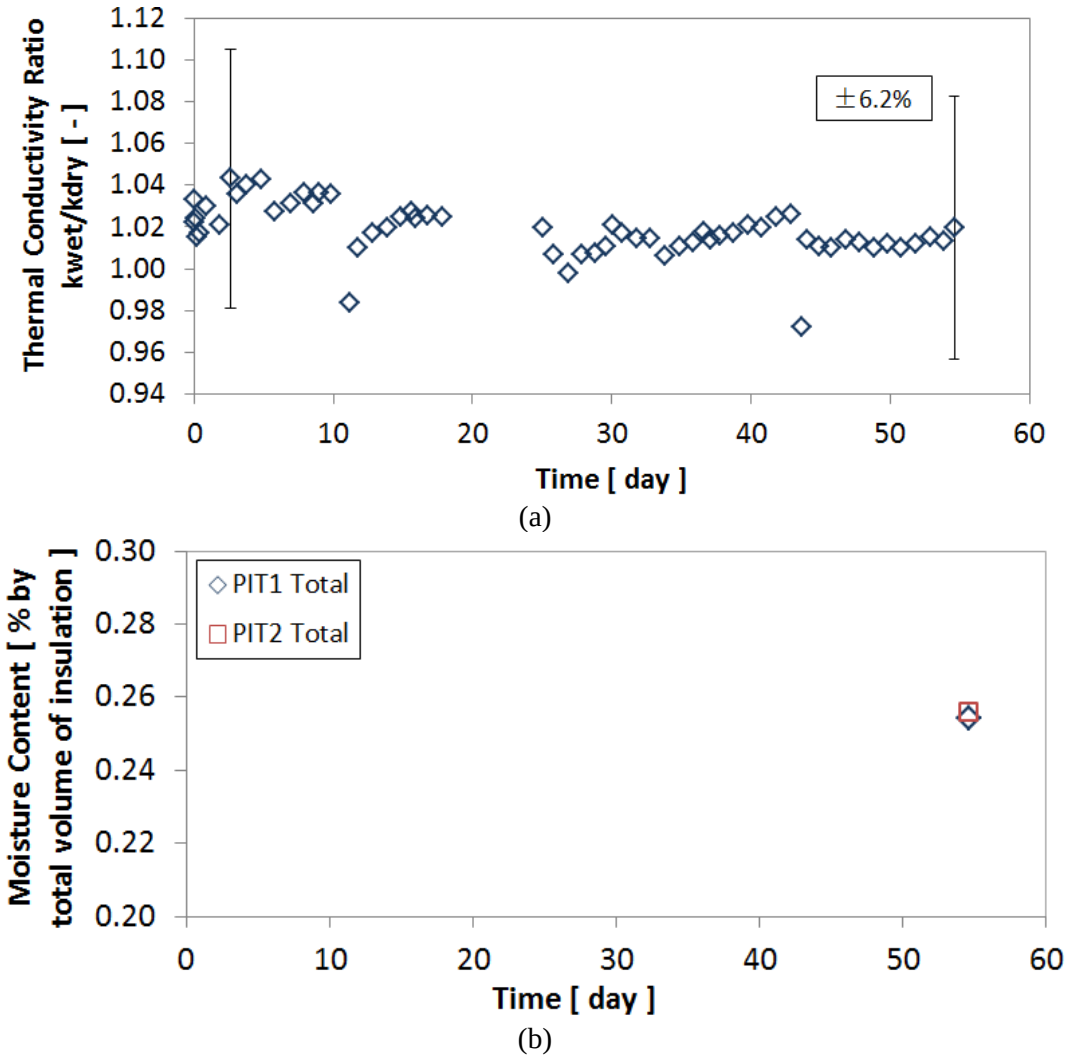

Figure 6.15: Experimental results on pipe insulation system FG4: (a) system thermal conductivity versus time during the wet test period (b) moisture content on the 2nd PIT and the 1st PIT on last day of wet test.

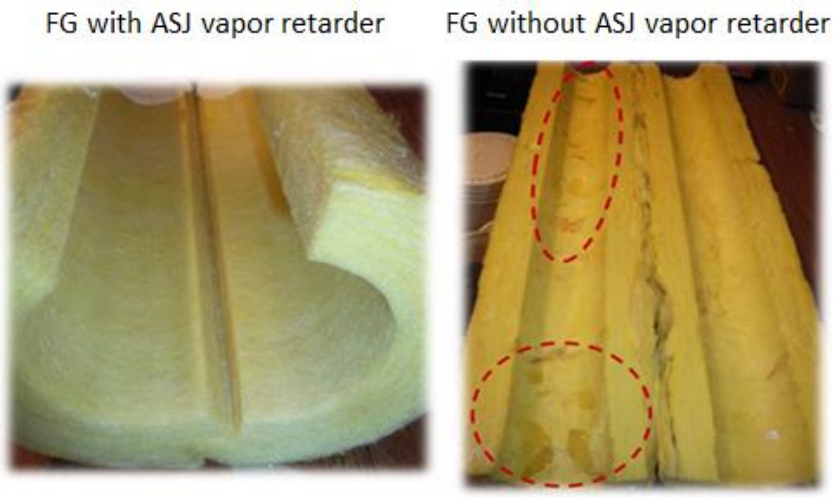

Figure 6.16: comparison of the interior surface of pipe insulation systems FG4 in medium humidity environment and FG3B in high humidity environment.

6.3.4 Fiberglass Pipe Insulation System FG5

This fiberglass pipe insulation system FG5 was tested with ASJ vapor retarder jacket installed on the exterior surface of the pipe insulation. The ASJ vapor retarder jacket was manufacturer installed on the fiberglass pipe insulation system. The ASJ lap joints were sealed using the pressure sensitive adhesive on the inside of one of the laps. This system had a nominal wall thickness of 1.5 in. (38.1mm) and was tested at 90°F (32°C), 83% R.H. for 66 days. The dew point temperature of the ambient air was 84.2°F (29.0°C) and the pipe insulation surface temperatures ranged from 86°F (30°C) to 88.5°F (31.4°C). In this system, the first PIT was used for thermal conductivity measurement, and the second PIT was installed with 6-in. sectioned pieces to measure the moisture content. Figure 6.18 shows the schematic of the installation, and Figure 6.17 shows the locations where Foster 90-66 vapor sealant was applied on the first PIT. There was no vapor sealant applied on the longitudinal joints of the two C-shells. On both PITs, ASJ butt joint strips were applied between each section in order to compensate for the discontinuity of ASJ vapor retarder jacket.

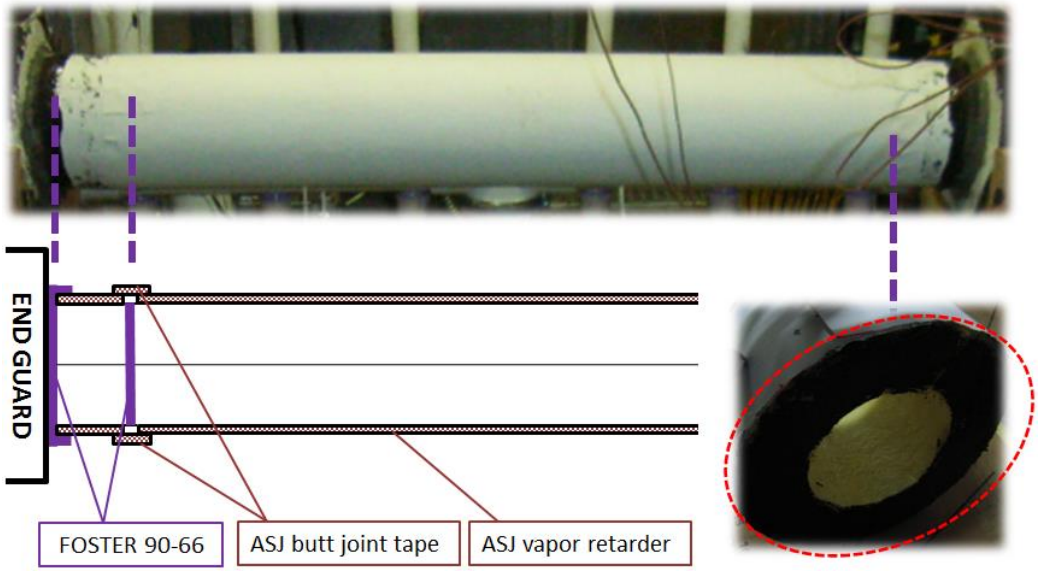

Figure 6.17: Photos and schematic of installation details of pipe insulation system FG5 on the 1st PIT.

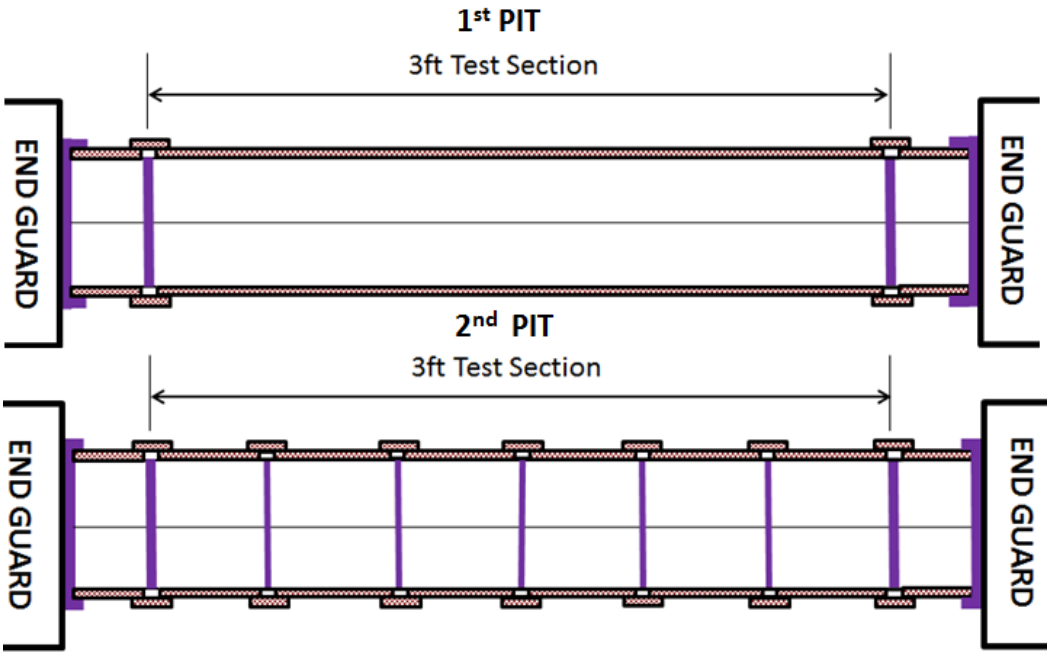

Figure 6.18: Schematics of installation of system FG5 for the wet test.

During the wet test, wet regions were observed on the exterior surface of the ASJ vapor retarder on both PITs, specifically on the bottom C-shells near the end sections as shown in Figure 6.19 (a) and (b). The formation of these condensation regions was due to a lower local temperature at the joints, where joint sealant was used to fill the micro gaps along the radial cross sections of two adjacent joints. As moisture accumulated on the exterior surface of the ASJ vapor retarder, the jacketing material became gradually wet and it darkened with time. A hypothesis was that, water condensation around the insulation joints might have entered the system through the micro-gaps of the ASJ butt joint strips. It should be noted that due to the low moisture content, the uncertainty was very high, and there was no specific correlation between the moisture content and thermal conductivity variation on the 1st PIT.

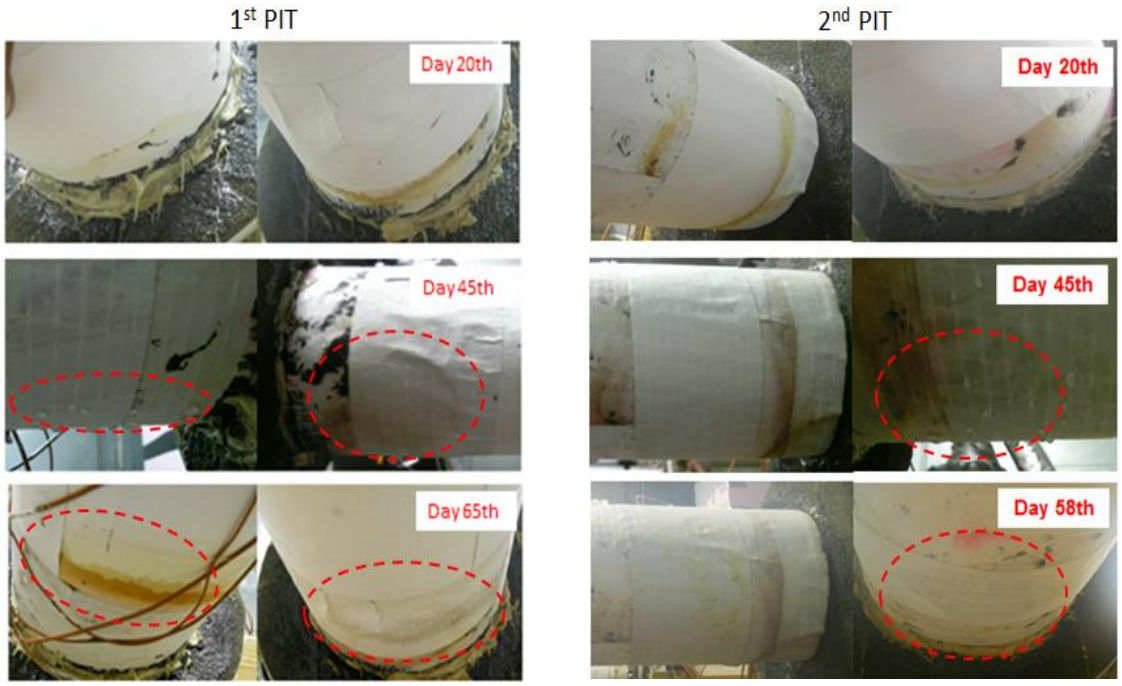

Figure 6.19: Development of wet regions on the exterior surface of pipe insulation system FG5 (a) fiberglass insulation test specimen on 1st PIT (b) fiberglass insulation test specimen on 2nd PIT.

Due to the existence of the ASJ vapor retarder jacket, the two-step variation observed in FG3A and FG3B was not obvious on fiberglass systems FG5, FG6 and FG7, because the vapor retarder jackets greatly reduced the transmission of water vapor into the fiberglass insulation specimens. It can be observed from Figure 6.20 (b) that at day 66, the thermal conductivity increased by about 7%. It should be noted that in Figure 6.20 (c), at day 10, 20 and 30, the moisture contents were measured at higher values than the remaining period of the moisture test. The reason to explain this phenomenon was the condensation formed at the bottom C-shells near the ends of the insulation specimen on the 2nd PIT, as shown in Figure 6.19 (b). During the measurement of the moisture content, the 6-in. sections at the two ends were measured first. The condensation at the bottom surface could have entered the insulation through unsealed gaps between the ASJ vapor retarder jacketing and the butt joint strips, and cause the inconsistent increase in the moisture content in the test samples at the ends. Therefore, it was reasonable to exclude the end sections because their moisture content was increased by a localized cooling phenomenon which was due to the interaction of the test specimen with the end thermal guard. The moisture content increased linearly with time until the last day of wet test as shown in the remaining data points in Figure 6.20 (c). Figure 6.20 (d) reported the periodical measurement of moisture content on PIT2 test insulation specimen and that of the insulation specimen on PIT1 at the last day of wet test. The moisture content on the 2nd PIT, at the last day of the wet test was higher than that on the 1st PIT. This was assumed to be the normal phenomenon because the insulation specimen on the 2nd PIT had more joints, and in addition it was disturbed at certain time intervals, more water vapor was likely to enter the insulation specimens on the 2nd PIT and cause the moisture content to increase. It should also be noted that the total moisture content of the insulation specimen on both PITs were less than 0.5% by volume, and the uncertainty was above $\pm$15%. It was observed from Figure 6.20 (a) that the thermal conductivity data appears to be discontinuous at day 10 and at

several other times. However, it should be emphasized that all the data in Figure 6.20 (a) have the uncertainty bars reported for two representative data points in the same figure.

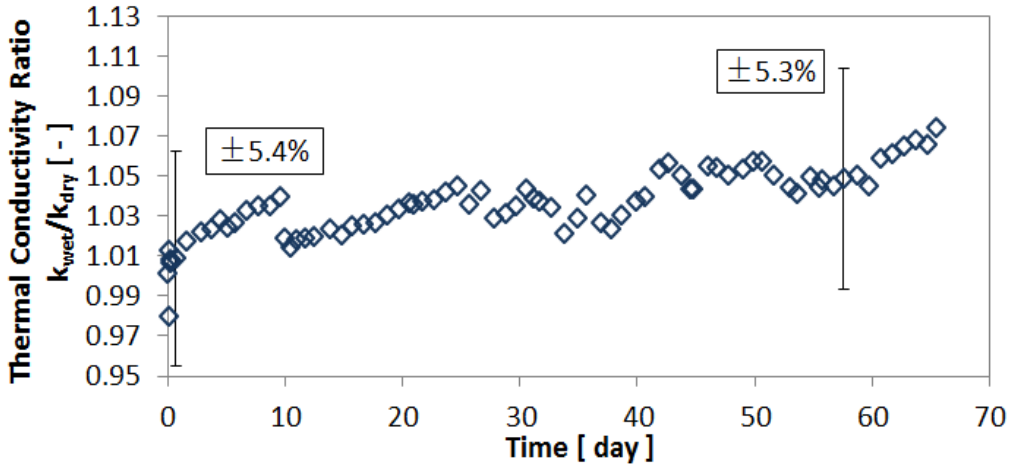

(a)

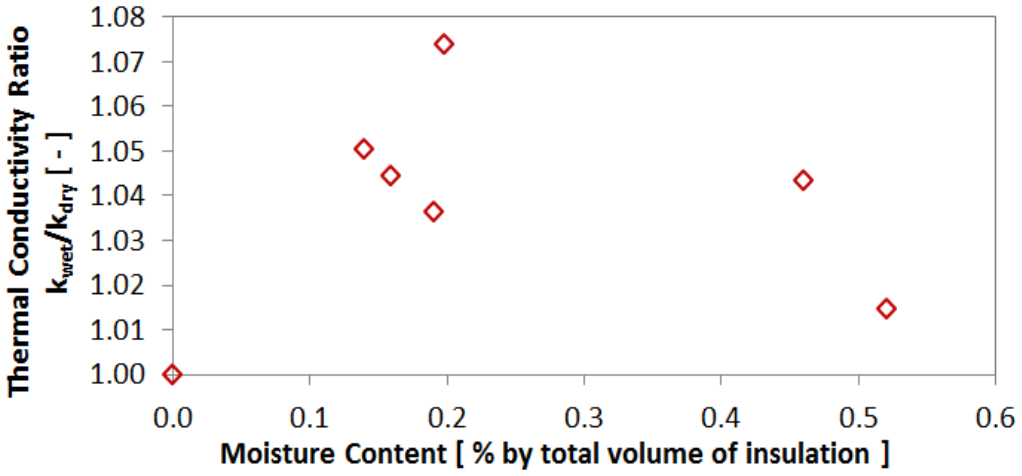

(b)

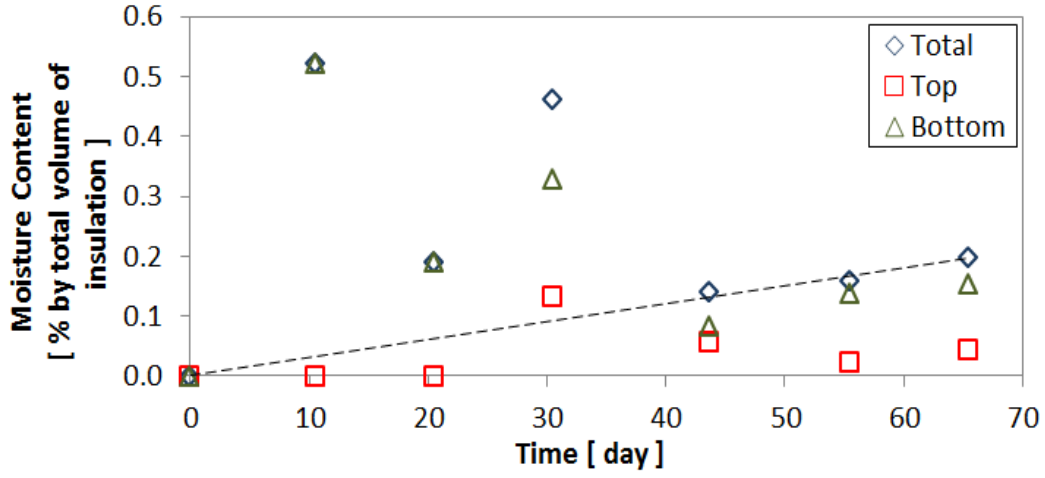

(c)

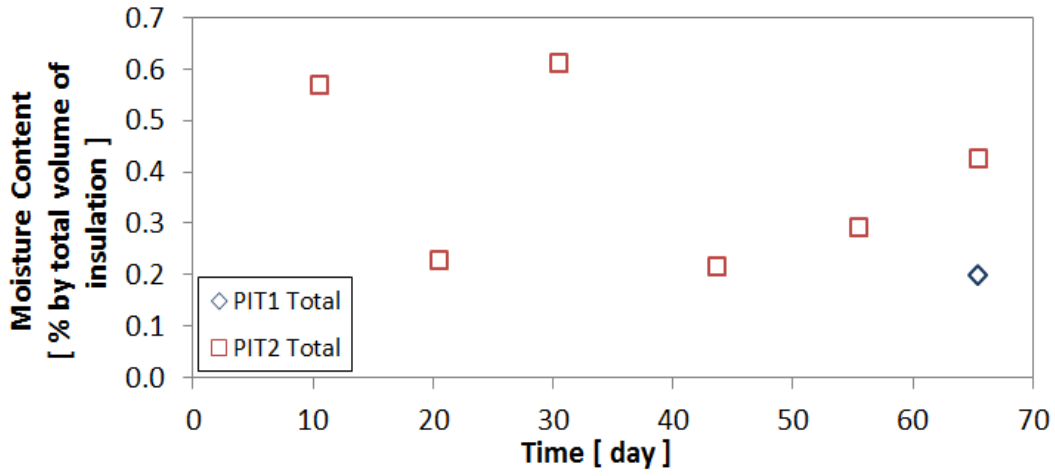

(d)

Figure 6.20: Experimental results on pipe insulation system FG5: (a) system thermal conductivity versus time during the wet test period (b) moisture accumulation during wet test (c) effect of moisture content on the pipe insulation system thermal conductivity ratio (d) periodical measurement of moisture content on the 2nd PIT and moisture content on 1st PIT at the completion of wet test.

6.3.5 Fiberglass Pipe Insulation System FG6

Fiberglass with a nominal wall thickness of 1.5 in. (38.1mm) was tested with ASJ vapor retarder jacket and then covered with 20 mil thick PVC jacketing, sealed at the joints. It should be noted that the ASJ vapor retarder jacket was manufacturer installed on the insulation system, while the PVC jacketing was installed above the ASJ vapor retarder by the authors according to the manufacturer recommendations. During the wet test of system FG6, the ambient temperature was controlled at about 90°F (32°C) and the relative humidity was set to 83 to 84% R.H. In this psychrometric condition, the air dew point was about 84.5°F (29.2°C).

Figure 6.21 shows the installation of system FG6. Foster 90-66 was used as the vapor sealant and applied on the cross-sectional end joints of the test specimen. There was not any vapor sealant applied on the longitudinal joints between the top and bottom C-shells. The fiberglass pipe insulation system FG6 was first installed with ASJ vapor retarder, and then covered with a 3.5ft-long piece of PVC jacketing. The PVC jacketing was sealed horizontally with PVC glue, and

vapor sealant Foster 90-66 was also applied on the two ends of the PVC jacketing along the circular edge perimeter of the PVC jacketing in order to eliminate any air gaps between the thermal guards and the PVC jacketing. The test specimen installed on the second PIT was divided into 6 small sections and each section was an exact replica of the test specimen installed on the first PIT.

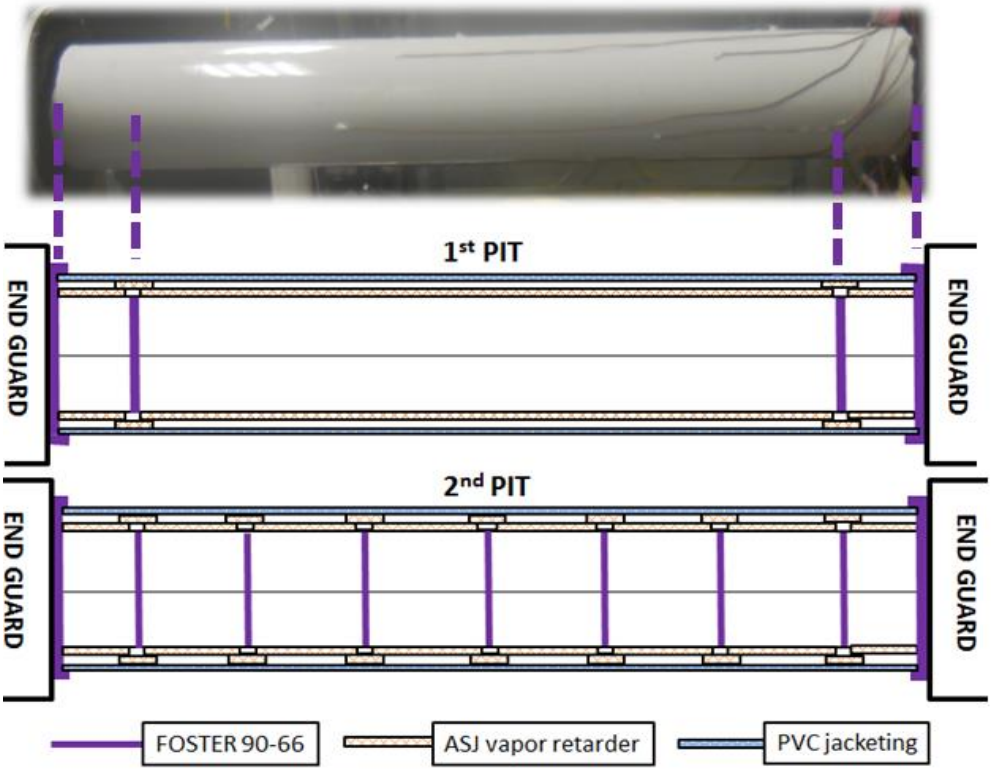

Figure 6.21: Photos and schematics of installation of system FG6 for the wet test.

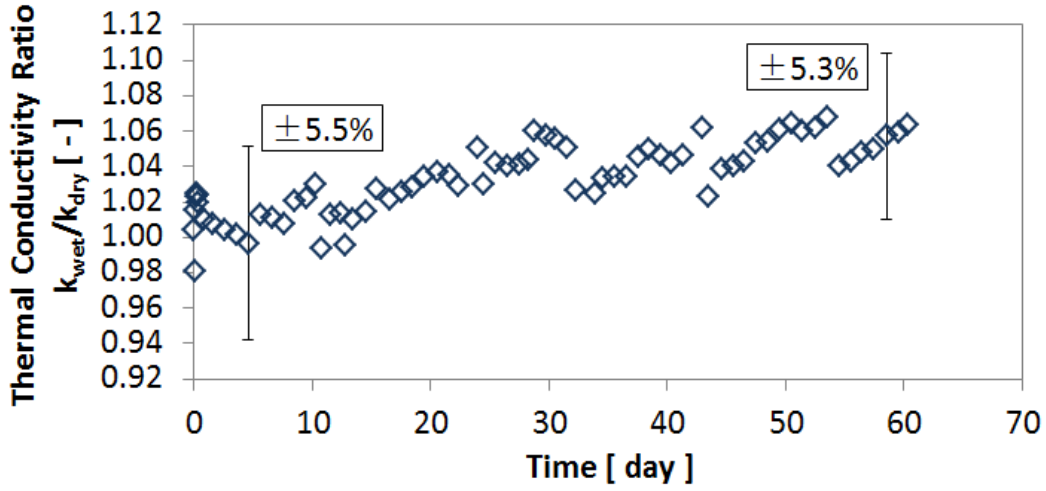
Thermal Conductivity Ratio
k_{wet}/k_{dry} [-]
1.12
1.10
1.08
1.06
1.04
1.02
1.00
0.98
0.96
0.94
0.92
±5.5%
±5.3%
0
10
20
30
40
50
60
70
Time [day]

(a)

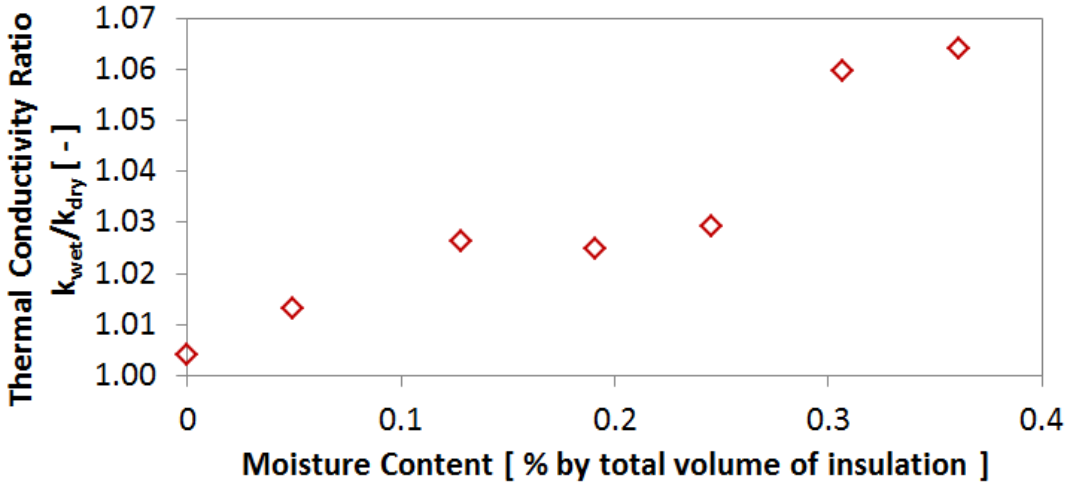
Thermal Conductivity Ratio
k_{wet}/k_{dry} [-]
1.07
1.06
1.05
1.04
1.03
1.02
1.01
1.00
0
0.1
0.2
0.3
0.4
Moisture Content [% by total volume of insulation]

(b)

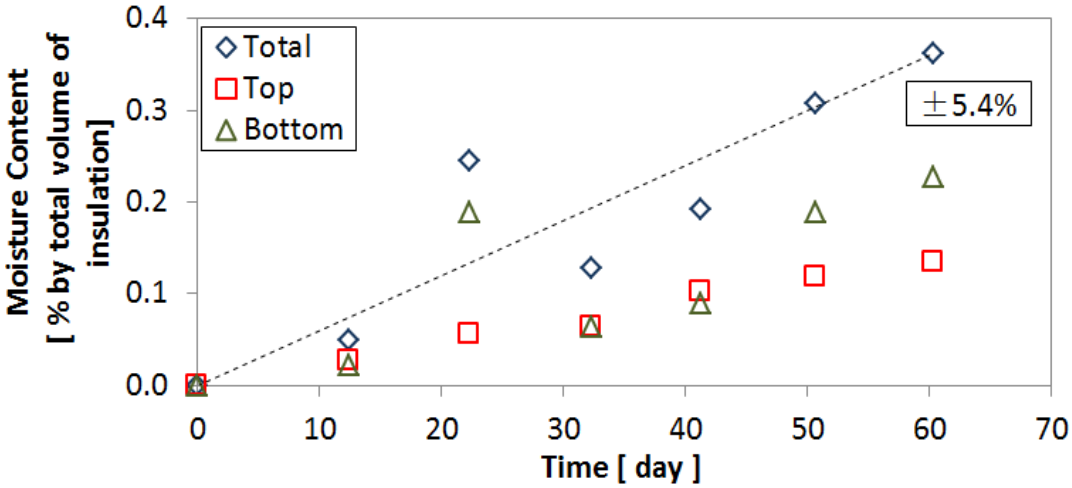
Moisture Content
[% by total volume of insulation]
0.4
0.3
0.2
0.1
0.0
Total
Top
Bottom
±5.4%
0
10
20
30
40
50
60
70
Time [day]

(c)

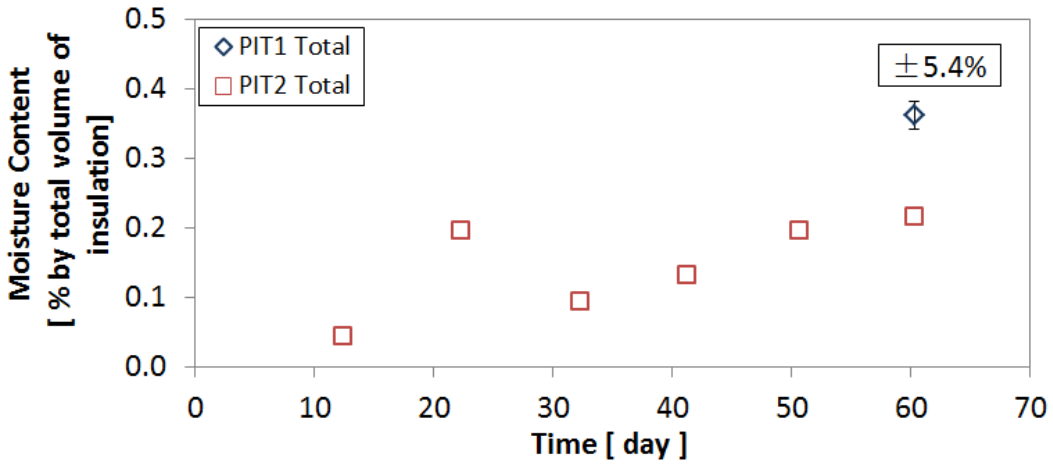

(d)

Figure 6.22: Experimental results on pipe insulation system FG6: (a) system thermal conductivity versus time during wet test period (b) moisture accumulation during wet test(c) effect of moisture content on the pipe insulation system thermal conductivity ratio (d) periodical measurement of moisture content on the 2nd PIT and moisture content on 1st PIT at the completion of wet test.

During the wet test of this system FG6, wet regions and water droplets were not observed on the exterior surface of the PVC jacketing. As shown in Figure 6.22(a) and (c), at the end of the wet test, the system thermal conductivity increased by about 7%, and the moisture content increased from 0 to about 0.35% by volume. The PVC vapor retarder was expected to have very low water permeability, less than 0.02 perm, and moisture could have entered the fiberglass insulation test specimen through the micro unsealed air gaps at the two ends, where the ASJ and PVC jackets were in contact with the thermal guards. The small amount of vapor ingress in the test specimen caused the system thermal conductivity to slightly increase during the 60 days of the wet test. Figure 6.22 (d) reported the periodical measurement of moisture content on PIT2 and the moisture content on PIT1 at the last day of wet test. The moisture content on the 2nd PIT was about 0.2% lower than that on the 1st PIT. This was caused by the fact that while the insulation test sample on the 1st PIT had the bottom C-shell water condensation at the two ends, the last insulation sample taken on the 2nd PIT did not have the condensation at the bottom C-shells at the two ends, which ruled out the possibility of water condensation entering the test insulation

specimen and causing the moisture content to increase. It was also observed in Figure 6.22 (a) that the data appeared to have discontinuity at some days. However, the small discontinuity steps are the results of the experimental error uncertainty of the measurements, which include the accuracy of the sensors, electric noise of the instrumentation, and electric interference with the power supply of the test facility equipment.

6.3.6 Fiberglass Pipe Insulation System FG7

This fiberglass pipe insulation system was tested with Polyester Foil Polyester (PFP) laminate vapor retarder jacket installed on the exterior surface of the insulation. The PFP vapor jacket was composed of a laminate consisting of 1 mil thick aluminum foil sandwiched between two layers of 0.5 mil thick polyester. And it was manufacturer installed on the pipe insulation systems. The lap joints were sealed using the pressure sensitive adhesive on the inside of one of the PFP vapor retarder laps. This fiberglass pipe insulation system FG7 had a nominal wall thickness of 1.5 in. (38.1mm) and a dark brown fiber color. It had a higher density of 3.86 lb/ft3 (62.2 kg/m3) than the fiberglass pipe insulation used in systems FG5 and FG6. Foster 90-66 was applied on the cross-sectional surfaces on both specimens installed on the first PIT and on the second PIT. Figure 6.23 shows the installation on the 1st PIT. PFP butt joint strips were overlapped in the regions between the insulation test specimen and the end sections, to compensate for the discontinuities of the PFP vapor retarder jacket, which was installed on the test specimen by the manufacturer.

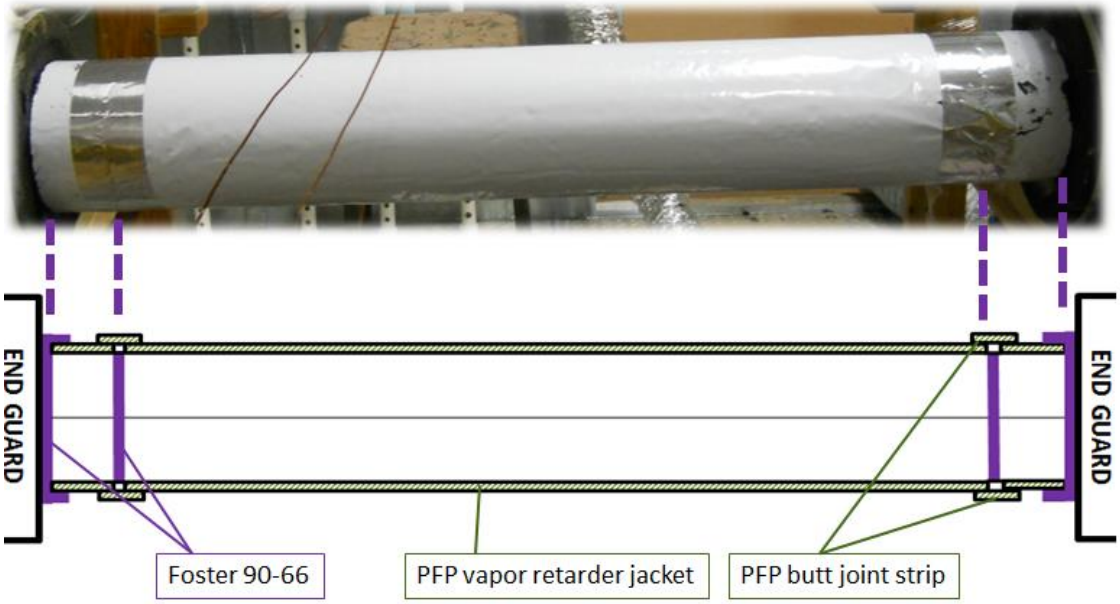

Figure 6.23: Photo and schematic of installation details of system FG7 on the 1st PIT.

This system FG7 was tested at 90°F (32°C) and 82.5% R.H. for 60 days. Similar to pipe insulation system FG5, wet regions were observed on the exterior surface of the PFP vapor jacketing paper of the bottom section at the ends of the test specimen during the wet test. Figure 6.24 (a) and (b) showed the locations and development of these wet regions. A possible reason that could explain the water condensation at the ends of the test specimen is shown in the infrared phots of both PITs in Figure 6.24 (c) and (d). It can be observed that in both infrared pictures, the local surface temperature at the two ends of the test specimen was about 2°F (1°C) lower than the middle section of the test insulation. This caused the surface temperature near the ends of the insulation test specimen to be lower than the ambient dew point temperature and led to water vapor condensation near these end regions.

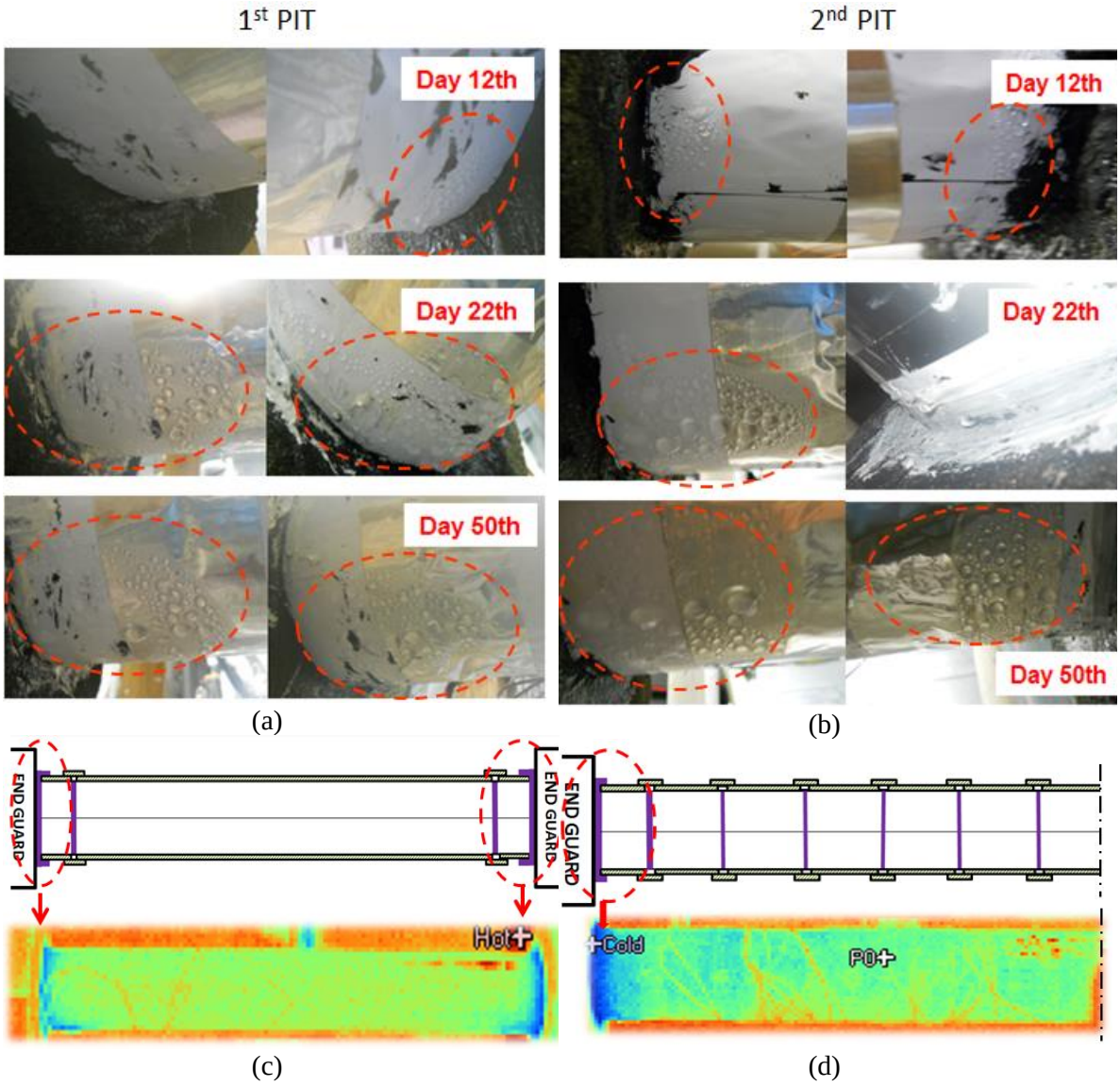

Figure 6.24: Development of wet regions on the exterior surface of pipe insulation system FG7 (a) fiberglass insulation test specimen on 1st PIT (b) fiberglass insulation test specimen on 2nd PIT (c) schematic and infrared photo of 1st PIT (d) schematic and infrared photo of 2nd PIT.

Figure 6.25 (a) shows that the system thermal conductivity ratio increased gradually from 1 to about 1.15 during the wet test period. Figure 6.25 (c) shows that at day 60, the system moisture content increased to about 1% by volume. It should be noted that on day 22, the moisture content increased significantly to 1.4% by volume. This phenomenon was very similar to what was observed on system FG5, and can also be explained by the water condensation on the bottom

surface of the vapor jacketing paper near the two ends of the test specimen. In this pipe insulation system FG7, water condensation on one of the end sections started to form at about day 10. The condensation region started from the region where the PFP vapor retarder jacket was in contact with the end thermal guards and then it expanded gradually toward the center part of the test specimen. At day 20, the condensation region was enlarged to cover part of the bottom surface of the 6-inch test section. It was likely that water condensation might have entered into the insulation specimen through micro gaps between the PFP vapor jacketing and the butt joint strip, and caused the large increase in the moisture content. This also could explain the measurement of the moisture content at day 20 shown in Figure 6.25 (c), because the moisture content was derived from the measurement of the 6-inch test section at the end. Therefore, it is reasonable not to consider the moisture content at day 22 because it was skewed by the localized cooling from the end side of the test specimen. If the moisture content at day 22 is not considered, the data in Figure 6.25 (c) suggest that moisture content increased gradually with time and the addition of water vapor condensation in the pipe insulation system augmented the thermal conductivity by about 13% in 60 days, as shown in Figure 6.25 (a). It was also observed in Figure 6.25 (d) that the moisture content of the test insulation specimen on the 1st PIT was higher than that on the 2nd PIT at the last day of the wet test. This was again caused by the fact that while the insulation test sample on the 1st PIT had the bottom C-shell water condensation at the two ends, the last insulation sample taken on the 2nd PIT did not have the condensation at the bottom C-shells at the two ends.

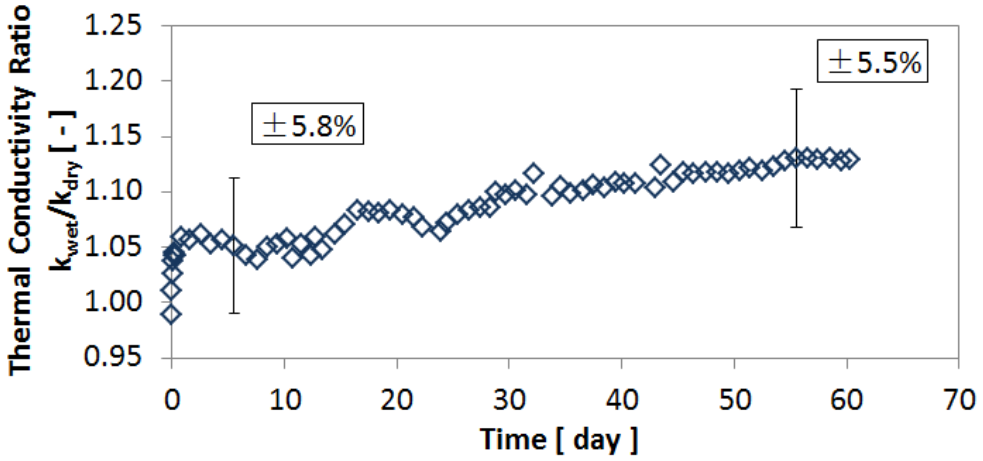
Thermal Conductivity Ratio
k_{wet}/k_{dry} [-]
1.25
1.20
1.15
1.10
1.05
1.00
0.95
±5.8%
±5.5%
0
10
20
30
40
50
60
70
Time [day]

(a)

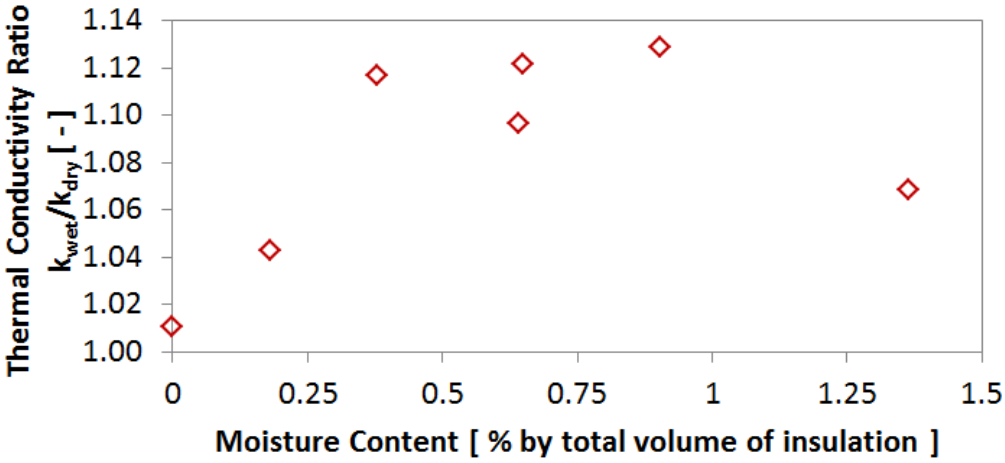
Thermal Conductivity Ratio
k_{wet}/k_{dry} [-]
1.14
1.12
1.10
1.08
1.06
1.04
1.02
1.00
0
0.25
0.5
0.75
1
1.25
1.5
Moisture Content [% by total volume of insulation]

(b)

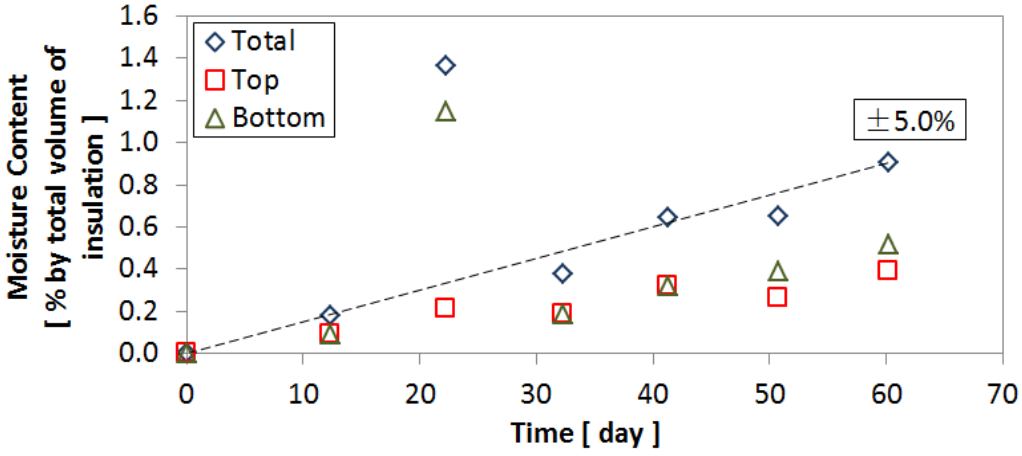
Moisture Content
[% by total volume of insulation]
1.6
1.4
1.2
1.0
0.8
0.6
0.4
0.2
0.0
Total
Top
Bottom
±5.0%
0
10
20
30
40
50
60
70
Time [day]

(c)

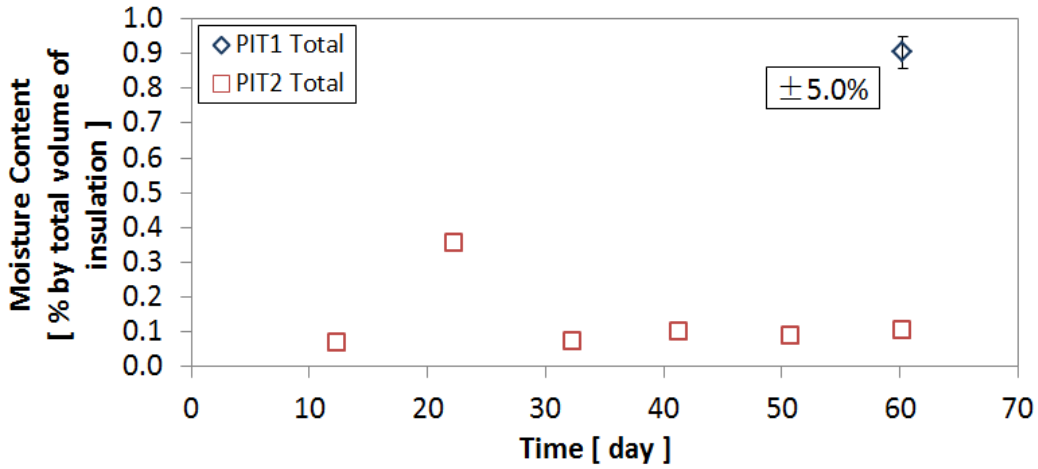

(d)

Figure 6.25: Experimental results on pipe insulation system FG7: (a) system thermal conductivity versus time during wet test period (b) moisture accumulation during wet test(c) effect of moisture content on the pipe insulation system thermal conductivity ratio (d) periodical measurement of moisture content on the 2nd PIT and moisture content on 1st PIT at the completion of wet test.

6.3.7 Elastomeric Pipe Insulation System ER1.5

Elastomeric rubber pipe insulation is typically manufactured as un-slit sleeves, or as an insulation wrap, and joint sealant might not be required during its installation. In the moisture test of the present work, elastomeric rubber pipe insulation system ER1.5 was tested as an insulation wrap with manufacturer applied adhesive tape along the longitudinal joint. A very thin plastic wire, visible in Figure 6.26, was wrapped around the exterior surface of the elastomeric rubber pipe insulation test specimen, in order to prevent the thermocouple wires from slipping away from the insulation surface. These thin plastic wires stayed on the test insulation specimen exterior surface during the entire period of the wet test. The test sample had a nominal wall thickness of 1.5 in. (38.1 mm) and the test samples were installed as one piece around the aluminum pipes of both 1st and 2nd PITs, as shown in Figure 6.26. The seam with the adhesive tape was installed as face-up on the top of the insulation system. During sampling procedure, one 6 in. (152.4 mm) section need to be directly cut out from the entire piece on the 2nd PIT. Then the void was replaced by another dry sample. Plastic film and joint sealant were used between the newly installed sample

and the adjacent pieces. Aeroseal was the sealant used at the edge seals and between each 6 in. (152.4 mm) sample. Elastomeric rubber pipe insulation system ER1.5 was tested at 90.6 °F (32.6 °C), with relative humidity at 83%, and the dew point was about 84.8 °F (29.3 °C). The wet test was conducted for 57 days. Wet regions were not observed on the exterior surface of the pipe insulation during the moisture test period. Two wet regions were observed on the interior surface, as shown in Figure 6.27, right after the test specimen was taken from the aluminum pipe. It seemed that the water condensate was on the interior surface but did not enter the insulation material because the water droplets were able to visibly move along the interior surface.

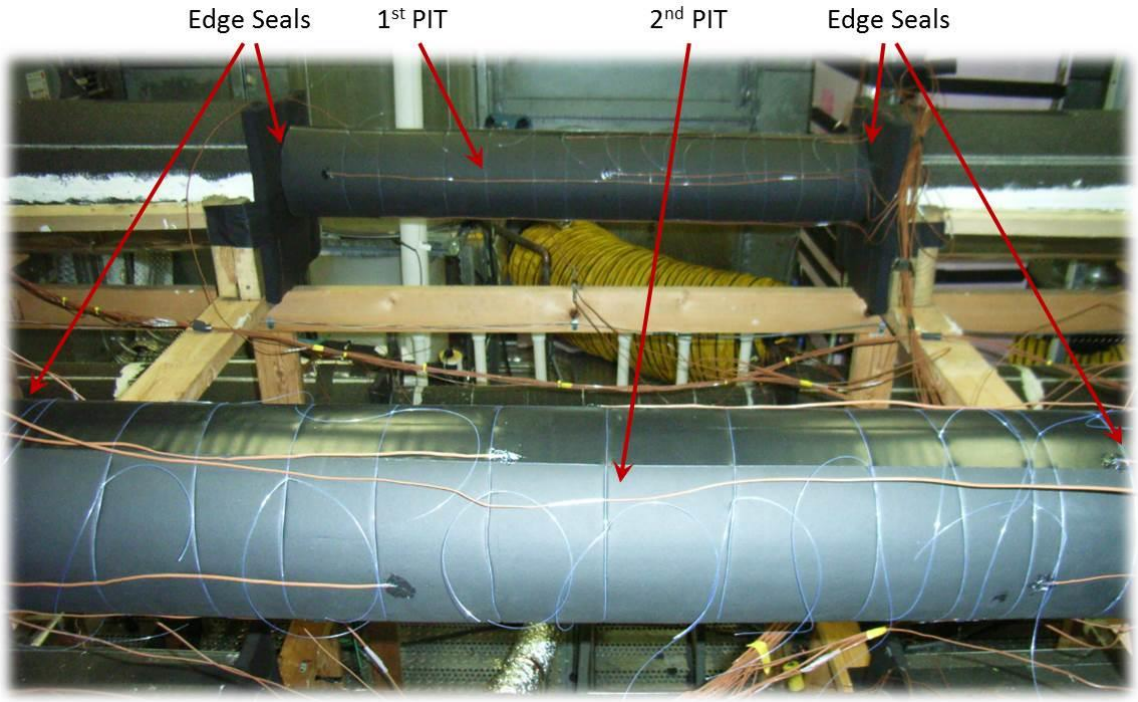

Figure 6.26: Photo of the installation details of pipe insulation system ER1.5 around the first PIT and the second PIT.

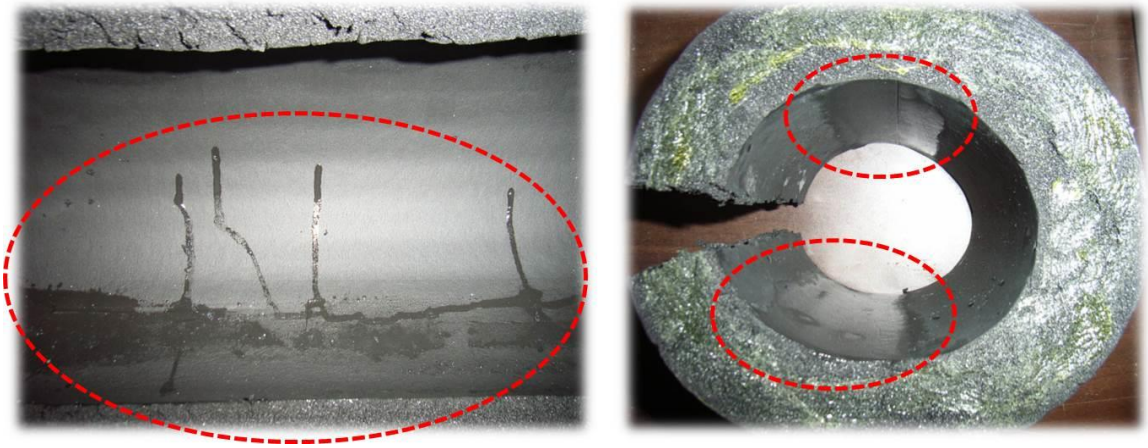

Figure 6.27: Photos of the interior surface of pipe insulation system ER1.5.

The experimental results on the variation of thermal conductivity and moisture content in the pipe insulation system ER1.5 are shown in Figure 6.28. In Figure 6.28 (a), a slight increase on the system thermal conductivity was observed at the beginning of the wet test, then the system thermal conductivity dropped back, and followed a gradually increase until the end of the test period. After 57 days of the continuous wet test, the system thermal conductivity increased by 4% when compared to the dry reference value at similar insulation mean temperature. Figure 6.28 (c) shows the moisture increased linearly with time. By the end of the moisture test period, the total water content was about 0.34% by volume. The amount of water trapped in the bottom shell was slightly higher than the one in the top shell. From the plot in Figure 6.28 (c), it seems that the system thermal conductivity follows a linear trend with the water content. Figure 6.28 (d) also showed that the moisture content of the test insulation specimen on both PITs at the last day of the wet test. The moisture content on the 2nd PIT was about 0.1% higher than that on the 1st PIT, and the possible reason was that more water vapor could have entered the insulation specimen on the 2nd PIT each time an insulation sample was taken, thus causing the moisture content on the 2nd PIT to be higher than the 1st PIT. The experimental uncertainty bars and noise interference

could also account for the appearing discontinuities of the thermal conductivity data points at several days in Figure 6.28 (a).

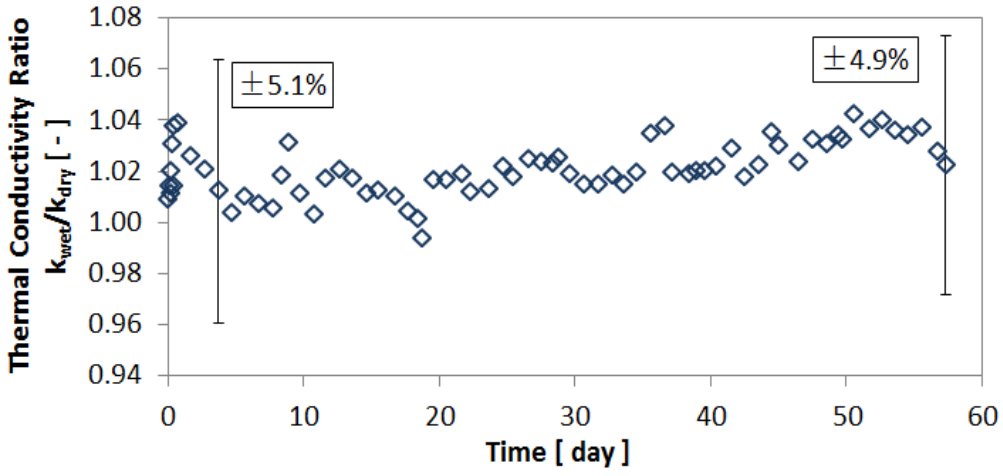

(a)

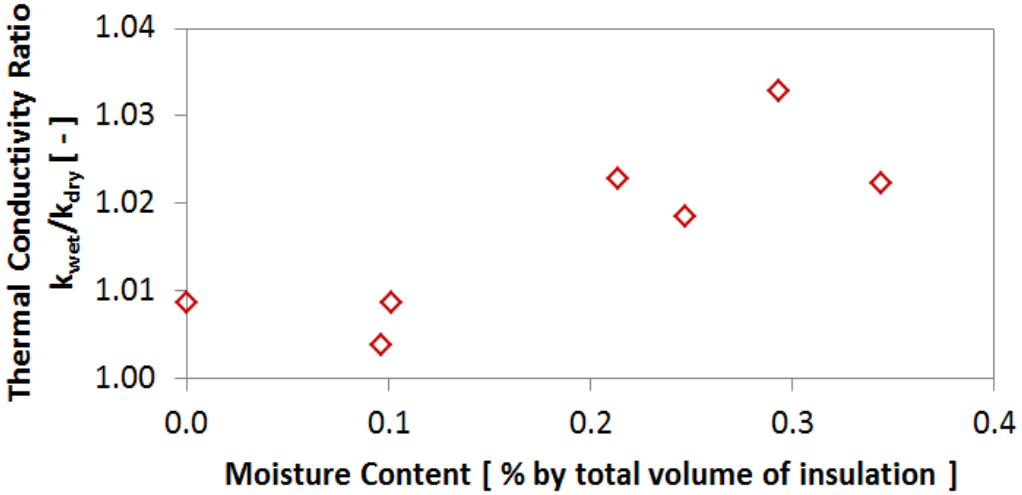

(b)

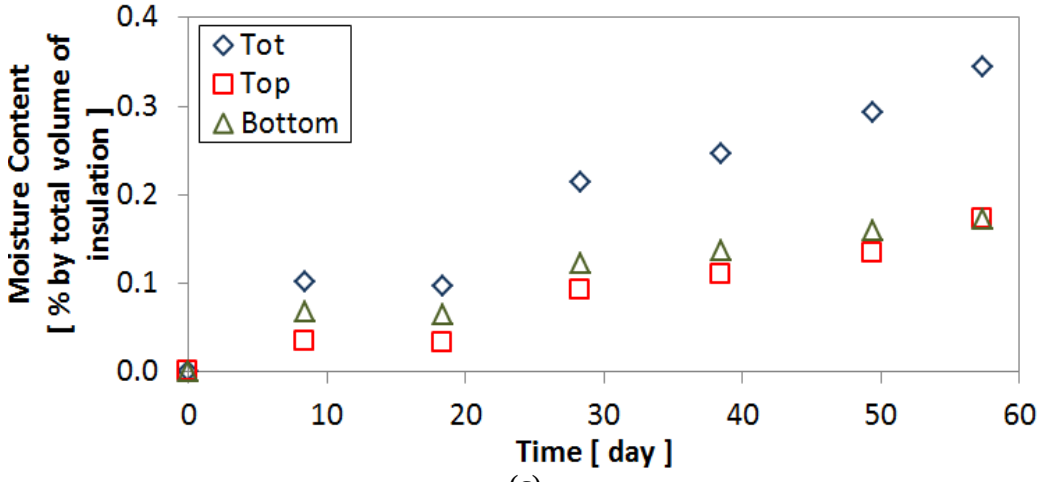

(c)

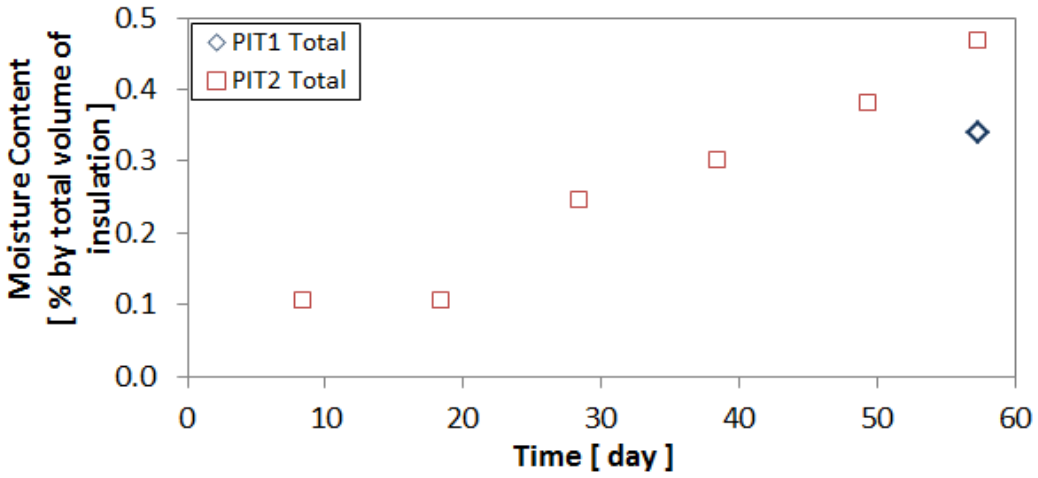

(d)

Figure 6.28: Experimental results on pipe insulation system ER1.5: (a) system thermal conductivity versus time during wet test period (b) moisture accumulation during wet test (c) effect of moisture content on the pipe insulation system thermal conductivity ratio (d) periodical measurement of moisture content on the 2nd PIT and moisture content on 1st PIT at the completion of wet test.

6.3.8 Cellular Glass Pipe Insulation Systems CGA and CGB

Cellular glass pipe insulation was tested twice at the similar ambient condition. The difference between system CGA and CGB is the aluminum pipe and the insulation fabrication joints. In the system CGA, cellular glass pipe insulation was installed around the bare aluminum pipe with thermocouple grooved exposed to the interior surface of the test sample, and in the system CGB, the aluminum pipe was sealed with aluminum tape and painted black to minimize radiation effects. Fabrication joints were visibly observed for the insulation samples of CGA but not for the insulation samples of CGB. The test samples in both systems had a nominal wall thickness of 1.5 in. (38.1 mm). Boss 368 butyl rubber sealant was applied as the joint sealant, and was also used for the edge joints on both PITs. System CGA was tested at an ambient temperature around 90°F (32 °C), and the relative humidity at 83%. At this condition, the dew point was about 84.8 °F (29.3 °C). System CGB was tested with ambient temperature at 90 °F (32 °C), relative humidity

at 83%, and the dew point was around 83.9°F (28.8 °C). The test length for system CGA and CGB are 57 and 64 days, respectively.

For both cellular glass pipe insulation systems, wet regions were not observed on the insulation surface, but a large amount of water condensate occurred near the joint sealant regions, and some water condensate dripped visibly along the exterior surface of the bottom C-shell, as shown in Figure 6.29. By the end of the moisture test, more water was observed to accumulate in the bottom C-shell on system CGA, and formed larger wet area at the interior surface. For the top shell, the wet region only formed next to the test insulation specimen ends, as circled out in Figure 6.30 (a). In pipe insulation system CGA, one piece of the test sample, which used as the bottom shell, had fabrication joints and wet regions appeared next to those fabrication joints on both interior and exterior surfaces. The fabrication joints and wet regions are shown in Figure 6.30 (b).

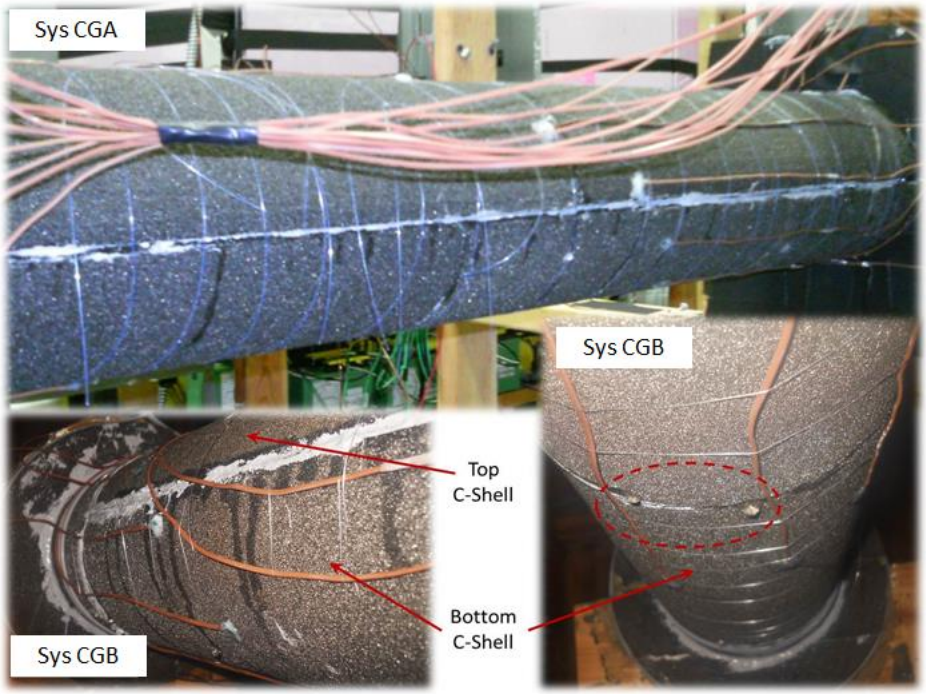

Figure 6.29: Photos of exterior surface condensation on pipe insulation system CGA and CGB.

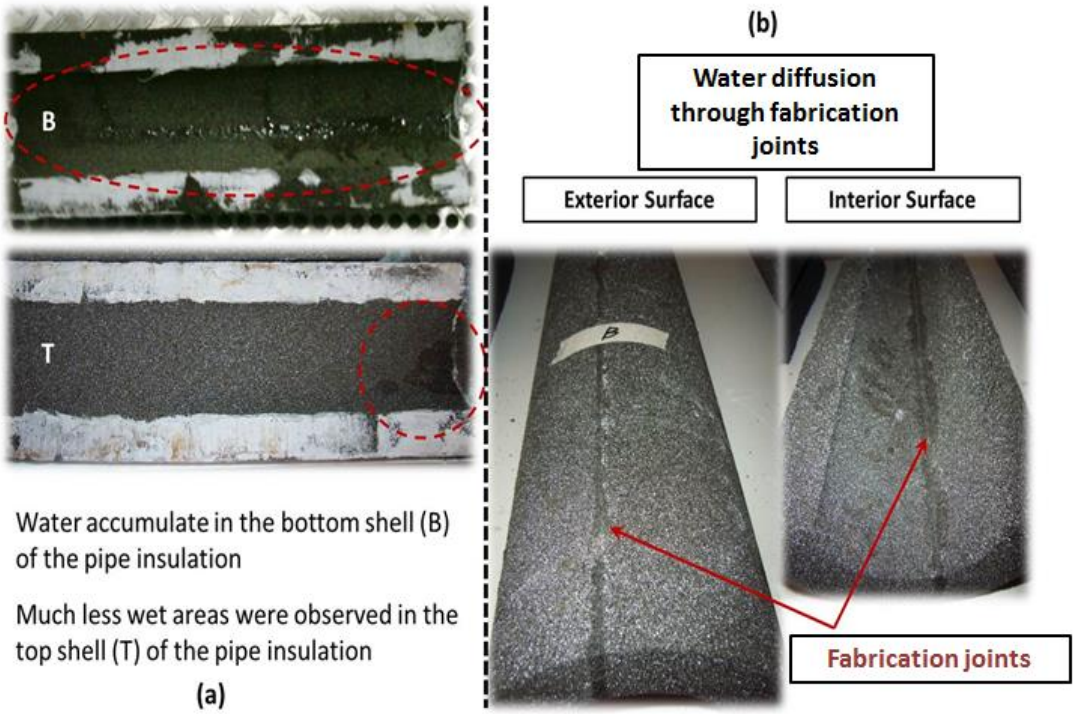

Figure 6.30: Photos of wet regions on pipe insulation system CGA.

The experimental results on the variation of thermal conductivity and moisture content in pipe insulation systems CGA and CGB are shown in Figure 6.31. In both systems, the thermal conductivity increased slightly at the beginning of the moisture test. In system CGA, the system thermal conductivity increased by 7% on day 15, and was almost constant until the end of the moisture test. The system thermal conductivity of CGB increased as well but it was more gradual than that of CGA, and showed a continuous increase until the last day of wet test period. Due to the small amount of water collected in the systems, the uncertainties in both cellular glass pipe insulation systems exceeded 15%. In system CGA, the total moisture content was 0.32% by volume after 57 days of the wet test. For system CGB, the moisture content was measured of 0.27% by volume after 64 days of test. One possible reason for the fact that system CGA was found at higher thermal conductivity and moisture content was the presence of fabrication joints. It should be noted that the difference on the results between these two systems were within the uncertainty

range of the test apparatus. Figure 6.31 (d) also compared the periodical measurement of test insulation specimen on the 2nd PIT with the total moisture content on the 1st PIT at last day of the wet test for both systems CGA and CGB. For CGA, the total moisture content on 2nd PIT at the last day of the wet test was lower than that on the 1st PIT, and this was probably caused by the fact that the last sample on the 2nd PIT had fewer fabrication joints, which introduced less water vapor condensation and thus leading to lower moisture content. It should also be noted that due to the low moisture content on both 1st PIT and 2nd PIT, as well as the localized water vapor condensation on the joint sealant areas or the fabrication joints areas, the moisture content on both PITs did not have certain patterns.

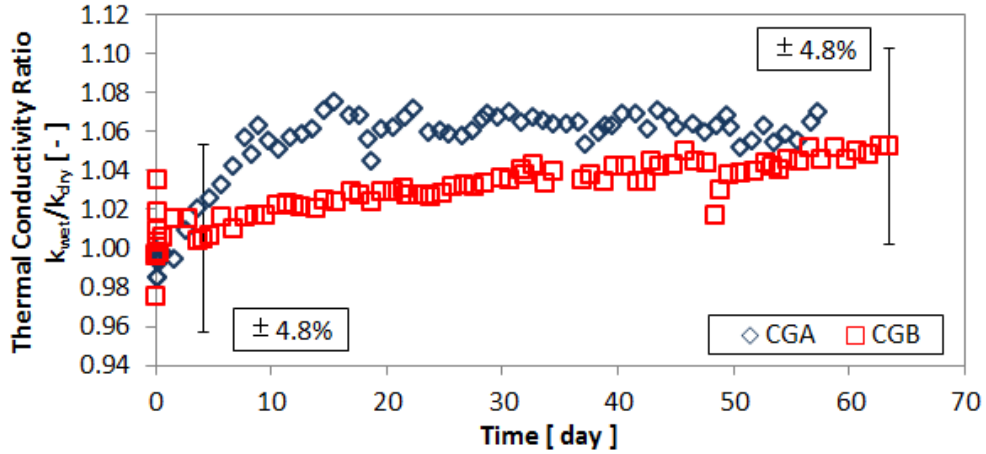

(a)

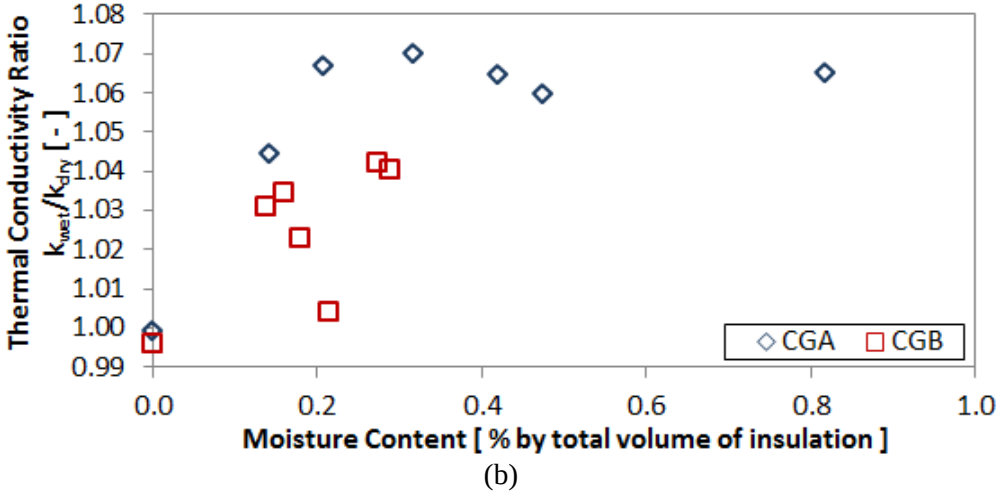

(b)

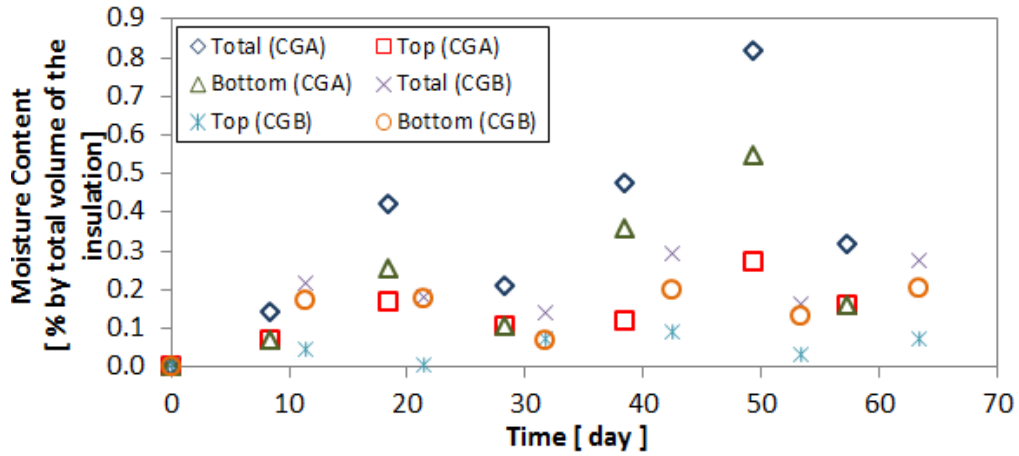

(c)

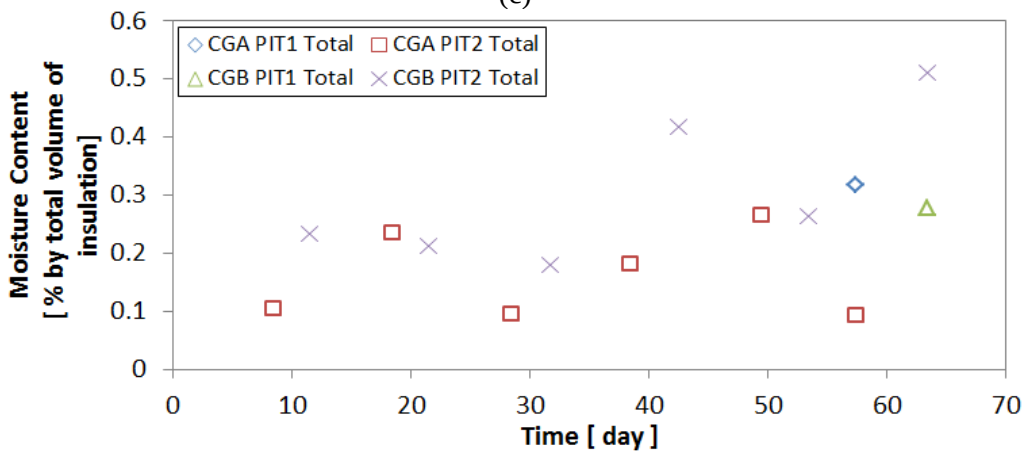

(d)

Figure 6.31: Experimental results on pipe insulation systems CGA and CGB: (a) System thermal conductivity versus time during wet test period (b) Moisture accumulation during wet test (c) Effect of moisture content on the pipe insulation system thermal conductivity ratio (d) periodical measurement of moisture content on the 2nd PIT and moisture content on 1st PIT at the completion of wet test.

6.3.9 Polyisocyanurate Pipe Insulation System PIR1

Polyisocyanurate (PIR) pipe insulation is a closed cell insulation for mechanical pipe insulation system applications. The PIR pipe insulation system PIR1 had a nominal wall thickness of 1 in. (25.4mm). A polymer polyvinylidene chloride (PVDC) film vapor retarder jacket was used with PIR and it consisted of a film of barrier PVDC coextruded with other polymers that provided strength and support. It should also be noted here that the PVDC vapor retarder jacket was

manufacturer installed on the PIR pipe insulation system. Figure 6.32 (a) shows the installation details of the PIR test specimen with the PVDC vapor retarder. Figure 6.32 (b) is an overview of the PIR insulation systems around the first PIT and the second PIT. The thermal conductivity was measured from the first PIT and the moisture content was measured from the six small sections installed on the second PIT. It should be noted that Foster 90-66 vapor sealant was not used on the cross section areas of the six 6-in. sections. This is because each 6-in. section had to be taken out at regular intervals during the wet test period but without damaging the adjacent sections. Unfortunately Foster 90-66 was an adhesive vapor sealant compound and it was not possible to remove each section without damaging the adjacent ones when this adhesive sealant was used.

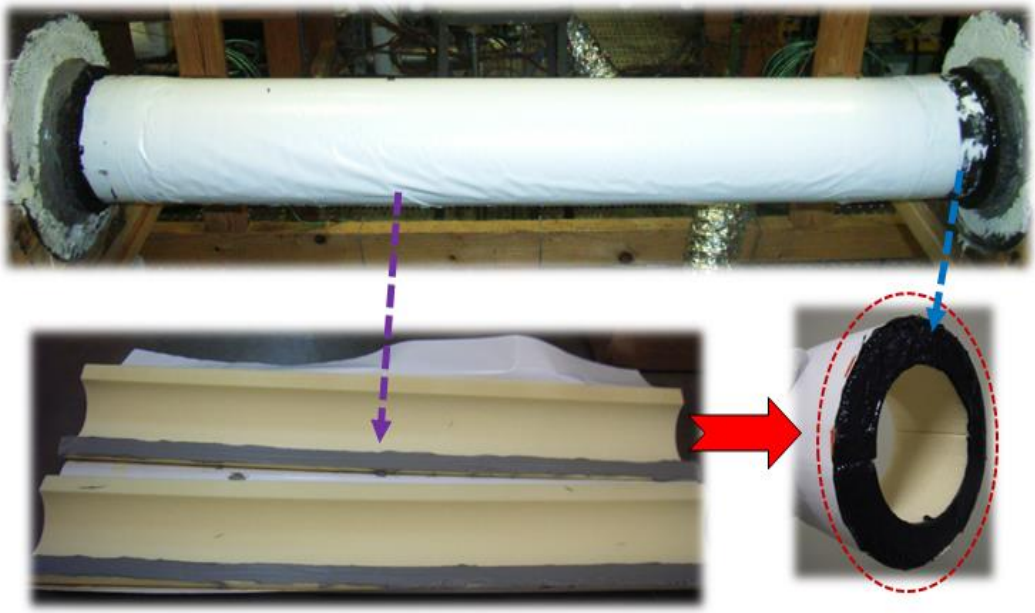

(a)

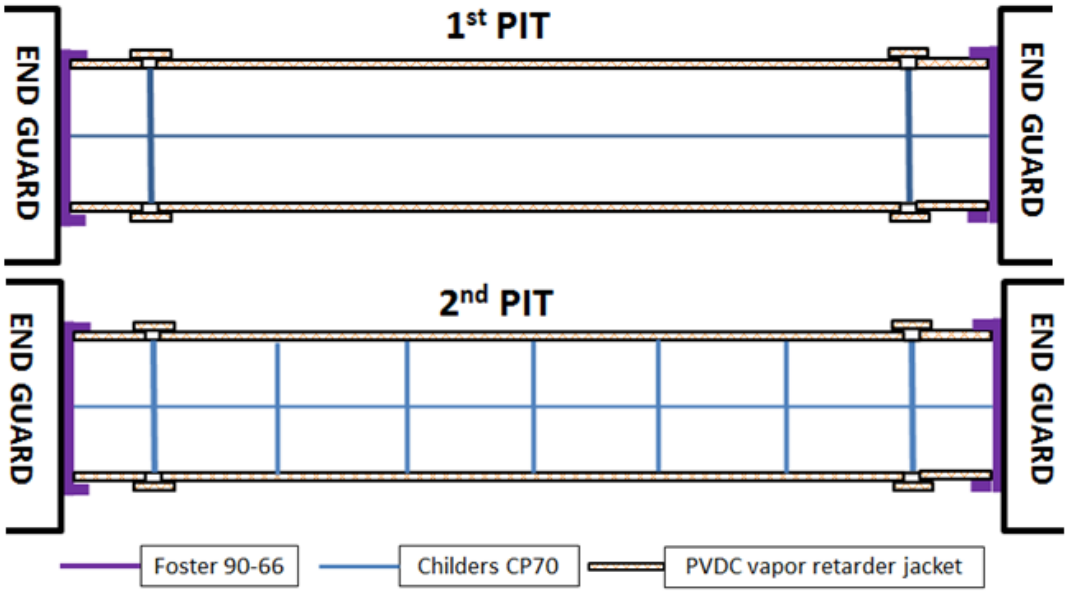

(b)

Figure 6.32: Photos and schematic of installation of pipe insulation system PIR1: (a) PIR pipe insulation test specimen on 1st PIT (b) schematic of installation details on both PITs.

To predict the moisture ingress on the long insulation test specimen installed on the 1st PIT, where only the initial and final values of the moisture content were measured, the intermediate moisture content data measured from the pipe insulation system installed on the 2nd PIT were used. The data were curve fit to generate a function of moisture content with time. For the 6 samples on the 2nd PIT, only the second and third sample showed total moisture content of 0.14 and 0.13% by total volume, while the other four samples showed basically 0% moisture content. This was due to the limitation of the sensitivity of the scale used for measuring the weight of the wet samples. It appeared that the moisture content inside the test specimen was sometimes below the sensitivity of the scale and thus it was defined to be 0%. At the 65th day of the wet test period, the moisture content on the 1st PIT was measured and resulted in about 0.1% by total volume. In this case, because the moisture content on the 2nd PIT was quite small and practically constant during the entire wet test period, we assumed that the moisture content in the PIR insulation on the 1st PIT was also small and practically constant throughout the wet test period. It should be

also noted that during the wet test period, condensation droplets were observed on the exterior surface of the jacket. The dew point temperature of the ambient was 84.0°F (28.9°C) and the pipe insulation surface temperature ranged from 86.9°F (30.5°C) to 87.3°F (30.7°C). However, as shown in Figure 6.33(b), the presence of joint sealant decreased the local surface temperature in the neighbor regions by about 1.8°F (1°C) with respect to the average exterior surface temperature of the pipe insulation system. This yielded to visible water droplet condensation covering exactly the joint lines of the pipe insulation system. It was possible that the condensation droplets on the exterior surface of the PVDC vapor retarder jacket entered the test specimen through micro unsealed gaps between the vapor jacket layers, causing the thermal conductivity of the test specimen on the 1st PIT to slightly increase with time. This could also be the reason for the insulation thermal conductivity on the 1st PIT to gradually increase by 4%, as can be seen from Figure 6.34(a). It should also be noted that since that moisture content on both PITs was below 0.2% by volume, the uncertainty exceeded 20%. In Figure 6.34 (d), it also can be seen that the total moisture content on 1st PIT at the last day of the wet test was higher than that on 2nd PIT. The possible reason to explain this phenomenon was that the last insulation sample on the 2nd PIT did not have water condensation on the bottom C-shells at the two ends, while the 3-ft. section on the 1st PIT had the condensation phenomenon at the two ends. And therefore, the moisture content of the insulation sample on 2nd PIT at the last day of wet test was not impacted by the possible intrusion of water vapor condensation. It was finally observed that while the thickness of the pipe insulation system was purposely selected to avoid condensation on the exterior surface, the presence of joints and joint sealant caused significant water droplet condensation at the joints. Thus, the thickness of the pipe insulation system should account for the local temperature near the joints in order to completely avoid condensation on the exterior surface of mechanical insulation systems when they are operating below ambient temperature in high humidity environments.

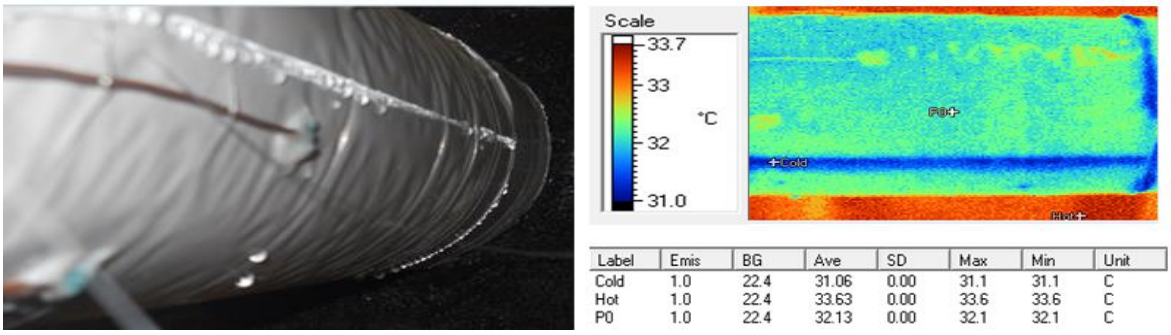

(a) (b)

Figure 6.33: (a) condensation following precisely the joint sealant areas on the pipe insulation system (b) infrared image showing the temperature difference between the region near the sealed joints and rest of the insulation

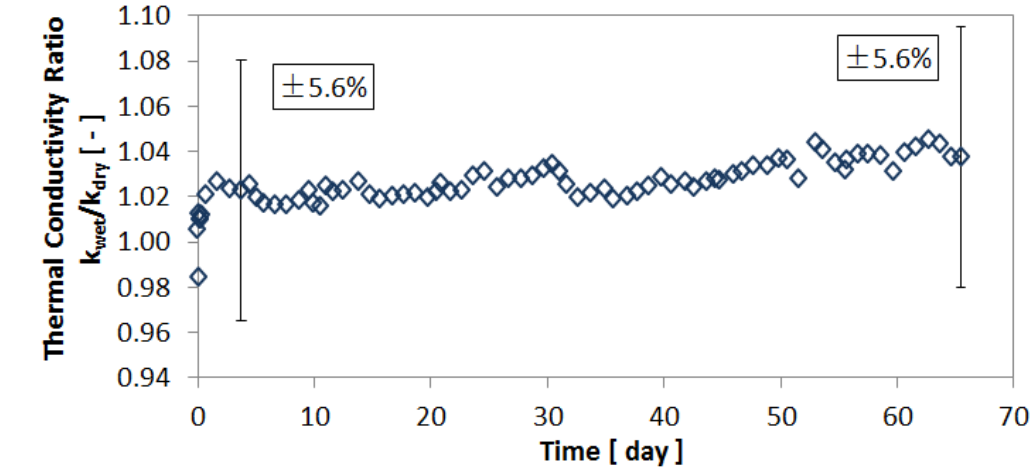

(a)

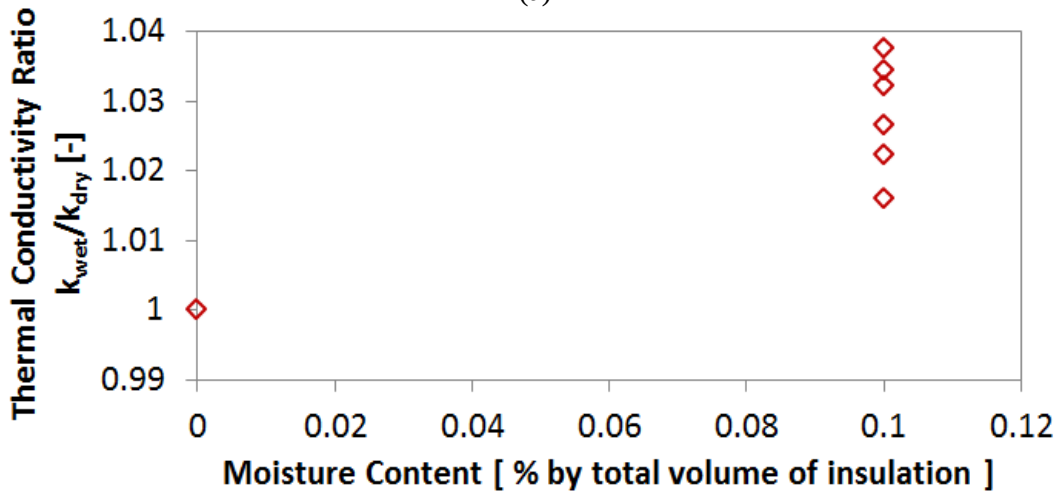

(b)

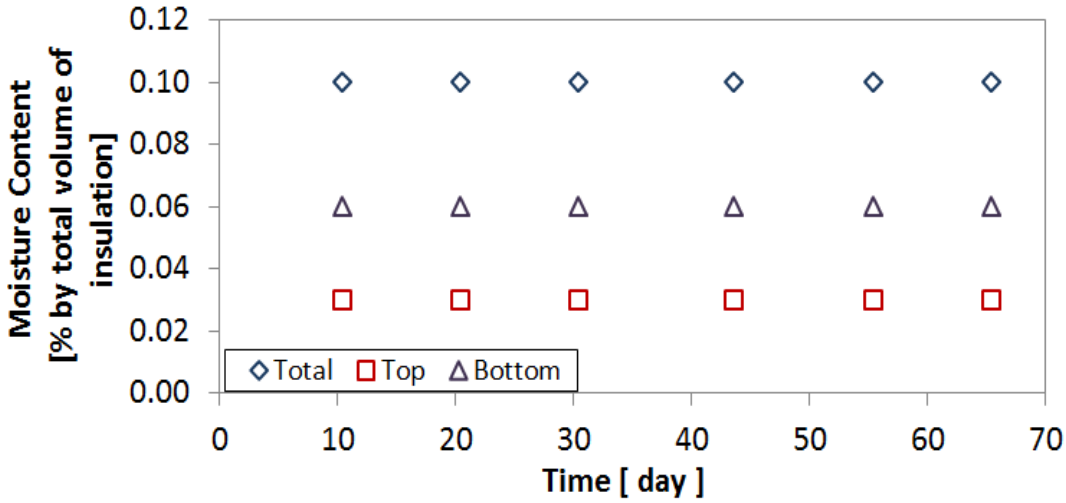

(c)

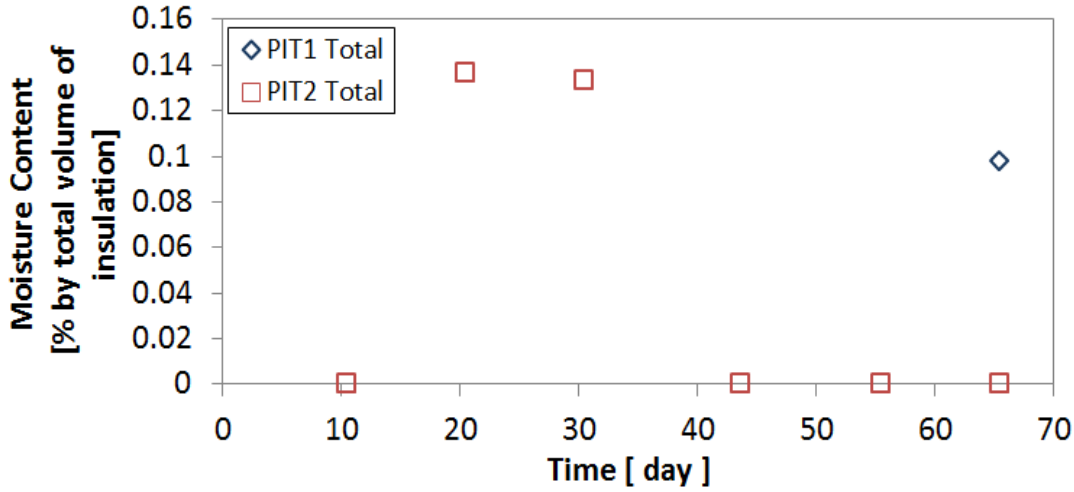

(d)

Figure 6.34: Experimental results on pipe insulation systems PIR1: (a) system thermal conductivity versus time during wet test period (b) moisture accumulation during wet test (c) effect of moisture content on the pipe insulation system thermal conductivity ratio (d) periodical measurement of moisture content on the 2nd PIT and moisture content on 1st PIT at the completion of wet test.

6.3.10 Polyisocyanurate Pipe Insulation System PIR1.5

The system PIR1.5 has a nominal wall thickness of 1.5 in. (38.1mm) and was tested without vapor retarder jacket. The wet test condition was set with the ambient temperature at 107°F (41.7°C), and the relative humidity at 81%. In this condition, the dew point temperature was about 100°F (37.8°C). Childers CP-70 was used as the vapor sealant and applied on all the

longitudinal and butt joints in the PIR pipe insulation system. Foster 90-66 was applied on the cross sectional surfaces between the end sections of the test specimen and the thermal guards of the test apparatus, which were made of cellular glass insulation. It should be emphasized that all the joint sealant was applied as uniformly as possible with 1/8 in. thickness layer on the entire longitudinal and cross sectional surfaces. Figure 6.35 below shows the schematic of the installation details of the system PIR1.5.

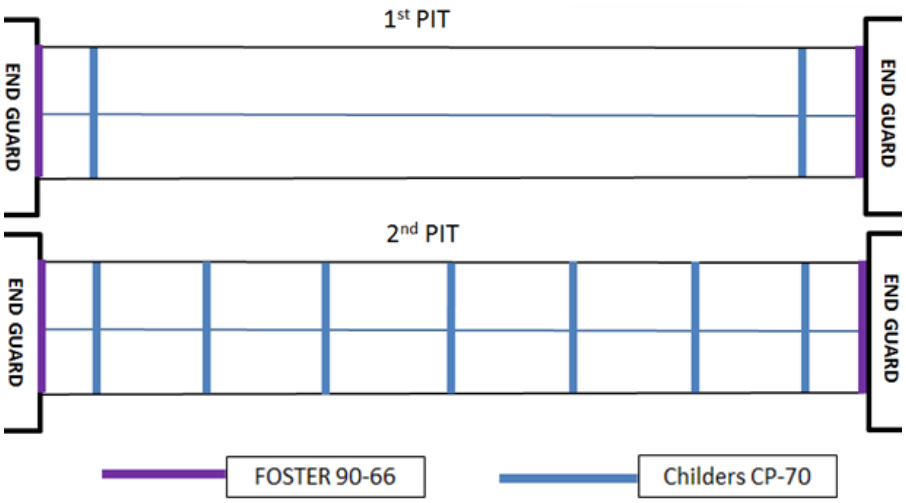

Figure 6.35: schematisc of installation of pipe insulation system PIR1.5.

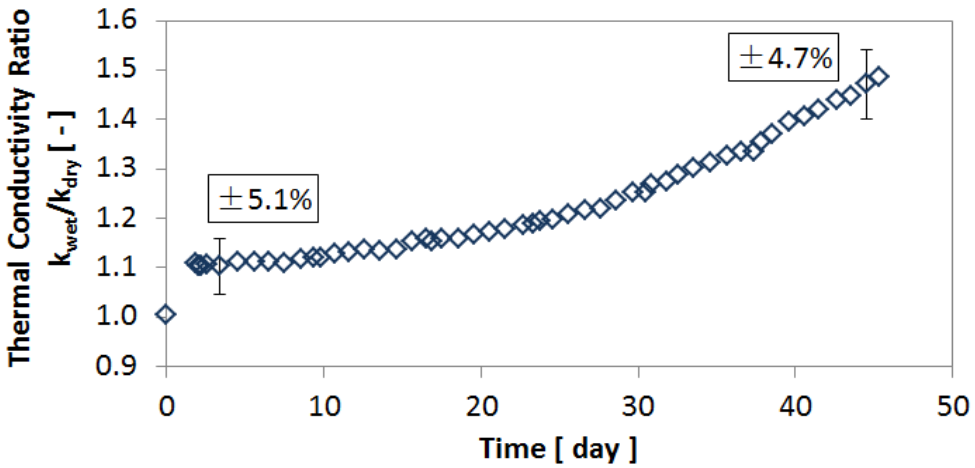

(a)

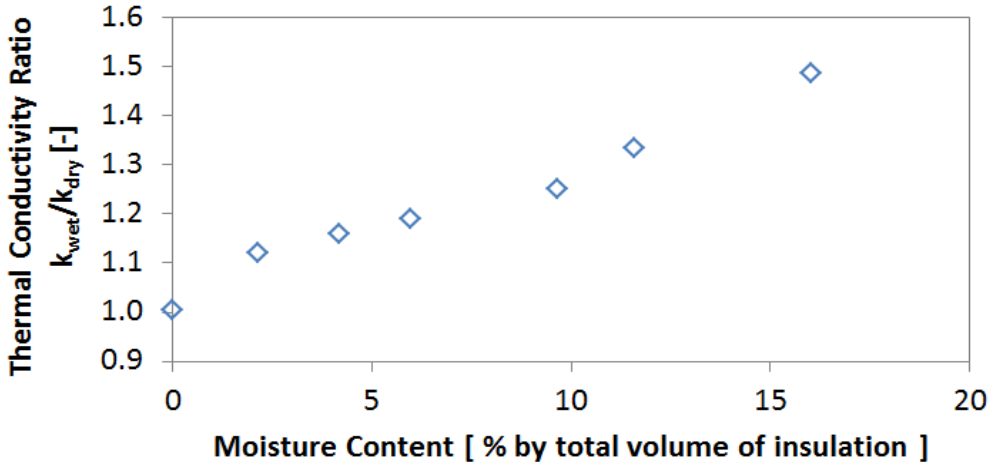

(b)

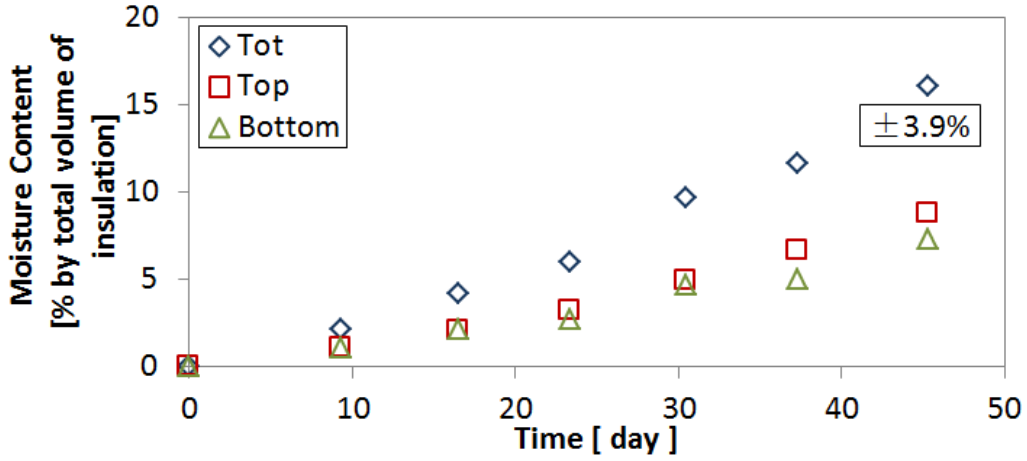

(c)

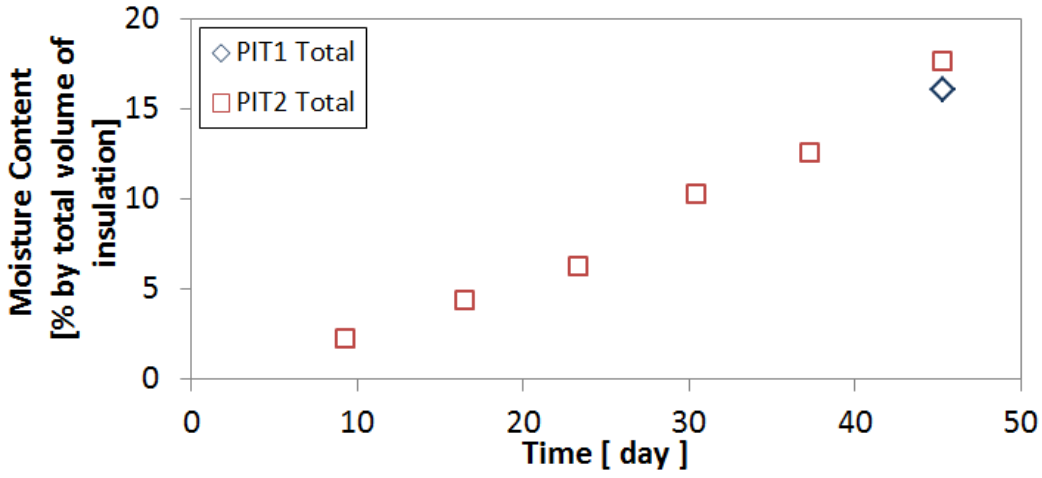

(d)

Figure 6.36: Experimental results on pipe insulation systems PIR1.5: (a) system thermal conductivity versus time during wet test period (b) moisture accumulation during wet test (c) effect of moisture content on the pipe insulation system thermal conductivity ratio (d) periodical measurement of moisture content on the 2nd PIT and moisture content on 1st PIT at the completion of wet test.

As shown in Figure 6.36(a), by the end of the wet test, the PIR system thermal conductivity increased to 1.5 times the dry reference value. At the beginning of the wet test, the humidifier was launched for two hours, and then it failed for 24 hours due to technical problems. The experimental results showed a 10% increase of the thermal conductivity during the time when the wet test condition was disrupted. The total moisture content accumulated in the system PIR1.5 was measured at 16% by total volume of the insulation specimen at the last day of the wet test. Because of the severe humidity conditions, the system PIR1.5 thermal conductivity kept increasing with the system moisture content for the entire period of the wet test. It should also be noted that, at day 38 and day 45, the moisture content of the bottom C-shells were lower than that of the top C-shells. This was due to the fact that during the later period of the wet test, the moisture content inside the bottom shells was so large that it dripped out from the insulation specimen and caused the bottom shells moisture content to decrease.

CHAPTER VII

7 CONCLUSIONS AND RECOMMENDATIONS

7.1 Conclusions

This thesis work presents an experimental apparatus to measure the thermal conductivity of mechanical pipe insulation systems at below ambient temperature in wet conditions with moisture ingress. The apparatus, referred throughout this report as pipe insulation test apparatus or PIT, utilized the heat transfer fluid in a cold copper core pipe inside an aluminum pipe which was 4 foot long and of 3-in NPS pipe diameter. The radial heat flux was calculated by surface temperature measurements on a copper pipe and on the aluminum pipe, which were installed concentric to each other. Dry sand was employed as filler of the annular gap in between the two pipes. Sealing of the aluminum pipe was a critical step to guarantee repeatability of the thermal conductivity measurements. The aluminum pipe surface temperature was controlled from 38 to 40°F (3.3 to 4.4°C) in order to be close to typical surface temperatures of pipes in building chilled water applications. The ambient temperature was varied from 75 to 107°F (24 to 42°C) and the mean pipe insulation temperature ranged from 57 to 73°F (14 to 23°C). With these temperature boundary conditions, the PIT capabilities were limited to radial heat transfer rate from 19.1 to 51.5 Btu/hr (5.6 to 15.1W) for a 3-foot section of pipe insulation system, that is, radial heat flux per unit length from 6.3 to 17.2 Btu/hr-ft (6.1 to 16.5W/m). If the radial heat flux was below 4.5 Btu/hr-ft (4.3 W/m) it was estimated that the uncertainty on the pipe insulation thermal conductivity was larger than ±10 %. For radial heat flux higher than 11.6 Btu/hr-ft (11.2 W/m) the uncertainty on the pipe insulation thermal conductivity was within ±5%.

Four PITs were constructed in the present work. Both groups of two PITs were identical and were built at the same time and utilized the same materials and instrumentation. The temperature sensors on the first PIT aimed to measure the thermal conductivity of the pipe insulation test specimens. The objective of the second PIT was to measure the moisture content in the pipe insulation system at intermediate time intervals during the wet test period. These measurements provided an indication of the moisture accumulation rate in the pipe insulation system during the wet test period.

The apparent thermal conductivity of nine pipe insulation systems was measured in dry non-condensing conditions at below ambient temperature, and Table 7-1 provides a summary of the experimental results for the nine pipe insulation systems at 55 ºF (12.8 ºC) and at 75 ºF (24 ºC) insulation mean temperature.

Table 7-1: Thermal conductivities of cylindrical shape pipe insulation systems at 55 ºF (12.8 ºC) and at 75 ºF (24 ºC) pipe insulation mean temperature.

Pipe Insulation Material	Nominal Wall Thickness		Joint Sealant Type	Apparent Thermal Conductiity[1] at 55°F (13°C)		Apparent Thermal Conductivity[1] at 75°F (24°C)	
	(inch)	(mm)		(Btu-in/hr-ft^2-F)	(W/m-K)	(Btu-in/hr-ft^2-F)	(W/m-K)
(1)Fiberglass FG1	2	50.8	N/A	0.25	0.035	0.29	0.041
(2)Fiberglass FG2	2	50.8	N/A	0.25	0.036	0.28	0.040
(3A)Fiberglass FG3A	2	50.8	Childers CP-30	0.25	0.036	0.27	0.039
(3B)Fiberglass FG3B	2	50.8	Childers CP-30	0.27	0.039	0.28	0.040
(4)Fiberglass FG4	1.5	38.1	Childers CP-30	0.25	0.036	0.27	0.038
(5)Fiberglass FG5	1.5	38.1	N/A	0.26	0.038	0.29	0.042
(6)Fiberglass FG6	1.5	38.1	N/A	0.25	0.037	0.27	0.041
(7)Fiberglass FG7	1.5	38.1	N/A	0.26	0.036	0.28	0.039
(8)Elastomeric Rubber ER2	2	50.8	Aeroseal	0.26	0.038	0.29	0.042
(9)Elastomeric Rubber ER1.5	1.5	38.1	Aeroseal	0.28	0.040	0.30	0.043
(10A)Cellular Glass CGA	1.5	38.1	Boss 368 butyl rubber	0.37	0.054	0.38	0.055
(10B)Cellular Glass CGB	1.5	38.1	Boss 368 butyl rubber	0.36	0.051	0.35	0.049
(11)Polyisocyanurate (PIR1)	1	25.4	Childers CP-70	0.26	0.037	0.25	0.036
(12)Polyisocyanurate (PIR1.5)	1.5	38.1	Childers CP-70	0.26	0.038	0.27	0.039

[1] These values of apparent thermal conductivity, under dry conditions, are obtained from the measurements of the present work.

The fiberglass pipe insulation systems FG1 and FG2 were tested at the very beginning and toward the end of this research project. The experimental results of these two fiberglass pipe insulation systems were compared with each other and the data showed consistency and repeatability of thermal conductivity measurements by using the newly developed experimental apparatus. In addition, the thermal conductivity data of FG1 and FG2 was also compared with one 2 in. thick fiberglass pipe insulation system from the previous research project ASHRAE RP-1356, and the results showed that the thermal conductivity data from both research phases were within the experimental uncertainty. This again validated the experimental data derived from the present experimental apparatus. Another fiberglass pipe insulation system FG3 was tested twice in dry non condensing conditions, and the results were within the experimental uncertainty range. The other four fiberglass pipe insulation systems FG4, FG5, FG6, and FG7 were tested with various vapor retarder jackets. Of these four fiberglass pipe insulation systems, FG4 and FG5 were installed with the same vapor retarder jacket system but tested in different ambient conditions. FG5, FG6 and FG7 were installed with different vapor retarder jacket systems while tested in the same ambient conditions. When comparing the test results of these four systems, their thermal conductivity in dry conditions were the same as shown in the fiberglass pipe insulation system results in Table 7-1. The small discrepancy was within the experimental uncertainty error of the test apparatus. These results confirmed that the vapor retarder jackets did not affect the apparent thermal conductivity in dry non-condensing conditions. Elastomeric rubber pipe insulation system ER2 without vapor retarder was tested only in dry conditions. The other elastomeric rubber pipe insulation system with a nominal wall thickness of 1.5 in. (38.1mm) was tested under both dry non-condensing conditions and wet conditions with moisture ingress. Two cellular glass pipe insulation systems CGA and CGB were tested during this project. The experimental results showed that the system thermal conductivity of CGA was higher than that of CGB. The reason was the presence of fabrication joints in the cellular glass pipe insulation samples for CGA, as well as different densities of CGA and CGB. A polyisocyanurate (PIR) pipe insulation system of

nominal wall thickness of 1 in. (25.4mm) with PVDC vapor retarder jacket was also tested in this project. The experimental results showed that the system thermal conductivity of PIR was practically constant for the range of insulation mean temperatures reported in Table 7-1. The other PIR pipe insulation system with a nominal wall thickness of 1.5 in. (38.1mm) was also tested. And the experimental results showed that the thermal conductivity of these two PIR systems were within the uncertainty range. For all tests in dry non-condensing ambient conditions, the air dew point temperature was below the aluminum pipe surface temperature. Linear trends of the thermal conductivity were observed with respect to the insulation mean temperature from 57 to 73°F (14 to 23°C).

The developed experimental apparatus was suitable for conducting thermal conductivity measurements of pipe insulation systems at below ambient temperature and under wet condensing conditions, in which water vapor could potentially enter the insulation system. The ambient condition for the wet tests was varied from 78°F to 90°F (25.5°C to 32.2°C), with relative humidity from 55 to 83%. The air dew point temperature was significantly higher than the aluminum surface temperature and water vapor sometimes condensate visibly and water droplets dripped from the exterior surface of insulation systems. In severe wet conditions, wet regions were observed on the top and bottom surfaces of the test specimens and wet regions were observed on the bottom surface of some pipe insulation systems near the end radial joints of the insulation test specimens. Thermal conductivity was measured and correlated with the measured moisture content. The experimental data are given in terms of thermal conductivity ratio, that is, the ratio of the thermal conductivity in wet conditions with respect to the corresponding thermal conductivity in initial dry conditions at the same pipe insulation mean temperature and the results are summarized in Table 7-2. The thermal conductivity increased with moisture accumulating into the insulation. For the fiberglass pipe insulation systems FG4, FG5, FG6 and FG7, which were tested with vapor retarder jacket systems, the maximum moisture contents were less than

2% by total volume of the insulation. For fiberglass system FG3B tested without vapor retarder jacket, the moisture content increased to 16% of the total volume at the last day of the wet test. The latent heat transfer by vapor diffusion was observed during the first several hours of transient stage in wet test. This was also the reason that the system thermal conductivity increased greatly during the beginning of the wet test. For closed cell type pipe insulation systems CGA and CGB, and elastomeric rubber pipe insulation system ER1.5, which were tested without any vapor retarder jacket, the maximum moisture contents during the wet tests were less than 1% by volume because of the low water permeability of the insulation material. The system PIR1 was tested with the PVDC vapor retarder jacket in wet conditions for 65 days, and its maximum moisture content at the end of the test was less than 1% by total volume of the insulation. The other PIR pipe insulation system PIR1.5 was tested in severe conditions without vapor retarder jacket for 45 days. The maximum moisture content was 16% by total volume of the insulation while the thermal conductivity ratio increased to 1.5 at the last day of the wet test. The moisture contents of the top and bottom shells were measured and the distribution of water condensate on the exterior surface of the pipe insulation systems was discussed. For several pipe insulation systems with vapor retarder jacket, water vapor condensation was observed on the jacket system along lines that overlapped exactly with the joints of the insulation system. This water condensation could possibly enter the insulation test specimen and cause the thermal conductivity and moisture content to increase. Another possible reason was postulated to be the water vapor that was trapped inside the system during the installation phase. Once the vapor retarder jacket was wrapped around the pipe insulation system, the water vapor would redistribute it-self and increase the system thermal conductivity. During the wet test, several thermal images of the insulation systems in wet conditions were taken to investigate this localized water vapor condensation phenomenon, and the regions near the joints had 1 to 2°C (1.8 to 3.6°F) lower local temperature than the average temperature of the remaining section of the insulation surface. This caused the joint sealant regions to be lower than the ambient dew point temperature, resulting in water vapor

condensation in these regions. Several digital photos of the wet regions in the pipe insulation systems were also reported to document the progression of the wetted regions on the exterior surface of the pipe insulation systems during continuous exposure to high humidity environments.

Table 7-2: Thermal conductivity ratio of pipe insulation under wet conditions with moisture ingress

Pipe Insulation Material	Nominal Wall Thickness		Joint Sealant Type	Test Length	Max. Thermal Conductivity Ratio (k_{wet}/k_{dry})	Max. Moisture Content
	(inch)	(mm)		(day)		%
(3A)Fiberglass FG3A	2	50.8	Childers CP-30	54	3.51	15.08
(3B)Fiberglass FG3B	2	50.8	Childers CP-30	55	1.48	1.66
(4)Fiberglass FG4	1.5	38.1	Childers CP-30	55	1.02	0.26
(5)Fiberglass FG5	1.5	38.1	N/A	65	1.07	0.52
(6)Fiberglass FG6	1.5	38.1	N/A	60	1.06	0.36
(7)Fiberglass FG7	1.5	38.1	N/A	60	1.13	1.36
(9)Elastomeric Rubber ER1.5	1.5	38.1	Aeroseal	57	1.04	0.34
(10A)Cellular Glass CGA	1.5	38.1	Boss 368 butyl rubber	57	1.07	0.82
(10B)Cellular Glass CGB	1.5	38.1	Boss 368 butyl rubber	63	1.05	0.29
(11)Polyisocyanurate (PIR1)	1	25.4	Childers CP-70	65	1.04	0.10
(12)Polyisocyanurate (PIR1.5)	1.5	38.1	Childers CP-70	45	1.49	16.04

7.2 Some Recommendations for the Future Improvements of the Test Apparatus

Water condensation along the joints as well as at the bottom C-shells of the insulation test specimen could be an issue when measuring thermal conductivity and moisture content shown in the thermal photos in Figure 6.24 and Figure 6.33. The joint sealant regions in some of the pipe insulation system had a lower temperature than the test insulation exterior surface, and even lower than the ambient air dew point, causing water condensation to form in these regions. The condensation might have entered the test insulation specimen through air gaps and caused the apparent thermal conductivity to increase. When this phenomenon occurs on the second PIT, the condensation will result in an inconsistent higher moisture content measurement of one of the 6-in. test sections at a specific time interval, which will further lead to a misinterpretation of the

moisture content accumulation rate of the insulation test specimen on the first PIT. From this observation, there are two possible approaches that could improve the current test apparatus. One way is to increase the length of the aluminum pipe. This approach minimizes the edge effect of water condensation on the bottom C-shell sections near the ends of the test specimen on the overall moisture content measurement. The aluminum pipe length could be extended such that the water condensation near the two ends will not expand to the bottom C-shell sections of any part of the test section. Unfortunately, this option requires a large space to house the PIT, which might not be easy to control for uniform air, ambient temperature, humidity and velocity. A second option could be to increase the thickness of the pipe insulation near the end sides, and stagger a second layer of pipe insulation to overlap and completely cover the end side joints of the insulation test specimen. Unfortunately, with this approach, the heat flux along the insulation test specimen might not be uniform. Thus, the measurement of the apparent thermal conductivity might be skewed by the presence of the additional pipe insulation located at the end sides. This approach would need to tested and calibrated in future laboratory experiments.

Another recommendation was regarding the calculation of the latent heat transfer component of thermal conductivity of fiberglass pipe insulation systems tested without vapor retarder jacket in wet condensing conditions. In the above research, it was observed that for fiberglass systems FG3A and FG3B, the system thermal conductivity during wet test period both showed a two-step variation. The thermal conductivity increased greatly during the first several hours in the transient stage of wet conditions, and then the increasing trend became moderate for the remaining period of the wet test period. This phenomenon was proved to be caused by the additional heat transfer of vapor diffusion. In future research, in order to better explain and prove this theory, it is recommended that the insulation test specimen sample be taken out right after the transient period of the wet test, and the water content in the insulation sample be calculated for vapor flow density. By performing this procedure, the corresponding latent heat flux can be calculated and

the latent heat component of the equivalent thermal conductivity of the pipe insulation system during the transient stage could be more accurate and convincing.

REFERENCES

Al-Hammad, A.-M., Abdelrahman, M. A., Grondzik, W., & Hawari, A. (1994). Comparison between actual and published k-values for Saudi insulation materials. *Journal of thermal insulation and building envelopes, 17*, 378-385.

ASTM. (2009). *ASTM C 585 - 09, Standard Practice for Inner and Outer Diameters of Thermal Insulation for Normal Sizes of Pipe and Tubing*. West Conshohocken, PA: ASTM International.

ASTM. (2010a). *ASTM C177 - 10 Standard, Test Method for Steady-State Heat Flux Measurements and Thermal Transmission Properties by Means of the Guarded-Hot-Plate Apparatus*. West Conshohocken, PA: ASTM International.

ASTM. (2010b). *ASTM C335 / C335M - 10e1 Standard Test Method for Steady-State Heat Transfer Properties of Pipe Insulation*. West Conshohocken, PA: ASTM International.

ASTM. (2010c). *ASTM C518 - 10 Standard Test Method for Steady-State Thermal Transmission Properties by Means of the Heat Flow Meter Apparatus*. West Conshohocken, PA: ASTM International.

Batty, W. J., O'Callaghan, P. W., & Probert, S. D. (1981). APPARENT THERMAL CONDUCTIVITY OF GLASS-FIBER INSULANT: EFFECTS OF COMPRESSION AND MOISTURE CONTENT. *Applied energy, 9*(1), 55-76. doi: 10.1016/0306-2619(81)90042-8

Bezjak, M., & Zvizdić, D. (2011). Dynamic Measurements of the Thermal Conductivity of Insulators. *International Journal of Thermophysics, 32*(7-8), 1467-1478. doi: 10.1007/s10765-011-1025-8

Cai, S. (2013). *Thermal Performance of Mechanical Pipe Insulation Systems at Below-ambient Temperature.* (Doctor of Philosophy Doctoral Dissertation), Oklahoma State University.

Chalumeau, A., & Felix-Henry, A. (2006). *Water absorption effect on syntactic foam thermal insulation of a flexible pipe.* Paper presented at the 25TH International Conference on Offshore Mechanics and Arctic Engineering, OMAE 2006, June 4, 2006 - June 9, 2006, Hamburg, Germany.

Chyu, M.-C., Zeng, X., & Ye, L. (1997a). *Performance of fibrous glass pipe insulation subjected to underground water attack.* Paper presented at the Proceedings of the 1997 ASHRAE Winter Meeting, January 26, 1997 - January 29, 1997, Philadelphia, PA, USA.

Chyu, M.-C., Zeng, X., & Ye, L. (1997b). *Effect of moisture content on the performance of polyurethane insulation used on a district heating and cooling pipe.* Paper presented at the Proceedings of the 1997 ASHRAE Winter Meeting, January 26, 1997 - January 29, 1997, Philadelphia, PA, USA.

Crall, G. C. (2002). The use of wicking technology to manage moisture in below-ambient insulation systems *Insulation Materials: Testing and Applications, ASTM Special Technical Publication: 4th Volume, ASTM 1426* (pp. 326-334). West Conshohocken, PA: American Society for Testing and Materials.

Cremaschi, L., Cai, S., Ghajar, A., & Worthington, K. (2012). ASHRAE RP 1356 final report: Methodology to measure thermal performance of pipe insulation at below ambient temperatuers: ASHRAE, available by request to ASHRAE.

Guldbrandsen, T., Karlsson, P. W., & Korsgaard, V. (2011). Analytical model of heat transfer in porous insulation around cold pipes. *International Journal of Heat and Mass Transfer, 54*, 288-292.

Gustafsson, S. E., Karawacki, E., & Khan, M. N. (1978). TRANSIENT HOT-STRIP METHOD FOR SIMULTANEOUSLY MEASURING THERMAL CONDUCTIVITY AND THERMAL DIFFUSIVITY OF SOLIDS AND FLUIDS. *Journal of Physics D: Applied Physics, 12*(9), 1411-1421.

Johnson, A. B., Simonson, C. J., and Besant, R. W. (1998). *Uncertainty analysis in the testing of air-to-air heat/energy exchangers installed in buildings*. Paper presented at the ASHRAE Transactions, San Francisco, CA, USA.

Klein, S. A. (2006). Engineering Equation Solver (Version V7.723-3D). Madison, WI, USA: F-Chart Software.

Korsgaard, V. (1993). *Innovative concept to prevent moisture formation and icing of cold pipe insulation*. Paper presented at the ASHRAE Transactions, Chicago, US.

Kulkarni, S. P., & Vipulanandan, C. (2006). Hot wire method to characterize the thermal conductivity of particle-filled polymer grouts used in pipe-in-pipe application. *Journal of Testing and Evaluation, 34*(3), 224-231.

Kumaran, M. K. (1987). MOISTURE TRANSPORT THROUGH GLASS-FIBRE INSULATION IN THE PRESENCE OF A THERMAL GRADIENT. *Journal of thermal insulation, 10*, 243-255.

Langlais, C., Hyrien, M., & Klarsfeld, S. (1983). *INFLUENCE OF MOISTURE ON HEAT TRANSFER THROUGH FIBROUS-INSULATING MATERIALS.* Paper presented at the Thermal Insulation, Materials, and Systems for Energy Conservation in the '80s., Clearwater Beach, FL, USA.

Log, T. (1993). Transient hot-strip (THS) method for measuring thermal conductivity of thermally insulating materials. *Fire and Materials, 17*(3), 131-138.

McFadden, T. (1986). *MOISTURE EFFECTS ON EXTRUDED POLYSTYRENE INSULATION*. Paper presented at the Cold Regions Engineering, Proceedings of the Fourth International Conference., Anchorage, AK, USA.

McFadden, T. (1988). THERMAL PERFORMANCE DEGRADATION OF WET INSULATIONS IN COLD REGIONS. *Journal of Cold Regions Engineering, 2*(1), 25-34.

Modi, D. K., & Benner, S. M. (1985). MOISTURE GAIN OF SPRAY-APPLIED INSULATIONS AND ITS EFFECT ON EFFECTIVE THERMAL CONDUCTIVITY - PART I. *Journal of thermal insulation, 8*, 259-277.

Moore, J. P., McElroy, D. L., & Jury, S. H. (1985). TECHNIQUE FOR MEASURING THE APPARENT THERMAL CONDUCTIVITY OF FLAT INSULATIONS. *Journal of thermal insulation, 9*, 102-110.

Musgrave, D. S. (1979). THERMAL PERFORMANCE OF URETHANE FOAM PIPE INSULATION AT CRYOGENIC TEMPERATURES. *Journal of thermal insulation, 3*, 3-21.

Ogniewicz, Y., & Tien, C. L. (1981). ANALYSIS OF CONDENSATION IN POROUS INSULATION. *International Journal of Heat and Mass Transfer, 24*(3), 421-429.

Ohmura, T. (2007). *Study on comparison of thermal conductivities of thermal insulations using different measurement methods in wide range of temperature.* Paper presented at the 2007 ASME/JSME Thermal Engineering Summer Heat Transfer Conference, HT 2007, July 8, 2007 - July 12, 2007, Vancouver, BC, Canada.

Ramsden, R. (1985). INSULATION USED ON CHILLED WATER PIPES IN SOUTH AFRICAN GOLD MINES. *Journal of the Mine Ventilation Society of South Africa, 38*(5), 49-54.

Rawlins, A. (2005). Chilled water pipe insulation materials, their properties and application. *Journal of the Mine Ventilation Society of South Africa, 58*(2), 45-57.

Sabuga, W., & Hammerschmidt, U. (1995). New method for the evaluation of thermal conductivity and thermal diffusivity from transient hot strip measurements. *International Journal of Thermophysics, 16*(2), 557-565.

Salmon, D. R., & Tye, R. P. (2011). An inter-comparison of a steady-state and transient methods for measuring the thermal conductivity of thin specimens of masonry materials. *Journal of Building Physics, 34*(3), 247-261. doi: 10.1177/1744259109360060

Taylor, J. R. (1997). An introduction to error analysis : the study of uncertainties in physical measurements (pp. xvii, 327 p.). Sausalito, Calif.: University Science Books.

Tseng, C.-J., & Kuo, K.-T. (2002). Thermal properties of phenolic foam insulation. *Journal of the Chinese Institute of Engineers, Transactions of the Chinese Institute of Engineers,Series A/Chung-kuo Kung Ch'eng Hsuch K'an, 25*(6), 753-758.

Whitaker, T. E., & Yarbrough, D. W. (2002). *Review of thermal properties of a variety of commercial and industrial pipe insulation materials.* Paper presented at the Insulation Materials: Testing and Applications: 4th Volume, October 21, 2002 - October 22, 2002, Charleston, SC, United states.

Wilkes, K. E., & Childs, P. W. (1995). *Thermal performance of fiberglass and cellulose attic insulations.* Paper presented at the Proceedings of the ASHRAE/DOE/BTECC Conference, Dec 7 - 10 1992, Clearwater Beach, FL, United states.

Wilkes, K. E., Desjarlais, A. O., Stovall, T. K., McElroy, D. L., Childs, K. W., & Miller, W. A. (2002). A Pipe Insulation Test Apparatus for Use Below Room Temperature *Insulation Materials: Testing and Applications, ASTM Special Technical Publication: 4th Volume, ASTM 1426* (pp. 24-256). West Conshohocken, PA: American Society for Testing and Materials.

Ye, Z., Wells, C. M., Carrington, C. G., & Hewitt, N. J. (2006). Thermal conductivity of wool and wool-hemp insulation. *International Journal of Energy Research, 30*(1), 37-49. doi: 10.1002/er.1123

Zehendner, H. (1983). THERMAL CONDUCTIVITY OF THERMAL INSULATION MATERIALS ON PIPES. *Journal of thermal insulation, 7*, 52-68.

APPENDICES

Appendix A: Data Summary of Pipe Insulation Systems Experimental Results

Table A-1: Data summary for system FG1

FG1-PIT 1			
Insulation Radius, inches	3.75	Insulation OD, inch	7.60
Pipe Radius, inches	1.75	Insulation ID, inches	3.60
Insulation Thickness, inches	2.00	Test Specimen Length, inches	36.00
Scan Interval, seconds	2.00	Insulation Surface Area, sq. inches	859.54
Initial Specimen Density, lbs/ft^3	4.37		
Summary			
Dry tests			
k_eff [Btu-in/hr-ft^2-°F]		k_ins [Btu-in/hr-ft^2-°F]	
2.7364		0.2556	
2.7623		0.2614	
2.7863		0.2677	

Table A-2: Data summary for system FG2

FG2-PIT 1			
Insulation Radius, inches	3.75	Insulation OD, inches	7.70
Pipe Radius, inches	1.75	Insulation ID, inches	3.70
Insulation Thickness, inches	2.00	Test Specimen Length, inches	36.00
Scan Interval, seconds	2.00	Insulation Surface Area, sq. inches	870.85
Initial Specimen Density, lbs/ft^3	4.37		
Summary			
Dry tests			
k_eff [Btu-in/hr-ft^2-°F]		k_ins [Btu-in/hr-ft^2-°F]	
2.9722		0.2547	
2.9876		0.2586	
3.0109		0.2736	

Table A-3: Data summary for system FG3A

FG3A-PIT 1			
Insulation Radius, inches	3.25	Insulation OD, inches	7.50
Pipe Radius, inches	1.75	Insulation ID, inches	3.50
Insulation Thickness, inches	2.00	Test Specimen Length, inches	36.00
Scan Interval, seconds	2.00	Insulation Surface Area, sq. inches	848.23
Initial Specimen Density, lbs/ft^3	4.37		
Summary			
Dry Tests		Wet Tests	
k_eff [Btu-in/hr-ft²-F]	k_ins [Btu-in/hr-ft²-F]	k_eff [Btu-in/hr-ft²-F]	k_ins [Btu-in/hr-ft²-F]
2.7559	0.2523	2.7516	0.6546
2.7454	0.2596	2.7554	0.7229
2.7215	0.2614	2.7556	0.7470

Table A-4: Data summary for system FG3B

FG3B-PIT 1			
Insulation Radius, inches	3.25	Insulation OD, inches	7.50
Pipe Radius, inches	1.75	Insulation ID, inches	3.50
Insulation Thickness, inches	2.00	Test Specimen Length, inches	36.00
Scan Interval, seconds	2.00	Insulation Surface Area, sq. inches	848.23
Initial Specimen Density, lbs/ft^3	4.37		
Summary			
Dry Tests		Wet Tests	
k_eff [Btu-in/hr-ft²-F]	k_ins [Btu-in/hr-ft²-F]	k_eff [Btu-in/hr-ft²-F]	k_ins [Btu-in/hr-ft²-F]
3.1610	0.2734	3.1442	0.4077
3.1292	0.2798	3.1462	0.4102
3.0880	0.2810	3.1477	0.4108

Table A-5: Data summary for system FG4

FG4-PIT 1			
Insulation Radius, inches	3.25	Insulation OD, inches	6.60
Pipe Radius, inches	1.75	Insulation ID, inches	3.50
Insulation Thickness, inches	1.50	Test Specimen Length, inches	36.00
Scan Interval, seconds	2.00	Insulation Surface Area, sq. inches	746.44
Initial Specimen Density, lbs/ft^3	3.48		
Summary			
Dry Tests		Wet Tests	
k_eff [Btu-in/hr-ft²-F]	k_ins [Btu-in/hr-ft²-F]	k_eff [Btu-in/hr-ft²-F]	k_ins [Btu-in/hr-ft²-F]
2.6075	0.2427	2.5922	0.2496
2.5875	0.2440	2.5832	0.2482
2.5669	0.2448	2.6068	0.2440

Table A-6: Data summary for system FG5

FG5-PIT 1			
Insulation Radius, inches	3.25	Insulation OD, inches	6.70
Pipe Radius, inches	1.75	Insulation ID, inches	3.70
Insulation Thickness, inches	1.50	Test Specimen Length, inches	36.00
Scan Interval, seconds	2.00	Insulation Surface Area, sq. inches	757.75
Initial Specimen Density, lbs/ft^3	3.18		
Summary			
Dry Tests		Wet Tests	
k_eff [Btu-in/hr-ft^2-°F]	k_ins [Btu-in/hr-ft^2-°F]	k_eff [Btu-in/hr-ft^2-°F]	k_ins [Btu-in/hr-ft^2-°F]
2.6647	0.2609	2.7971	0.2636
2.7060	0.2646	2.8014	0.2679
2.7947	0.2759	2.8281	0.2728

Table A-7: Data summary for system FG6

FG6-PIT 1			
Insulation Radius, inches	3.25	Insulation OD, inches	6.80
Pipe Radius, inches	1.75	Insulation ID, inches	3.80
Insulation Thickness, inches	1.50	Test Specimen Length, inches	36.00
Scan Interval, seconds	2.00	Insulation Surface Area, sq. inches	769.06
Initial Specimen Density, lbs/ft^3	3.18		
Summary			
Dry Tests		Wet Tests	
k_eff [Btu-in/hr-ft^2-°F]	k_ins [Btu-in/hr-ft^2-°F]	k_eff [Btu-in/hr-ft^2-°F]	k_ins [Btu-in/hr-ft^2-°F]
2.5964	0.2552	2.8583	0.2528
2.6297	0.2563	2.7134	0.2455
2.7044	0.2645	2.9349	0.2669

Table A-8: Data summary for system FG7

FG7-PIT 1			
Insulation Radius, inches	3.25	Insulation OD, inches	6.60
Pipe Radius, inches	1.75	Insulation ID, inches	3.60
Insulation Thickness, inches	1.50	Test Specimen Length, inches	36.00
Scan Interval, seconds	2.00	Insulation Surface Area, sq. inches	746.44
Initial Specimen Density, lbs/ft^3	3.89		
Summary			
Dry Tests		Wet Tests	
k_eff [Btu-in/hr-ft^2-°F]	k_ins [Btu-in/hr-ft^2-°F]	k_eff [Btu-in/hr-ft^2-°F]	k_ins [Btu-in/hr-ft^2-°F]
3.2230	0.2597	3.1590	0.2738
3.2027	0.2590	3.0593	0.2826
3.1807	0.2704	3.0820	0.2981

Table A-9: Data summary for system ER2

ER2-PIT 1			
Insulation Radius, inches	3.75	Insulation OD, inches	7.70
Pipe Radius, inches	1.75	Insulation ID, inches	3.70
Insulation Thickness, inches	2.00	Test Specimen Length, inches	36.00
Scan Interval, seconds	2.00	Insulation Surface Area, sq. inches	870.85
Initial Specimen Density, lbs/ft^3	2.50		
Summary			
Dry tests			
k_eff [Btu-in/hr-ft^2-°F]		k_ins [Btu-in/hr-ft^2-°F]	
2.6219		0.2637	
2.6527		0.2703	
2.6835		0.2726	

Table A-10: Data summary for system ER1.5

ER1.5-PIT 1			
Insulation Radius, inches	3.25	Insulation OD, inches	6.80
Pipe Radius, inches	1.75	Insulation ID, inches	3.80
Insulation Thickness, inches	1.50	Test Specimen Length, inches	36.00
Scan Interval, seconds	2.00	Insulation Surface Area, sq. inches	769.06
Initial Specimen Density, lbs/ft^3	2.50		
Summary			
Dry Tests		Wet Tests	
k_eff [Btu-in/hr-ft^2-°F]	k_ins [Btu-in/hr-ft^2-°F]	k_eff [Btu-in/hr-ft^2-°F]	k_ins [Btu-in/hr-ft^2-°F]
2.7446	0.2822	2.7756	0.2937
2.7656	0.2906	2.7676	0.2959
2.7848	0.2925	2.7790	0.2955

Table A-11: Data summary for system CGA

CGA-PIT 1			
Insulation Radius, inches	3.25	Insulation OD, inches	6.80
Pipe Radius, inches	1.75	Insulation ID, inches	3.80
Insulation Thickness, inches	1.50	Test Specimen Length, inches	36.00
Scan Interval, seconds	2.00	Insulation Surface Area, sq. inches	769.06
Initial Specimen Density, lbs/ft^3	7.49		
Summary			
Dry Tests		Wet Tests	
k_eff [Btu-in/hr-ft^2-°F]	k_ins [Btu-in/hr-ft^2-°F]	k_eff [Btu-in/hr-ft^2-°F]	k_ins [Btu-in/hr-ft^2-°F]
3.2831	0.3753	3.1486	0.3870
3.2534	0.3766	3.1626	0.3952
3.2255	0.3770	3.1661	0.3966

Table A-12: Data summary for system CGB

CGB-PIT 1			
Insulation Radius, inches	3.25	Insulation OD, inches	6.60
Pipe Radius, inches	1.75	Insulation ID, inches	3.60
Insulation Thickness, inches	1.50	Test Specimen Length, inches	36.00
Scan Interval, seconds	2.00	Insulation Surface Area, sq. inches	746.44
Initial Specimen Density, lbs/ft^3	7.21		

Summary			
Dry Tests		Wet Tests	
k_eff [Btu-in/hr-ft^2-°F]	k_ins [Btu-in/hr-ft^2-°F]	k_eff [Btu-in/hr-ft^2-°F]	k_ins [Btu-in/hr-ft^2-°F]
3.1811	0.3570	3.0620	0.3612
3.1014	0.3541	3.0538	0.3664
3.0450	0.3512	3.0546	0.3668

Table A-13: Data summary for system PIR1

PIR1-PIT 1			
Insulation Radius, inches	2.75	Insulation OD, inches	5.70
Pipe Radius, inches	1.75	Insulation ID, inches	3.70
Insulation Thickness, inches	2.00	Test Specimen Length, inches	36.00
Scan Interval, seconds	2.00	Insulation Surface Area, sq. inches	644.65
Initial Specimen Density, lbs/ft^3	1.79		

Summary			
Dry Tests		Wet Tests	
k_eff [Btu-in/hr-ft^2-°F]	k_ins [Btu-in/hr-ft^2-°F]	k_eff [Btu-in/hr-ft^2-°F]	k_ins [Btu-in/hr-ft^2-°F]
3.2969	0.2582	3.1079	0.2516
3.2661	0.2564	3.1359	0.2563
3.1942	0.2542	3.1726	0.2560

Table A-14: Data summary for system PIR1.5

PIR1.5-PIT 1			
Insulation Radius, inches	3.25	Insulation OD, inches	6.80
Pipe Radius, inches	1.75	Insulation ID, inches	3.50
Insulation Thickness, inches	1.50	Test Specimen Length, inches	36.00
Scan Interval, seconds	2.00	Insulation Surface Area, sq. inches	848.23
Initial Specimen Density, lbs/ft^3	1.99		

Summary			
Dry Tests		Wet Tests	
k_eff [Btu-in/hr-ft^2-F]	k_ins [Btu-in/hr-ft^2-F]	k_eff [Btu-in/hr-ft^2-F]	k_ins [Btu-in/hr-ft^2-F]
2.7826	0.2644	2.8323	0.3140
2.7898	0.2633	2.8196	0.3391
2.7943	0.2679	2.7768	0.4302

Appendix B: Examples of Experimental Data Sheets

Table B-1: Experimental results for system FG1 in dry conditions

RH	%	8.97	8.32	7.50
T_{Room}	F	85.48	90.55	95.56
T_{Outins}	F	83.37	88.23	93.06
T_{Al}	F	36.88	36.98	36.57
T_{Cu}	F	26.85	25.79	24.04
ΔT_{out}	F	46.49	51.25	56.50
ΔT_{in}	F	10.03	11.19	12.53
T_{sand}	F	31.86	31.38	30.30
T_{test}	F	60.13	62.61	64.82
k_{eff}	Btu-in/hr-ft^2-F	2.74	2.76	2.77
Q_{sand}	Btu/hr	24.07	27.04	30.46
k_{test}	Btu-in/hr-ft^2-F	0.2556	0.2605	0.2661
func (1in)	Btu-in/hr-ft^2-F	0.2334	0.2343	0.2352
ΔT_{Al}	F	0.98	1.12	1.24
ΔT_{Outins}	F	1.49	1.74	1.85

Table B-2: Experimental results for system FG2 in dry conditions

RH	%	12.86	11.01	9.67
T_{Room}	F	76.90	81.86	86.78
T_{Outins}	F	75.86	80.60	85.34
T_{Al}	F	37.94	37.67	37.90
T_{Cu}	F	30.56	29.23	28.57
ΔT_{out}	F	37.92	42.93	47.43
ΔT_{in}	F	7.38	8.44	9.33
T_{sand}	F	34.25	33.45	33.24
T_{test}	F	56.90	59.14	61.62
k_{eff}	Btu-in/hr-ft^2-F	2.9720	2.9817	2.9875
Q_{sand}	Btu/hr	19.24	22.06	24.43
k_{test}	Btu-in/hr-ft^2-F	0.2547	0.2580	0.2586
func (1in)	Btu-in/hr-ft^2-F	0.2321	0.2330	0.2340
ΔT_{Al}	F	1.02	1.03	1.03
ΔT_{Outins}	F	1.81	1.95	2.06

Table B-3: Experimental results for system FG3A in dry conditions

RH	%	14.74	13.88	11.58
T_{Room}	F	76.87	81.68	86.58
T_{Outins}	F	75.77	80.45	85.09
T_{Al}	F	36.62	36.82	34.91
T_{Cu}	F	28.48	27.74	24.13
ΔT_{out}	F	39.15	43.62	50.18
ΔT_{in}	F	8.15	9.09	10.78
T_{sand}	F	32.55	32.28	29.52
T_{test}	F	56.20	58.64	60.00
k_{eff}	Btu-in/hr-ft^2-F	2.7558	2.7478	2.7453
Q_{sand}	Btu/hr	19.68	21.89	25.95
k_{test}	Btu-in/hr-ft^2-F	0.2523	0.2519	0.2595
func (1in)	Btu-in/hr-ft^2-F	0.2390	0.2428	0.2449
ΔT_{Al}	F	1.83	1.88	1.73
ΔT_{Outins}	F	1.58	1.78	1.97

Table B-4: Experimental results for system FG3B in dry conditions

RH	%	15.59	13.52	11.45
T_{Room}	F	76.85	81.71	86.71
T_{Outins}	F	75.61	80.28	85.11
T_{Al}	F	39.74	39.53	39.50
T_{Cu}	F	32.58	31.22	30.07
ΔT_{out}	F	35.86	40.76	45.61
ΔT_{in}	F	7.17	8.30	9.43
T_{sand}	F	36.16	35.37	34.79
T_{test}	F	57.68	59.91	62.31
k_{eff}	Btu-in/hr-ft^2-F	3.1609	3.1433	3.1290
Q_{sand}	Btu/hr	19.86	22.88	25.85
k_{test}	Btu-in/hr-ft^2-F	0.2734	0.2771	0.2798
func (1in)	Btu-in/hr-ft^2-F	0.2328	0.2354	0.2382
ΔT_{Al}	F	1.51	1.48	1.50
ΔT_{Outins}	F	1.27	1.24	1.29

Table B-5: Experimental results for system FG4 in dry conditions

RH	%	15.59	13.52	11.45
T_{Room}	F	76.97	81.74	86.71
T_{Outins}	F	75.53	80.09	84.82
T_{Al}	F	40.49	40.50	40.68
T_{Cu}	F	31.28	29.95	28.79
ΔT_{out}	F	35.04	39.60	44.14
ΔT_{in}	F	9.21	10.55	11.89
T_{sand}	F	35.89	35.23	34.74
T_{test}	F	58.01	60.30	62.75
k_{eff}	Btu-in/hr-ft^2-F	2.7156	2.7030	2.6908
Q_{sand}	Btu/hr	21.93	24.99	28.05
k_{test}	Btu-in/hr-ft^2-F	0.2527	0.2548	0.2566
func (1in)	Btu-in/hr-ft^2-F	0.2431	0.2436	0.2442
ΔT_{Al}	F	1.70	1.73	1.77
ΔT_{Outins}	F	2.15	2.41	2.52

Table B-6: Experimental results for system FG5 in dry conditions

RH	%	21.13	18.23	13.72
T_{Room}	F	77.14	80.10	85.07
T_{Outins}	F	75.32	78.12	82.78
T_{Al}	F	37.81	37.57	37.83
T_{Cu}	F	27.67	26.64	25.70
ΔT_{out}	F	37.51	40.54	44.95
ΔT_{in}	F	10.14	10.94	12.13
T_{sand}	F	32.74	32.11	31.76
T_{test}	F	56.56	57.85	60.31
k_{eff}	Btu-in/hr-ft^2-F	2.6646	2.6806	2.7059
Q_{sand}	Btu/hr	23.68	25.70	28.77
k_{test}	Btu-in/hr-ft^2-F	0.2609	0.2621	0.2646
func (1in)	Btu-in/hr-ft^2-F	0.1994	0.1999	0.2009
ΔT_{Al}	F	1.33	1.43	1.56
ΔT_{Outins}	F	1.31	1.46	1.88

Table B-7: Experimental results for system FG6 in dry conditions

RH	%	21.13	18.23	13.72
T_{Room}	F	76.99	80.00	84.68
T_{Outins}	F	75.55	78.37	82.83
T_{Al}	F	37.97	37.74	37.95
T_{Cu}	F	28.01	27.00	26.15
ΔT_{out}	F	37.57	40.63	44.89
ΔT_{in}	F	9.96	10.74	11.80
T_{sand}	F	32.99	32.37	32.05
T_{test}	F	56.76	58.06	60.39
k_{eff}	Btu-in/hr-ft^2-F	2.5962	2.6078	2.6296
Q_{sand}	Btu/hr	22.68	24.55	27.21
k_{test}	Btu-in/hr-ft^2-F	0.2552	0.2555	0.2563
func (1in)	Btu-in/hr-ft^2-F	0.1995	0.2000	0.2009
ΔT_{Al}	F	1.03	1.07	1.12
ΔT_{Outins}	F	0.76	0.88	1.09

Table B-8: Experimental results for system FG7 in dry conditions

RH	%	12.86	11.01	9.67
T_{Room}	F	77.12	82.16	87.16
T_{Outins}	F	75.54	80.30	85.06
T_{Al}	F	38.84	38.48	38.67
T_{Cu}	F	30.48	28.94	28.08
ΔT_{out}	F	36.71	41.82	46.38
ΔT_{in}	F	8.36	9.54	10.60
T_{sand}	F	34.66	33.71	33.37
T_{test}	F	57.19	59.39	61.86
k_{eff}	Btu-in/hr-ft^2-F	3.2228	3.2114	3.2025
Q_{sand}	Btu/hr	23.61	26.85	29.75
k_{test}	Btu-in/hr-ft^2-F	0.2597	0.2593	0.2590
func (1in)	Btu-in/hr-ft^2-F	0.2323	0.2331	0.2341
ΔT_{Al}	F	1.59	1.52	1.53
ΔT_{Outins}	F	1.36	1.46	1.74

Table B-9: Experimental results for system ER2 in dry conditions

RH	%	11.18	8.97	8.32
T_{Room}	F	74.88	84.32	89.14
T_{Outins}	F	73.74	82.62	87.25
T_{Al}	F	37.19	36.74	36.74
T_{Cu}	F	28.81	26.26	25.16
ΔT_{out}	F	36.55	45.88	50.51
ΔT_{in}	F	8.37	10.48	11.59
T_{sand}	F	33.00	31.50	30.95
T_{test}	F	55.46	59.68	62.00
k_{eff}	Btu-in/hr-ft^2-F	2.58	2.62	2.64
Q_{sand}	Btu/hr	18.92	24.10	26.86
k_{test}	Btu-in/hr-ft^2-F	0.2599	0.2636	0.2669
func (1in)	Btu-in/hr-ft^2-F	0.2442	0.2465	0.2477
ΔT_{Al}	F	0.70	0.75	0.80
ΔT_{Outins}	F	1.57	1.64	1.67

Table B-10: Experimental results for system ER1.5 in dry conditions

RH	%	11.18	8.97	8.32
T_{Room}	F	75.48	84.16	89.00
T_{Outins}	F	73.96	83.13	87.90
T_{Al}	F	38.23	38.32	38.50
T_{Cu}	F	28.33	25.90	24.68
ΔT_{out}	F	35.73	44.80	49.39
ΔT_{in}	F	9.90	12.43	13.82
T_{sand}	F	33.28	32.11	31.59
T_{test}	F	56.10	60.73	63.20
k_{eff}	Btu-in/hr-ft^2-F	2.72	2.74	2.76
Q_{sand}	Btu/hr	23.58	29.90	33.47
k_{test}	Btu-in/hr-ft^2-F	0.2791	0.2821	0.2865
func (1in)	Btu-in/hr-ft^2-F	0.0000	0.0000	0.0000
ΔT_{Al}	F	0.76	0.78	0.84
ΔT_{Outins}	F	2.53	3.39	3.82

Table B-11: Experimental results for system CGA in dry conditions

RH	%	11.18	8.97	8.32
T_{Room}	F	74.51	84.00	88.92
T_{Outins}	F	72.46	81.46	86.25
T_{Al}	F	39.62	39.99	40.31
T_{Cu}	F	29.55	27.20	25.99
ΔT_{out}	F	32.84	41.47	45.95
ΔT_{in}	F	10.07	12.79	14.32
T_{sand}	F	34.58	33.59	33.15
T_{test}	F	56.04	60.72	63.28
k_{eff}	Btu-in/hr-ft^2-F	3.31	3.28	3.27
Q_{sand}	Btu/hr	29.24	36.81	41.06
k_{test}	Btu-in/hr-ft^2-F	0.3765	0.3753	0.3778
func (1in)	Btu-in/hr-ft^2-F	0.2963	0.3008	0.3033
ΔT_{Al}	F	0.70	0.79	0.80
ΔT_{Outins}	F	0.99	0.90	0.89

Table B-12: Experimental results for system CGB in dry conditions

RH	%	14.74	13.88	11.58
T_{Room}	F	77.01	81.95	86.88
T_{Outins}	F	74.79	79.51	84.11
T_{Al}	F	40.02	40.55	38.93
T_{Cu}	F	29.00	28.13	24.36
ΔT_{out}	F	34.77	38.96	45.18
ΔT_{in}	F	11.02	12.42	14.57
T_{sand}	F	34.51	34.34	31.64
T_{test}	F	57.41	60.03	61.52
k_{eff}	Btu-in/hr-ft^2-F	3.1809	3.1640	3.1012
Q_{sand}	Btu/hr	30.73	34.44	39.62
k_{test}	Btu-in/hr-ft^2-F	0.3570	0.3570	0.3541
func (1in)	Btu-in/hr-ft^2-F	0.3493	0.3483	0.3478
ΔT_{Al}	F	1.32	1.31	1.30
ΔT_{Outins}	F	1.56	1.72	1.76

Table B-13: Experimental results for system PIR1 in dry conditions

RH	%	21.13	18.23	13.72
T_{Room}	F	77.13	80.18	85.27
T_{Outins}	F	73.97	76.67	81.29
T_{Al}	F	38.87	38.64	39.00
T_{Cu}	F	28.78	27.66	26.80
ΔT_{out}	F	35.09	38.03	42.29
ΔT_{in}	F	10.10	10.98	12.20
T_{sand}	F	33.82	33.15	32.90
T_{test}	F	56.42	57.66	60.15
k_{eff}	Btu-in/hr-ft^2-F	3.2967	3.2711	3.2659
Q_{sand}	Btu/hr	29.19	31.50	34.93
k_{test}	Btu-in/hr-ft^2-F	0.2582	0.2571	0.2564
func (1in)	Btu-in/hr-ft^2-F	0.1945	0.1950	0.1960
ΔT_{Al}	F	1.29	1.26	1.11
ΔT_{Outins}	F	1.18	1.54	2.13

Table B-14: Experimental results for system PIR1.5 in dry conditions

RH	%	21.13	18.23	13.72
T_{Room}	F	77.13	80.11	84.94
T_{Outins}	F	76.02	78.89	83.47
T_{Al}	F	38.21	37.99	38.23
T_{Cu}	F	28.52	27.52	26.71
ΔT_{out}	F	37.81	40.90	45.24
ΔT_{in}	F	9.69	10.47	11.52
T_{sand}	F	33.36	32.75	32.47
T_{test}	F	57.11	58.44	60.85
k_{eff}	Btu-in/hr-ft^2-F	2.7824	2.7796	2.7897
Q_{sand}	Btu/hr	23.64	25.50	28.17
k_{test}	Btu-in/hr-ft^2-F	0.2644	0.2636	0.2633
func (1in)	Btu-in/hr-ft^2-F	0.1948	0.1953	0.1962
ΔT_{Al}	F	1.44	1.44	1.58
ΔT_{Outins}	F	1.92	1.92	2.52

Appendix C: Examples of Calculation Procedures of j, $k_{sand,j}$, and $k_{ins,j}$

Table C-1: Example of FG1

Actual time during the test period j [day]	Actual time during the test period j [hour]	Status of the test period	$k_{sand,j}$ [Btu-in/hr-ft^2-°F]	$k_{ins,j}$ [Btu-in/hr-ft^2-°F]
0.00	0.00	first test of the dry tests	2.6995	0.2626
0.25	6.00	second test of the dry tests	2.7363	0.2556
0.80	19.20	third test of the dry tests	2.7561	0.2611
⋮	⋮	⋮	⋮	⋮
2.96	71.04	last test of the dry tests	2.7547	0.2593

Table C-2: Example of FG2

Actual time during the test period j [day]	Actual time during the test period j [hour]	Status of the test period	$k_{sand,j}$ [Btu-in/hr-ft^2-°F]	$k_{ins,j}$ [Btu-in/hr-ft^2-°F]
0.00	0.00	first test of the dry tests	2.9722	0.2547
0.11	2.64	second test of the dry tests	2.9821	0.2580
0.20	4.80	third test of the dry tests	2.9880	0.2586
⋮	⋮	⋮	⋮	⋮
0.48	11.52	last test of the dry tests	3.0114	0.2736

Table C-3: Example of FG3A

Actual time during the test period j [day]	Actual time during the test period j [hour]	Status of the test period	$k_{sand,j}$ [Btu-in/hr-ft^2-°F]	$k_{ins,j}$ [Btu-in/hr-ft^2-°F]
0.00	0.00	first test of the dry tests	2.7559	0.2523
0.24	5.76	second test of the dry tests	2.7482	0.2519
0.46	11.04	third test of the dry tests	2.7460	0.2596
⋮	⋮	⋮	⋮	⋮
1.43	34.32	last test of the dry tests	2.7551	0.2543
1.86	44.64	first test of the wet tests	2.7437	0.2546
1.93	46.32	second test of the wet tests	2.7435	0.2643
1.97	47.28	third test of the wet tests	2.7429	0.3588
⋮	⋮	⋮	⋮	⋮
54.20	1300.80	last test of the wet tests	2.8321	0.7678

Table C-4: Example of FG3B

Actual time during the test period j [day]	Actual time during the test period j [hour]	Status of the test period	$k_{sand,j}$ [Btu-in/hr-ft^2-°F]	$k_{ins,j}$ [Btu-in/hr-ft^2-°F]
0.00	0.00	first test of the dry tests	3.1609	0.2734
0.25	6.00	second test of the dry tests	3.1429	0.2771
0.36	8.64	third test of the dry tests	3.1290	0.2798
⋮	⋮	⋮	⋮	⋮
0.70	16.80	last test of the dry tests	3.0867	0.2808
2.70	64.80	first test of the wet tests	3.1191	0.2813
2.74	65.76	second test of the wet tests	3.1239	0.3086
2.78	66.72	third test of the wet tests	3.1429	0.3993
⋮	⋮	⋮	⋮	⋮
57.30	1375.20	last test of the wet tests	3.0829	0.4024

Table C-5: Example of FG4

Actual time during the test period j [day]	Actual time during the test period j [hour]	Status of the test period	$k_{sand,j}$ [Btu-in/hr-ft^2-°F]	$k_{ins,j}$ [Btu-in/hr-ft^2-°F]
0.00	0.00	first test of the dry tests	2.7158	0.2527
0.25	6.00	second test of the dry tests	2.7026	0.2548
0.36	8.64	third test of the dry tests	2.6909	0.2566
⋮	⋮	⋮	⋮	⋮
0.70	16.80	last test of the dry tests	2.6527	0.2590
2.70	64.80	first test of the wet tests	2.6968	0.2598
2.74	65.76	second test of the wet tests	2.6962	0.2570
2.78	66.72	third test of the wet tests	2.6963	0.2577
⋮	⋮	⋮	⋮	⋮
57.30	1375.20	last test of the wet tests	2.6714	0.2562

Table C-6: Example of FG5

Actual time during the test period j [day]	Actual time during the test period j [hour]	Status of the test period	$k_{sand,j}$ [Btu-in/hr-ft^2-°F]	$k_{ins,j}$ [Btu-in/hr-ft^2-°F]
0.00	0.00	first test of the dry tests	2.6647	0.2609
0.13	3.12	second test of the dry tests	2.6803	0.2664
0.17	4.08	third test of the dry tests	2.6808	0.2636
⋮	⋮	⋮	⋮	⋮
3.60	86.40	last test of the dry tests	2.6686	0.2588
4.37	104.88	first test of the wet tests	2.8031	0.2634
4.44	106.56	second test of the wet tests	2.7976	0.2569
4.51	108.24	third test of the wet tests	2.8010	0.2653
⋮	⋮	⋮	⋮	⋮
68.85	1652.40	last test of the wet tests	2.8323	0.2780

Table C-7: Example of FG6

Actual time during the test period j [day]	Actual time during the test period j [hour]	Status of the test period	$k_{sand,j}$ [Btu-in/hr-ft^2-°F]	$k_{ins,j}$ [Btu-in/hr-ft^2-°F]
0.00	0.00	first test of the dry tests	2.5964	0.2552
0.13	3.12	second test of the dry tests	2.6063	0.2588
0.17	4.08	third test of the dry tests	2.6068	0.2551
⋮	⋮	⋮	⋮	⋮
3.60	86.40	last test of the dry tests	2.6224	0.2565
3.92	94.08	first test of the wet tests	2.8329	0.2506
3.97	95.28	second test of the wet tests	2.8268	0.2447
4.03	96.72	third test of the wet tests	2.8297	0.2530
⋮	⋮	⋮	⋮	⋮
64.67	1552.15	last test of the wet tests	2.9542	0.2657

Table C-8: Example of FG7

Actual time during the test period j [day]	Actual time during the test period j [hour]	Status of the test period	$k_{sand,j}$ [Btu-in/hr-ft^2-°F]	$k_{ins,j}$ [Btu-in/hr-ft^2-°F]
0.00	0.00	first test of the dry tests	3.2230	0.2597
0.11	2.64	second test of the dry tests	3.2115	0.2593
0.20	4.80	third test of the dry tests	3.2024	0.2590
⋮	⋮	⋮	⋮	⋮
0.48	11.52	last test of the dry tests	3.1681	0.2687
1.28	30.72	first test of the wet tests	3.1897	0.2665
1.33	31.92	second test of the wet tests	3.1870	0.2611
1.39	33.36	third test of the wet tests	3.1893	0.2716
⋮	⋮	⋮	⋮	⋮
61.55	1477.20	last test of the wet tests	3.0634	0.3002

Table C-9: Example of ER2

Actual time during the test period j [day]	Actual time during the test period j [hour]	Status of the test period	$k_{sand,j}$ [Btu-in/hr-ft^2-°F]	$k_{ins,j}$ [Btu-in/hr-ft^2-°F]
0.00	0.00	first test of the dry tests	2.5777	0.2599
0.25	6.00	second test of the dry tests	2.6219	0.2637
0.80	19.20	third test of the dry tests	2.6447	0.2664
⋮	⋮	⋮	⋮	⋮
2.96	71.04	last test of the dry tests	2.6439	0.2675

Table C-10: Example of ER1.5

Actual time during the test period j [day]	Actual time during the test period j [hour]	Status of the test period	$k_{sand,j}$ [Btu-in/hr-ft^2-°F]	$k_{ins,j}$ [Btu-in/hr-ft^2-°F]
0.00	0.00	first test of the dry tests	2.7168	0.2791
0.25	6.00	second test of the dry tests	2.7447	0.2822
0.80	19.20	third test of the dry tests	2.7624	0.2859
⋮	⋮	⋮	⋮	⋮
2.96	71.04	last test of the dry tests	2.7612	0.2883
5.27	126.48	first test of the wet tests	2.7595	0.2918
5.35	128.40	second test of the wet tests	2.7607	0.2932
5.42	130.08	third test of the wet tests	2.7636	0.2932
⋮	⋮	⋮	⋮	⋮
62.61	1502.64	last test of the wet tests	2.7790	0.2955

Table C-11: Example of CGA

Actual time during the test period j [day]	Actual time during the test period j [hour]	Status of the test period	$k_{sand,j}$ [Btu-in/hr-ft^2-°F]	$k_{ins,j}$ [Btu-in/hr-ft^2-°F]
0.00	0.00	first test of the dry tests	3.3130	0.3765
0.25	6.00	second test of the dry tests	3.2831	0.3753
0.80	19.20	third test of the dry tests	3.2748	0.3778
⋮	⋮	⋮	⋮	⋮
2.96	71.04	last test of the dry tests	3.2656	0.3763
5.27	126.48	first test of the wet tests	3.1593	0.3686
5.35	128.40	second test of the wet tests	3.1572	0.3670
5.42	130.08	third test of the wet tests	3.1594	0.3666
⋮	⋮	⋮	⋮	⋮
62.61	1502.64	last test of the wet tests	3.1661	0.3966

Table C-12: Example of CGB

Actual time during the test period j [day]	Actual time during the test period j [hour]	Status of the test period	$k_{sand,j}$ [Btu-in/hr-ft^2-°F]	$k_{ins,j}$ [Btu-in/hr-ft^2-°F]
0.00	0.00	first test of the dry tests	3.1811	0.3570
0.24	5.76	second test of the dry tests	3.1640	0.3570
0.46	11.04	third test of the dry tests	3.1014	0.3541
⋮	⋮	⋮	⋮	⋮
1.43	34.32	last test of the dry tests	3.1217	0.3534
1.86	44.64	first test of the wet tests	2.9590	0.3389
1.93	46.32	second test of the wet tests	2.9591	0.3393
1.97	47.28	third test of the wet tests	2.9542	0.3318
⋮	⋮	⋮	⋮	⋮
63.29	1518.96	last test of the wet tests	2.9561	0.3583

Table C-13: Example of PIR1

Actual time during the test period j [day]	Actual time during the test period j [hour]	Status of the test period	$k_{sand,j}$ [Btu-in/hr-ft^2-°F]	$k_{ins,j}$ [Btu-in/hr-ft^2-°F]
0.00	0.00	first test of the dry tests	3.2969	0.2582
0.13	3.12	second test of the dry tests	3.2650	0.2596
0.17	4.08	third test of the dry tests	3.2640	0.2562
⋮	⋮	⋮	⋮	⋮
3.60	86.40	last test of the dry tests	3.2658	0.2554
4.37	104.88	first test of the wet tests	3.0936	0.2492
4.44	106.56	second test of the wet tests	3.0930	0.2441
4.51	108.24	third test of the wet tests	3.0940	0.2510
⋮	⋮	⋮	⋮	⋮
68.85	1652.40	last test of the wet tests	3.1867	0.2573

Table C-14: Example of PIR1.5

Actual time during the test period j [day]	Actual time during the test period j [hour]	Status of the test period	$k_{sand,j}$ [Btu-in/hr-ft^2-°F]	$k_{ins,j}$ [Btu-in/hr-ft^2-°F]
0.00	0.00	first test of the dry tests	2.7826	0.2644
0.13	3.12	second test of the dry tests	2.7762	0.2669
0.17	4.08	third test of the dry tests	2.7756	0.2628
⋮	⋮	⋮	⋮	⋮
3.60	86.40	last test of the dry tests	2.7749	0.2630
4.27	102.48	first test of the wet tests	2.8084	0.2726
4.38	105.12	second test of the wet tests	2.7977	0.3029
4.50	108.00	third test of the wet tests	2.7963	0.3012
⋮	⋮	⋮	⋮	⋮
45.10	1082.40	last test of the wet tests	2.6326	0.4079

VITA

Weiwei Zhu

Candidate for the Degree of

Master of Science

Thesis: MEASUREMENTS OF THERMAL CONDUCTIVITY OF PIPE INSULATION SYSTEMS AT BELOW-AMBIENT TEMPERATURE AND IN WET CONDENSING CONDITIONS WITH MOISTURE INGRESS

Major Field: Mechanical Engineering

Biographical:

Education:

Completed the requirements for the Master of Science in Mechanical Engineering at Oklahoma State University, Stillwater, Oklahoma in December 2014.

Completed the requirements for the Bachelor of Science in HVAC at Suzhou University, Suzhou, China, 2012.

Experience: Research/ Teaching Assistant at Oklahoma State University

Professional Membership: ASHRAE Student Member